Investigations of degradation in LNT catalysts systems: from noble metal to novel perovskite materials

By

Travis Jacques Wentworth

Submitted to the graduate degree program in Chemical and Petroleum Engineering and the Graduate Faculty of the University of Kansas in partial fulfillment of the requirements for the degree of Doctor of Philosophy.

_____

Chairperson: Susan M. Stagg-Williams

_____

Christopher Depcik

_____

Kevin Leonard

_____

Karen Nordheden

_____

Kyle Camarda

Date Defended: 8/11/2015

The Thesis Committee for Travis Wentworth

certifies that this is the approved version of the following thesis:

Investigations of degradation in LNT catalysts systems: from noble metal to novel perovskite materials

_____

Chairperson: Susan M. Stagg-Williams

Date approved: 8/11/2015

Abstract

The reduction in emissions from mobile and stationary sources has become a global priority. With the impacts of global warming already being felt, all avenues for reduction in greenhouse gas emissions are being investigated. Proposed miles per gallon standards of 54.5 MPG by 2025 have made increased engine efficiency a priority for all auto manufacturers. Lean-burn diesel engines are one potential strategy to reach the MPG targets, however current automotive catalysts struggle to reduce NO_x emission in the oxidative environments of lean-burn diesel engines.

Lean NO_x trap (LNT) catalysis is an ideal approach to reducing NO_x in oxidative environments. LNT catalysts are similar to traditional three-way catalysts in that they are inserted directly into engine exhausts and require no additional reductant systems. These catalysts can be improved by investigation into the specific catalytic components. Platinum serves to oxidize NO, facilitates NO_x storage, and reduce NO_x. Barium stores NO_x during lean phase operation, and common additives such as cerium improve tolerance to chemical thermal and physical degradation. As catalysts formulations are changed it is extremely important to understand how these catalysts will perform over the lifetime of operation.

The following work has taken a systematic approach to investigating aging characteristics of LNT catalysts, from simplistic noble metal alumina supported materials, to novel platinum free ceramic catalysts. A global kinetic model has been developed, and through the implementation of adaptive kinetic parameters, degradation of NO oxidation has been accurately modeled with changes in noble metal morphology. Investigations into aging of $Pt/Ba/Al_2O_3$ and $Pt/Ba/Ce/Al_2O_3$ have shown that NO oxidation profiles change substantially with thermal aging and that both the oxidation state and particle size of Pt affects conversion. Investigation of NO_x

storage over $Pt/Ba/Ce/Al_2O_3$ after thermal aging have shown that thermal aging induces formation of $BaAl_2O_4$ at aging temperatures as low as 600ºC and small amounts of $BaAl_2O_4$ can promote storage. Finally, a Pt-free $LaSrCoO_3$ catalyst has been shown to both oxidize and store NO_x but was unable to perform NO_x reduction. The work lays the foundation for investigations of non-platinic perovskites catalysts which represent the next generation of LNT catalysts.

Acknowledgements

I would like to acknowledge the support of my family and friends throughout my entire journey through graduate school. Without their support, encouragement and patience I would not have been able to get to this point in my life and my career. I would like to thank my mother Julie Wentworth and father Tylor Wentworth for their support and belief in me no matter what direction I choose to take in my life and career. I would also like to thank my wonderful fiancé Anisha Patel for her patience and encouragement, she has been with me throughout the entire process and I could not have done this without her.

I would like to thank my PhD advisor Dr. Susan Williams, for direction, advice and, genuinely helpful conversations. The list of things Dr. Williams has helped me with could go on but I hope it is sufficient to say I would have been unable to complete this achievement without her help and guidance. Finally, I would like to thank all of the researchers and staff at the University of Kansas who have helped me along the way. The list of people who have been extremely helpful and knowledgeable, in helping me complete my research is too long; however I hope I have been able to express my gratitude for all of their services over the years I have been here.

Table of Contents

List of Figures

List of Tables

Chapter 1: The Evolution of NO_x and MPG Standards in Tandem

1.1 NSF-IGERT requirement

As an NSF-IGERT Climate Change Humans and Nature in A Global Environment (C-CHANGE) fellow, part of my fellowship requires the inclusion of a thesis chapter that frames the research conducted within the context of global policy, human, and environmental changes. As such, I have chosen to include a historical review of the policies that are driving technology development in my field. Automotive catalysis is driven by the need for improving emissions from both a policy and environmental standpoint. I have, therefore, included this chapter entitled "The History of NO_x Emission Standards: A study in policy and technology development in tandem".

1.2 Abstract

Beginning in the 1970's, fuel economy standards set by the United States (US) Energy Policy and Conservation Act (EPCA) established the Corporate Average Fuel Economy Standards (CAFE). The CAFE standards in conjunction with the Clean Air Act amendments have had a major impact on technology developments, due to the interrelated nature of fuel economy and exhaust emissions. One of the easiest metrics to discern the impact of emissions standards and technology developments associated with fuel economy is nitrogen oxides (NO_x) emissions reduction technology. Current technology is struggling to meet emissions and fuel efficiency standards as a result of substantially decreased NO_x emissions standards and radical increases in miles per gallon (MPG) standards. This paper aims to show the history of NO_x emissions and fuel efficiency standards in the United States from 1970 to present and explain why these standards, while necessary and important have not been immediately met with technologic success in achieving them.

1.3 Introduction

In 1975, the US Energy Policy and Conservation Act (EPCA), established the Corporate Average Fuel Economy Standards (CAFE). Originally, the purpose of the CAFE standards were to reduce US dependence on foreign oil as a response to the 1973-74 Arab oil embargo [1]. In the same decade, the Clean Air Act began the process of setting and enforcing national ambient air quality standards, part of which included the regulation of emissions from mobile sources, primarily automobiles. This marked the first time in US history that fleet wide fuel efficiency standards were set for the automobile industry, and this also coincided with the first major enforcement effort of automobile emissions standards. The goal of nearly doubling the fuel efficiency of each automakers fleet of cars in six years whilst maintaining emissions standards that had previously been of little concern was extremely ambitious.

Both miles per gallon (MPG) and emissions standards are critically important to the sustainability and improvement of the environment in a global climate. According to the EPA, the two most prominent greenhouse gases produced in the United States in 2010 were carbon dioxide (CO_2) and methane (CH_4), representing 84% and 10% of total greenhouse gases produced, respectively [2].

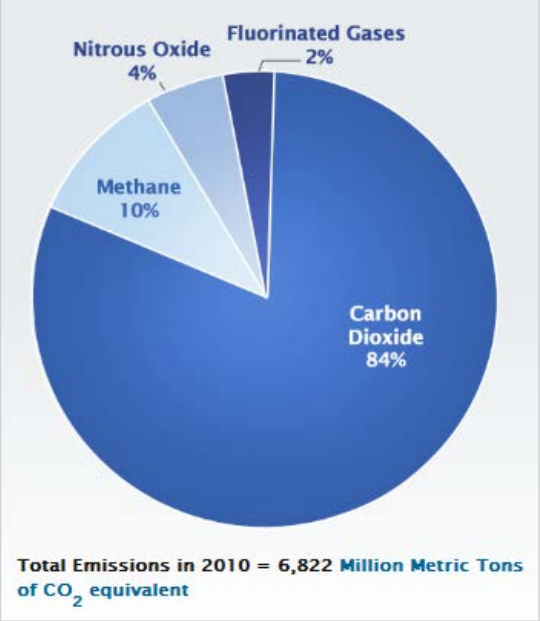

Figure 1-1: US Greenhouse gas emission by source 2010 [3]

Mobile source emissions of CO_2 represent the second largest source of CO_2 emissions in the United States. Emission of methane is also facilitated in part by the production and transport of oil. Increasing fuel efficiency of automobiles represents an extremely important avenue that is being used to reduce emission of CO_2 and methane by reducing the consumption of gasoline and diesel by automobiles [3].

The production and emission of NO_x also has a negative impact on the environment. NO_x contributes to the formation of ground level ozone, as well as fine particulate pollution and nitrogen dioxide (NO_2) has been linked to a number of respiratory health issues [4]. Figure 1-2 shows the breakdown of NO_x emission by source. Nearly two thirds of national NO_x emissions are produced by mobile sources [5].

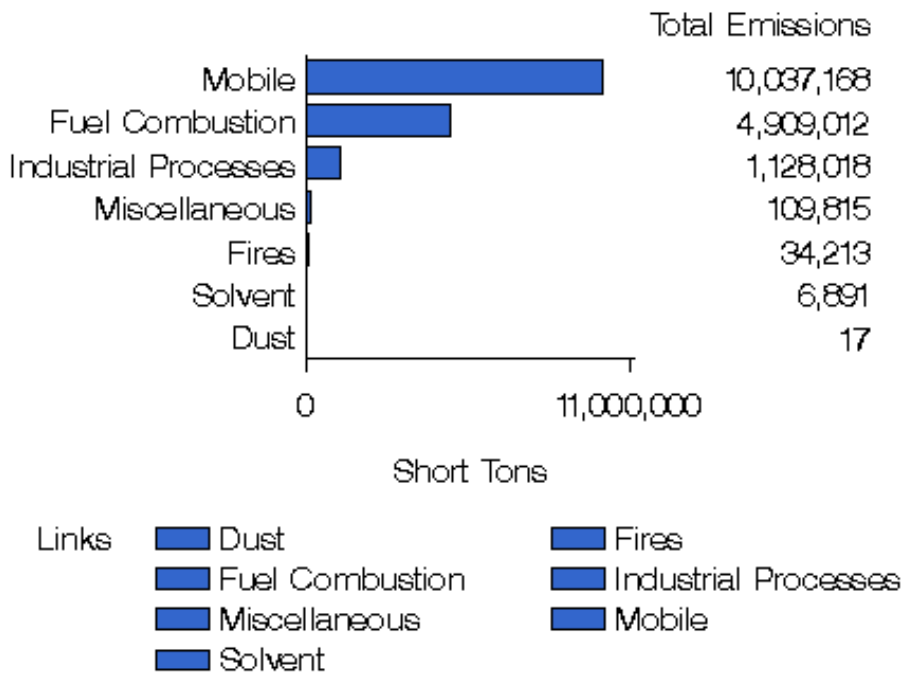

Figure 1-2: National nitrogen oxides emissions by source sector in 2008 [5]

Automobiles represent a significant contribution to both global climate change, as well as the increase in NO_x concentrations. Emissions and fuel efficiency are also intimately linked technologically. Therefore, it is extremely important to understand the relationship between the two in the context of historical regulation and how these regulations affect current standards.

1.4 Standards on Mobile Sources in the United States

Prior to the 1970's, the industries and manufacturers associated with automobiles, fuels and emissions, were still operating outside the realm of environmental accountability. During the House of Representatives debate on the Clean Air Act of 1970 a small town mayor was quoted as saying "If you want this town to grow, it has got to stink" [6]. This quote epitomizes

the attitude many American car manufacturers carried. The manufacturers and executives believed economic growth and technology development would result in environmental degradation. With the implementation of national ambient air quality, mobile source emissions and domestic automobile fuel efficiency standards, the United States government declared that the manufacturing community will be held responsible for maintenance of environmental air quality.

In the 1970's the United States began implementation of standards governing the consumption of petroleum fuels in miles per gallon (MPG) and emissions in parts per million (PPM) of organic compounds by mobile sources such as carbon monoxide (CO) and nitrogen oxides (NO_x). Regulations were applied to a number of different mobile sources by category; domestically purchased automobiles (cars), light trucks, public transportation diesel and gasoline engines. The regulations also applied to emissions during cold start up and after estimated vehicle life expiration. To meet the 1970's standards which were outlined and implemented in a relatively short period of time, technology in automotive emissions and vehicle MPG's required significant advances in a myriad of different fields. The standards required technology development in both chemical and mechanical engineering, as well as advances in environmental engineering and life cycle analysis. The technologies are in many ways at odds with one another from a design standpoint, meaning that optimizing one often times results in a suboptimal operating condition for the other technology. The dichotomy between technology and the policies as it relates to fuel efficiency and automotive emissions marks an important crossroads in the American policy and science relationship.

A prime example of the yin and yang between policy and technology is the relationship between the fuel efficiency of diesel engines and the emissions of particulate matter (PM) and

(NO_x). As fuel efficiency standards increase a promising strategy to reach MPG targets is to run engines lean. Traditional stoichiometric engines operate at an air to fuel ratio of approximately 14 to 1 and lean burn diesel engines operate at an air to fuel ratio of 25 to 1 or greater. The significant increase in available oxygen promotes complete combustion of the hydrocarbons leading to greater fuel efficiency and a decrease in the emission of carbon monoxide**.** However, the diesel direct injection process, combined with available oxygen for nitrogen dissociation, results in more PM and NO_x generated [7]. To add another level of technological complexity, PM emission resulting from direct injection can be virtually eliminated at the expense of significantly more NO_x production, or NO_x emission could be significantly reduced resulting in increased PM emission, through injection timing modulation. This is also known as the NO_x PM trade off. It is clear just from this brief discussion of lean burn technology that even without the increasing political demands in emissions and fuel efficiency, the implementation of lean burn technology is a complex problem to solve [8].

In 1970, the Clean Air Act (CAA) was amended to include national ambient air quality standards. The act authorized the establishment of national emissions standards for hazardous air pollutants and authorized requirements for the control of motor vehicle emissions. The CAA set the precedence for the future of environmental legislation in the United States, asserting that air quality cannot be sufficiently regulated and controlled regionally and those mobile and stationary sources of air pollution must be regulated and held accountable. Mobile emissions regulated by the amendments included carbon monoxide (CO), volatile organic compounds (VOC's) and NO_x. The NO_x standard set by the amendments was 3.1 grams per mile (GPM) for both cars and light duty trucks to be met by 1975 [9]. The 1970 CAA suffered a similar fate to the air quality act of 1967 in that it failed to meet the air quality targets set, and suffered from lack of enforcement.

However, the framework for effective regulation of automotive emissions was laid and would be the backbone of future amendments aimed at effectively reducing emissions from mobile sources.

In tandem with the air quality standards developments, the United States government was also developing the first set of fuel economy standards. With the establishment of the 1975 CAFE standards, the US set the first regulations on domestic automobile fuel economy. The fleet standards were set at 18 MPG in 1978 and were to rise, to a then staggering, 27.5 MPG in 1985 [10]. Although the response to CAFE standards was positive from a national security standpoint, with the estimated reduction in dependency on foreign oil, and reduction in pollutant emissions, response to the newly formed fleet fuel efficiency standards was mixed. The responses to the standards were especially negative from the automotive manufacturers themselves. One Ford executive was quoted in testimony to congress as saying, "[CAFE standards] would require a Ford product line consisting of either all sub-Pinto sized vehicles or some mix of vehicles ranging from a sub-sub compacts to perhaps a Maverick" [11]. The automotive industry also argued that, with the size reduction required to meet the standards, vehicle safety would be compromised [12]. The aversion of the automotive industry to the rapid changes in fuel efficiency standards made sense from a business perspective as they had already established a customer base in the current car market of large vehicles and, at this time, American automakers had a large majority of the automotive market in the US. Also, the regulations seemingly did little to entice consumers and/or facilitate profits. At first glance, the CAFE standards required large modifications to existing lines of automobiles, as well as significant technology development to meet these changes with little return in the form of consumer satisfaction.

By 1975, the initial targets and framework had been laid for the regulation of automobile fuel efficiency and emission in the US. The regulations set out by the 1970 CAA and the CAFE standards of 1975 required significant advancements in technology and a drastically new approach to car design. The effects of these independent standards on the automotive industry were not initially recognized by the US government. Emissions standards required the implementation of a catalytic converter; this technology required research in catalyst development, as well as implementation. The implementation of the devices had a considerable effect on engine performance and car cost and required use of costly noble metals [13]. The CAFE standards also required significant strides in development and implementation of technology to increase fuel efficiency. This represented a cost to the customer and had the potential to drastically change the emissions profiles of the vehicle.

After the initial CAFE standards were implemented and effectively met by the mid 1980's, the political landscape had changed as it pertained to fuel efficiency standards. This was due to the increases in fuel efficiency in domestic vehicles, the changing geopolitical environment and the recession of the 1980's dropping fuel demand[14]. It can be seen in Figure 1-3 that by 1990 oil prices in dollars per barrel had dropped to nearly the pre-embargo prices of the early 1970's.

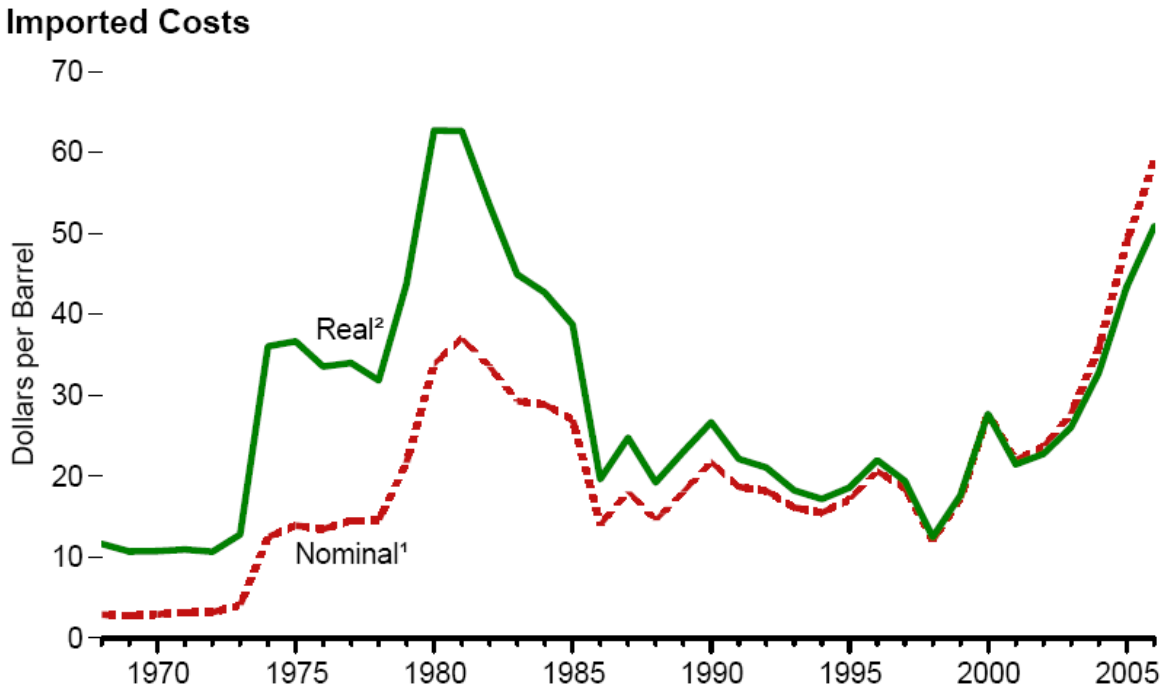

Figure 1-3: Real and nominal costs in dollars per barrel of oil in the United States between 1965 and 2005 [15]

As a result, the fuel efficiency standards stagnated between 1986 and 2002. Over the aforementioned time period, light passenger car fuel efficiency never wavered from the 27.5 MPG benchmark, and the 2 and 4-wheel drive (2WD/4WD) truck standard increased a meager 0.2 MPG from 20.5 to 20.7 [16].

Despite the stagnation in CAFE, emissions standards following the CAA amendments passed in 1970 continued to develop. The 1977 CAA amendments decreased maximum allowable NO_x to 2.0 GPM for cars, and the limits were again decreased to 1.0 GPM in 1981. The changes from 1975 to 1981 demonstrate nearly a 70% decrease in maximum tolerable NO_x emissions from the 1970 standards [2]. This represented a large change to car manufacturers,

considering just seven years earlier there had been no regulations of this kind imposed on automobile emissions. However, these changes were a stepping stone to the goal of limiting emissions to parts per million (PPM) levels.

The attitude towards the 1977 amendments is best summarized in an EPA press release. Douglas M. Costle, who was the EPA administrator at the time states, "The legislation enacted by the Congress will resolve a number of critical issues…. It will provide an acceptable schedule for continued future reduction in emissions from automobiles" [17]. The statement shows that although the standards are increasing, the 1977 amendments did not represent a giant leap forward like those of 1970 or the regulations that would follow.

The introduction of the CAA amendments of 1990 did in fact make great strides in the progression towards PPM emissions standards. The 1990 amendments specified 189 toxic pollutants required for regulation by the EPA, including those that were initially designated for regulation by the National Emission Standard for Hazardous Air Pollutants [2]. The act expanded enforcement authority and reformed the attainment requirements for the National Ambient Air Quality Standards. The new NO_x standard was set at 0.6 GPM for light cars, this is an additional 40% reduction in allowable GPM from the 1981 standards. Also, standards for light and heavy duty trucks were implement ranging from 0.6 GPM to 1.53 GPM dependent upon weight. These standards were to implemented and met by 1994 [18]. It is clear from the 1990 CAA amendments that the rapid reduction in allowable NO_x was a major priority for mobile emission regulation. Also included in the act was the prioritization of clear and swift enforcement of the emissions standards. As the development of the emissions standards is outlined, it is extremely important to keep in mind the relationship of these standards to fuel economy technology.

When the CAA amendment passed, it was the first time a major amendment passed with the consideration of global warming present in the national discourse. In an article written by Paul G. Rogers former Chair of the House Subcommittee on Health and Environment, Rogers states "Rising public concern over well-reported environmental problems such as acid rain, global warming and fouled beaches, coupled with the high profile that environmental issues took in the 1988 presidential elections, provides Congress with one of the most promising opportunities for legislative initiatives on clean air in recent years" [6]. This quote also explains in part why the standards changed so drastically during this time period as environmental issues were at the forefront of the 1988 presidential elections. This is another example of the lack of communication between policy makers and those developing the technology. It was noted earlier that the late 80's and early 90's were a time of rapid development in standards but it is important to understand what was driving this progression. It was due in large part to political campaign issues in the 1988 elections.

Furthermore the major reduction in allowable emissions implemented by the 1990 amendments to the CAA generated the necessity for lean burn diesel NO_x catalyst development. In 1996, Takahashi of the Toyota motor group published the first paper outlining the design of a Lean NO_x Trap (LNT) catalyst [19]. This marks the first time a mobile NO_x reduction strategy has been published that utilized the framework of the existing Three-Way Catalyst (TWC) system. The benefits that the LNT and TWC catalyst systems share are their use of exhaust gas constituents to convert harmful gases such as CO, unreacted hydrocarbons (HCs) and NO_x while maintaining a relatively maintenance free system. In these systems, there is no need for alternate conversion sources, feedback control systems, or storage tanks for other reaction components. It is important to note that these systems are not without flaw. For example, the use of noble

metals, such as platinum and palladium, represent a significant cost and represent an area automotive researchers are continuing to optimize to drive costs down [13]. Without the CAA and CAFE standards, research interests in this area would be extremely limited if they existed at all. The timing of the development of the LNT catalyst by the Takahashi group is another prime example of the strong interdependence between the social/political environments and technology development.

In the late 90's, the standards for NO_x emissions continued to increase. In 1998, the northeast states in conjunction with major auto manufacturers and support from the Clinton administration passed a voluntary agreement for the reduction of automotive emission entitled National Low Emissions Vehicles (NLEV) [20]**.** The standards set by this voluntary group decreased NO_x emissions to 0.3 GPM for cars and 0.5 GPM for light trucks. These voluntary standards preempted the 1999 EPA proposed Tier 2 standards and set the bar for continued NO_x emissions reductions into the 21st century. Directly following the voluntary standards, the EPA Tier 2 standards were proposed for implementation by 2004. Tier 2 set NO_x emissions goals for both cars and light trucks at the same level for the first time since the inception of the standards by the CAA amendments in 1970. Table 1-1 shows the changes in NO_x GPM standards from 1975 to 2009. Tier 2 set targets at 0.07 GPM which represented a 74-78% reduction in allowable NO_x for cars and a 94-96% reduction in allowable NO_x for light duty from previous targets [18].

Table 1-1 Figure NO_x Emissions Standards 1975-2009 for Cars and Light trucks NO_x Standards for Cars[18]

Year	1975	1977	1981	1994	1999	2004-2009
NO_x Standard (GPM)	3.1	2.0	1.0	0.6	0.3	0.07
NO_x Reduced (from previous standard)		35%	50%	40%	50%	77%

NO_x Standards for light duty trucks (6000lb and less)

Year	1975	1979	1988	1994	1999	2004-2009
NO_x Standard (GPM)	3.1	2.3	1.2	0.6	0.5	0.07
NO_x Reduced (from previous standard)		26%	48%	50%	17%	86%

Thus, from 1975 to 2004, the national NO_x standards went from unregulated to near elimination of NO/NO_2 emissions from automotive exhausts. It should be noted that over this time of continual tightening of emissions standards, fuel efficiency standards remained at 27.5MPG for light cars. One of the major reasons that emissions profiles did not change with MPG increases was related to how the MPG standards were achieved. In a CRS report to congress entitled Automobile and Light Truck Fuel Economy: CAFE Standards, the report states 70% of fuel economy improvement was achieved by improvements in weight reduction, transmissions, aerodynamics, use of front-wheel drive and fuel injection [16]. The majority of the listed improvements with the exception of fuel injection has very little impact on the characteristics of the engine burn profile and, therefore, does little to affect exhaust emissions. It is important to understand why fuel efficiency standards to this point were important. The CAFE standards of the 1975 EPCA forced auto manufacturers to deplete the avenues most easily implemented to increase fuel efficiency (the low lying fruit of technological development), such as decreasing vehicle weight. Once the simplest methods of improvement were depleted, the more advanced methods (such as lean-burn engine operation) became extremely important in meeting higher MPG standards. So, while the initial MPG standards did not substantially affect automobile exhaust profiles, they played a key role in creating the situation the automotive industry will find itself in when trying to reach future MPG standards.

In 2002, the National Academy of Sciences (NAS) released the Effectiveness and Impact of the Corporate Average Fuel Economy (CAFE) Standards. As a part of this study, it was proposed that fuel economy standards for light trucks including SUV's could be increased by another 40% over the following 10-15 years [12]. Furthermore, light trucks and SUV's represent a large percentage of domestically operating diesel engines and lean burn strategies have been investigated in large part for use in increased fuel efficiency. Again, policy is driving the development and implementation of lean burn diesel technologies.

In the years following, the state of California began enacting an even more rigorous standard for automotive emissions, where maximum allowable NO_x for cars and light duty trucks were set at 0.05 GPM and the standard for medium duty trucks was set to 0.2 GPM. The California emission standards were coupled with stricter standards on CO and PM, which generated the tightest standards in the country at the time [21]. A study by the North East State for Coordinated Air Use Management (NESCAUM) concluded about the LEV-II effectiveness "(LEV-II) compliance would lead to a drop in carbon dioxide emissions, considered by scientist to be a chief cause of global warming states would thus find it easier to meet state and regional climate change goals" [22]. Again the importance of climate change, as it relates to mobile emissions source reduction, is reiterated in the national discourse this time by a government agency.

In the 2000's, gas prices began to increase substantially and discussions of environmental sustainability had also come to the forefront of political and social discussions. As a result of both rising gas prices and increased national concern over environmental sustainability, consumers became more aware of fuel efficiency and environmental concerns subsequently impacting their decisions. After 30 years of CAFE standards, the last 10 years

represents a time period where automotive executives are becoming more acutely aware of the benefits of fuel efficiency. In a December 6, 2001 testimony Bernard Robertson, Senior Vice President of Engineering Technologies and Regulatory affairs for Daimler-Chrysler stated, “the industry achieved significant gains during the past twenty five years” and that replacements to the CAFE standards are “either politically unacceptable or have significant ‘unknowns’ or problems” [23].

As automotive executives began accepting CAFE standards as necessary and valuable, it has also become clear that MPG standards represent intrinsic value to the customer. In a study produced by the NAS, illustrated in Table 1-2, it was shown that an increase in fuel economy of light trucks to 21.0 MPG in 2005 and further to 22.2MPG in 2007 would represent a net benefit of 111 million dollars for model year (MY) 2005, 216 million dollars for MY 2006, and 421 million dollars for MY 2007. The study determined total benefits of nearly 1 billion dollars over the three year time frame of implementation.

Table 1-2 Figure Estimated Costs and Benefits from the MY2005-2007 light truck CAFE standards [16]

	Total Costs (million)	Total Societal Benefits (million)	Net Benefits (million)
MY2005	$108	$219	$111
MY2006	221	513	292
MY2007	373	794	421

With a decrease in resistance from domestic and foreign auto manufacturers, and growing demand from consumers, the environment for increased fuel efficiency standards had never been more positive. In 2007, Congress passed the most optimistic standards proposal to date, the Energy Independence and Security Act (EISA). In Title I of the act: Energy Security Through Improved Vehicle Economy, the standard for fleet wide fuel economy was set at 35 MPG by 2020. The EISA also established guidelines for the first five years of the proposed program. The fleet wide fuel economy was to be increased to 27.3 MPG this a marked increase from the fleet average 21 MPG during the stagnation period (where 27.5 MPG was the standard for light cars) and the average fuel economy, as well as reduction in GHG emission was to be 5% per year for 2011-2016 [24]. The plan also called for evaluation and implementation of similar standards increases over the following five years to successfully attain the 35 MPG goal.

It is important to contextualize the fuel efficiency standards within the framework of the emissions regulations passed through the 1990's and 2000's. As stated previously, the MPG standards achieved by the automotive industry from the fuel efficiency regulations pre 2007 were obtained predominantly through means unrelated to engine operating conditions. However, one must now recognize the situation created by both the CAFE and EPA emissions standards. EPA regulations set allowable NO_x emissions at 0.06 GPM for light cars and the EPA has mandated an average fleet fuel economy of no less than 27.3 MPG [25]. Light cars have the highest attainable fuel efficiency and as such, must have fuel efficiency much higher than the fleet average to compensate for vehicles such as trucks, vans, and sport utility vehicles (SUVs). Given this information, it is clear that strong consideration must be given to engine operating regimes, such as lean-burn diesel engines.

To give perspective on this issue, one could look at Europe, where similar problems are present. Fuel costs are dramatically higher in Europe and have been for an extended period of time, and this has already lead to the implementation of lean burn engines as a strategy to increase fuel efficiency and save consumers money [26]. Fuel costs led to the implementation of lean burn engines, and current EU NO_x standards are set at 0.18 GPM [27]. At that level, implementation of lean burn diesel engines in some applications are more viable than their American counterparts. I would argue that the fuel efficiency demand in Europe arose much earlier due to the higher cost of fuel, aligning the fuel economy policies and emissions standards. This allowed for more effective implementation of lean technology. This is another example showing the importance of the history of emissions and fuel economy standards development. Where European emissions standards seem to be working with fuel economy and technology development, the inverse seems to be true in the US

Current lean burn engines emit NO_x in concentrations upwards of 0.1 GPM [28]. This is nearly 100% more than is allowable by 2009 emission standards in the US. In August of 2013, the Obama administration released a statement that the DOT and EPA will be "building on the success" of MY2011 and MY2012 fuel efficiency standards, and have set a goal of 54.5 MPG for cars and light trucks by the year 2025 [29]. As a nation we are in an environment where fuel efficiency demands are increasing rapidly and, as a country, we are unwilling to sacrifice our ambient air quality and cleanliness of environment.

1.5 Conclusions

In the last 45 years emissions standards have increased significantly starting with the implementation of the CAA amendments in 1970 and culminating in the Tier 2 standards which have decreased allowable NO_x emission to 0.06 GPM. Over the same time period, fuel efficiency standards have increased from non-existent to a proposed 54.5 MPG in 2025. Both the changes in fuel efficiency and emissions are significantly large for a 30 year time scale, however, they are also extremely important for a number of reasons; global climate change, energy independence, and ambient air quality. It is clear that due to all of these factors, emissions and fuel economy must be considered in conjunction in the future and developments in technology must be at the forefront of political concern.

Finally, from a scientific perspective there are a number of reasons that make this problem extremely important, including the high standards set on both fuel efficiency and emissions, as well as the interplay between the two as it relates to automobile manufacturing. The problem is perpetuated by the fact that attempts to increase fuel efficiency further will likely result in both the increase of NO_x emissions, as well as a decrease in the efficiency of the conversion technology to due to the exhaust conditions. This means that, although the interdisciplinary nature of these topics may have been lost during the development of these standards, it must be developed and maintained as we move forward in these areas.

1.6 References

1. Hoffman, A.R., *The Origins of CAFE.* Forum on Physics and Society, 2007. **36**(4).
2. EPA, *Inventory of U.S. Greenhouse Gas Emissions and Sinks: 1990-2010*, U.S.E.P. Agency, Editor. 2012: Washington D.C.
3. EPA. *Greenhous Gas emission*. 2012 [cited 2012 November 12, 2012]; Available from: http://www.epa.gov/climatechange/ghgemissions/gases.html.
4. Paul Beggs, P.C., *Climate and Chronic Respiratory Diseas.* Health and Toxicology, 1997: p. 329-345.
5. NEI. *National Nitrogen Oxides Emission by Source sector*. 2008; Available from: http://www.epa.gov/cgi-bin/broker?_service=data&_debug=0&_program=dataprog.national_1.sas&polchoice=NOX.
6. Rogers, P.G., *The Clean Air Act of 1970.* EPA journal, 1990(January/February 1990).
7. Gable, C. *What is a Lean Burn Engine?* 2012; Available from: http://alternativefuels.about.com/od/glossary/g/leanburn.htm.
8. EPA, *Technical Bulletin: Nitrogen Oxides (NOx), Why and How they are Controlled*, O.o.A.Q.P.a. Standards, Editor. 1999: Research Triangle Park.
9. EPA, *Clean Air Amendments of 1970*, E.P. Agency, Editor. 1970: Washington DC.
10. Greene, D.L., *Why CAFE worked.* Energy Policy, 1998. **26**(8): p. 595-613.
11. record, c., *Congressional Record, V. 146, Pt. 8, June 13, 2000 to June 21, 2000*. 2000, Government Printing Office. p. 10954.
12. Effectiveness, C.o.t., I.o.C.A.F.E. Standards, and N.R. Council, *Effectiveness and Impact of Corporate Average Fuel Economy (CAFE) Standards*. 2002: The National Academies Press.
13. Chauhan, S., *Noble metal catalysts for monolithic converters.* Journal of Chemical and Pharmaceutical Research, 2010. **2**(4): p. 9.
14. Morris, M., *Motor Gasoline Consumption 2008: A Histrical Perspective and Short Term Projections*, D.o. Energy, Editor. 2008, Energy Information Administration: Washington D.C.
15. DOE, *Annual Energy Review 2011*, D.o. Energy, Editor. 2012, U.S. Energy Information Administration: washington D.C.
16. Yacobucci, B.D., *Automobile and Light Truck Fuel Economy: The CAFE Standards*, C.R. Service, Editor. 2007.
17. Costle, D.M., *Statemnet by Douglas M. Costle on Passage of Clean Air Act Amendments of 1977*, E.P. Agency, Editor. 1977.
18. McCarthy, J.E., *Clean Air Act: A summary of the Act and Its Major Requirements* C.R. Service, Editor. 2005.
19. Takahashi, N., et al., *The new concept 3-way catalyst for automotive lean-burn engine: NOx storage and reduction catalyst.* Catalysis Today, 1996. **27**(1–2): p. 63-69.
20. EPA, *Control of Air Pollution from New Motor Vehicles and New Motor Vehicle Engines: Finding of National Low Emissions Vehicle Program in Effect*, E.P. Agency, Editor. 1998: Washington D.C.
21. *Cars and Light-Duty Trucks - California*. 2012 July 2012 [cited 2012 November 25, 2012].
22. Marin, A.N., *National Research Council Report Supports States' Ability to Adopt California's Clean Vehicle Program*, T.C.A.A.o.t. Northeast, Editor. 2006: Boston, MA.
23. Congress, *Corporate Average Fuel Economy (CAFE) Reform: Hearing before the Committee on Commerce, science and, Transportation*, U. Senate, Editor. 2005, U.S. Government Printing Office: Washington, DC.
24. Congress, t., *Energy Independence and Security Act of 2007*, U.S.G. Information, Editor. 2007: Washington, D.C.

25. Anderson, T., *SUMMARY OF FUEL ECONOMY PERFORMANCE*, U.D.o. Transportation, Editor. 2011: Washington, DC.
26. University, C., *Fuel and Air Transport*, D.o.A. Transport, Editor. 2008.
27. *Emissions Standards - European Union: Cars and Light Trucks*. 2012 September 2012 November 25, 2012]; Available from: http://www.dieselnet.com/standards/eu/ld.php.
28. Canuteson, E., *NOx HyCat: A New Catalytic System for Diesel Engines*. 2012, Los Alamos National Lab.
29. Secretary, P., *Obama Adminitration Finalizes Historic 54.5 MPG Fuel Efficiency Standards*, T.W. House, Editor. 2012.

Chapter 2: Overview of LNT Catalysis

2.1 Introduction

Beginning in the 1970's, reduction of NO_x in oxidizing environments has been a reaction of interest in the automotive industry. In 1995, Matsumoto et al in the Toyota research group showed a promising method for facilitating this reaction [1]. They proposed the "NO_x Storage Reduction catalyst" (NSR) where NO and NO_2 (also known as NO_x) emitted by learn burn engines are stored during lean phase operation and then reduced during a short rich exhaust condition. They showed that through continuous cycling of lean/rich operation, NO_x can be substantially reduced. The authors proposed a noble metal/alkali earth metal catalyst combination on an oxide support, whereby the alkali earth metal stored NO_x and the noble metal component facilitated NO oxidation and NO_x uptake, as well as rich phase reduction.

The catalyst formulation most common in NSR or lean NO_x trap (LNT) literature consists of Pt as the noble metal component, and Ba as the NO_x storage component supported on high surface area γ-alumina, $Pt/BaO/Al_2O_3$. This material is either used as a powder in packed bed experiments or dip coated on monolith substrates [2-4]. Catalysts formulations which include Ce as an oxygen storage component (OSC) to facilitate NO_x uptake and conversion have been shown to have promise in recent years[5].

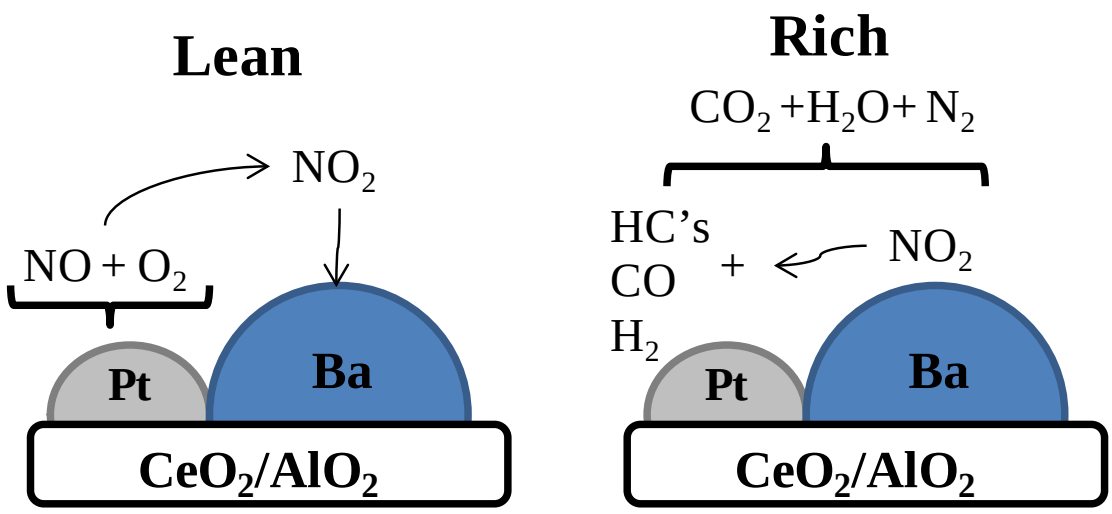

Figure 2-1: Diagram of traditional operation of LNT catalysts under lean and rich environments

Figure 2-1 shows a diagram of the fully formulated LNT catalyst illustrating the required Pt-Ba adjacency as well as the CeO_2/Al_2O_3 support. The following literature review is presented in a similar methodology to the way in which it was investigated. Literature is separated by individual component and presented clearly to elucidate the functionality of each component.

2.2 Investigations of platinum in LNT catalysts

Takahashi et al expanded upon the Matsumoto work and eventually proposed the first NO_x storage mechanism [6]. They were the first authors to identify variations in NO_x conversion with noble metal particle size. Total NO_x conversion increased with a decrease of platinum particle size from 15 – 1 nm. It is hypothesized that the increase in conversion with Pt dispersion is due to increased surface area for oxidation and reduction as well as an increase in the Pt-Ba interaction. However this was shown for platinum barium catalysts with complex oxidizing and

reducing environments. It is not possible to verify these hypotheses under the complex conditions and, as a result, subsequent investigations break down the complex systems and present smaller and more manageable experiments.

An investigation of the effect of support material on the oxidation of NO to NO_2 over platinum showed the effect of support material on LNT catalysts [7]. Varying support material showed a substantial effect on the catalysts ability to oxidize NO and SO_2. The most effective support material was SiO_2 where the order of effectiveness was $SiO_2 > Al_2O_3 > ZrO_2$. The reaction rate showed a strong correlation with particle size for NO oxidation where reaction rate increased with increased platinum particle size for both γ-Al_2O_3 and SiO_2 supports. No particle size correlation was found for the ZrO_2 support. SiO_2 showed the largest particle size variation in the range of 1%-5% platinum loading. The γ-Al_2O_3 support showed the highest platinum dispersions with equivalent loading and a less linear change in Pt dispersion due to the propensity of γ-Al_2O_3 to promote platinum dispersion. The Al_2O_3 catalyst with the largest platinum particle size had the highest conversions even when compared to an Al_2O_3 catalyst with double the platinum loading. This indicated a strong correlation between platinum particle size and the ability to oxidize. Further investigations into particle size effects were required to understand this phenomena.

Another important conclusion resulted from temperature programmed desorption (TPD) experiments. Pt/γ-Al_2O_3 desorbed the most NO/NO_2 after loading as compared to the other two support materials. The secondary desorption peak associated with desorption of NO from the support material occurred at the highest temperature for Al_2O_3 supported catalysts which indicated the most stable NO_x species were stored on Al_2O_3. This is perhaps the most important finding whereby the interaction of the support material with acidic molecules like SO_2 that would

normally be a detriment to the use of γ-Al_2O_3 supports in automotive applications was shown to positively impact NO and NO_2 uptake for use in an LNT catalyst.

The effect of Pt particle size on NO oxidation as well as NO_x reduction with Pt loading, showed an even greater impact of particle size on NO oxidation [8]. With a decrease in dispersion from 82% to 4.4% NO oxidation in the temperature range of 255ºC to 300ºC was increased nearly tenfold. NO_x reduction by propene with varying dispersion showed that noble metal dispersion has very little effect on the reduction of NO and it was concluded that due to the constant NO reduction with particle size, NO oxidation was not a fundamental step in the reduction mechanism.

The first LNT model developed specifically for NO oxidation over Pt/Al_2O_3 catalysts attempted to model variations in NO oxidation via oxygen surface coverage [9]. This was a preliminary idea that was later used as the basis for modeling variations with noble metal particle size. The model used Eley-Rideal (E-R) kinetics and the Arrhenius rate expression to described reaction rate constants:

$$\boldsymbol{k = Ae^{\frac{-E_A}{RT}}}$$

Many parameters, such as sticking coefficients, were taken from the literature but one of the key parameters, activation energy of oxygen desorption, was described by an empirical estimation based upon TPD experiments. Oxygen desorption profiles were found to change based upon adsorption conditions. As oxygen adsorption temperature was increased desorption temperature and maximum temperature of desorption also increased. Based upon this finding, oxygen desorption activation energy was determined to vary linearly with surface coverage and surface coverage was estimated based upon the TPD experiments. The model also varied

activation energy of NO_2 desorption based upon the hypothesis that surface concentrations of NO and NO_2 are dictated by surface coverage of O_2 where oxygen dominates the surface at low temperatures. The model predicted both the increase in NO conversion with temperature at low temperatures (kinetic regime), as well as the decrease in NO conversion at higher temperatures (equilibrium limited regime).

While Pt was the most common noble metal for LNT catalysts. Pt and Rh were shown to be the two most effective promoters in lean phase performance [10]. The authors show that Pt and Rh are the most effective promoters of both NO oxidation and NO_x storage. A strong correlation was found between the noble metal NO oxidation activity and the promotion of NO_x storage over the alkali earth component.

Another investigation compared Pt and Pd supported on BaO/Al_2O_3[11]. The Pd catalyst achieved slightly higher NO_x storage capacity at low temperatures (300ºC). At higher temperatures (400ºC), the Pt catalyst showed slightly better storage. During transient cycling the Pd catalyst showed early NO breakthrough when switching form rich to lean. The breakthrough was associated with the re-oxidation of the reduced Pd particles from the previous cycle. Because Pd required re-oxidation, a loss in overall NO_x reduction efficiency was observed. Also NO oxidation was limited over the Pd catalyst. Given that NO_x storage requires the oxidation of NO to NO_2, platinum was the more viable noble metal for use as an LNT catalyst.

Once it had been established that Pt was superior to other noble metal alternatives, investigations to facilitate real world applications were required. Degradation facilitated via the dissociation of NO_2 was investigated for Pt/Al_2O_3 and $Pt/Ba/Al_2O_3$ [12]. The increased activity with platinum particle size was attributed to the decrease in formation of platinum oxide for

larger platinum particles. NO_2 dissociation and NO oxidation over $Pt/Ba/Al_2O_3$ catalysts with the same pretreatment conditions did not show the same trends. $Pt/Ba/Al_2O_3$ showed lower Pt dispersion at each pretreatment temperature relative to the Pt/Al_2O_3. Ba addition was observed to impact both NO oxidation and NO_2 dissociation negatively. XPS measurements showed that Pt oxide formation was promoted via the Pt-Ba interaction whereby the alkalinity of the barium promoted PtO_2 formation resulting in the negative impact on both NO oxidation and NO_2 dissociation. This was the opposite effect of the Al_2O_3 support which was shown to help abate PtO_2 formation due to the acidic nature of the support material.

Real world effects on Pt LNT catalysts were also shown in the effects of lean phase gas concentrations [13]. Maximum conversion decreased with increasing NO concentration and maximum conversion temperature increased. Because NO conversion decreased with increased NO inlet it was concluded that the production of NO_2 inhibits NO oxidation. NO_2 inhibition could be regenerated via reconditioning above 650ºC in a reducing environment that showed NO_2 induced deactivation via oxidation of Pt particles. The proposed mechanism for Pt catalyst deactivation via NO_2 decomposition was hypothesized as:

$$2Pt + O_2 \rightarrow 2Pt - O_{ads}$$

$$NO + Pt - O_{ads} \leftrightarrow Pt + NO_2$$

$$NO_2 + Pt \leftrightarrow Pt - O_{ads} + NO$$

$$NO_2 + Pt \leftrightarrow PtO + NO$$

Pt-O formation with varying Pt particle size was investigated through induced oxidation of Pt via the NO_2 dissociation reaction. The theory of deactivation in NO oxidation due to Pt-O formation and increased Pt-O formation over smaller particle was confirmed [14]. It was shown

that the NO oxidation turnover rate (TOR) for thermally aged Pt/Al_2O_3 with an average particle size of 7 nm was four times higher than the TOR over the same catalyst formulation with average particle size of 2.4 nm. Then deactivation due to Pt-O formation was induced via exposure to NO_2 at low temperatures. Deactivation was characterized by oxygen uptake, through oxygen uptake it was observed that smaller Pt particles undergo oxidation increased due to increased surface exposure. Smaller Pt particles decrease metallic platinum stability [15].

Another way changes in NO oxidation with Pt particle size were elucidated was through single crystal studies [16-18]. It was identified that the (111) facet is representative of the large Pt > 5 nm particles and other facets such as the (110) are representative of stepped or kinked regions more closely associated with small Pt particles < 2 nm. In a study of NO oxidation on Pt(111) and Pt(321) large single crystals, compared with Pt support on Al_2O_3 and SBA-15 it was shown that Pt(111) surpassed even the largest Pt particles in catalytic activity [18]. TOR increased with particle size up to 9.1 nm where the Pt(111) single crystal showed TOR 3-4 times higher than even the 9 nm particles. Because TOR is a measurement of conversion normalized to the site the TOR increases all the way to the maximum particle size condition, the Pt (111) single crystal. The single crystal study clearly illustrates that increased catalytic oxidation with Pt particle size is continuous to even the largest platinum particles (represented by the Pt(111) single crystal. However, there will still exist a maximum in NO conversion because at constant Pt loadings increasing particle size decreases the number of available sites. The maximum will be where the number of available catalytic sites outweighs the increased conversion observed over larger particles.

Most recently, the effects of temperature and gaseous environment on noble metal sintering and catalyst performance in the NO oxidation reaction were investigated [19]. It is

shown specifically that successive aging of Pt/Al_2O_3 catalysts can be achieved at calcination temperatures between 500-900ºC, where 100ºC step changes provide sufficient aging in oxygen environments to achieve observable changes in Pt particle size and NO oxidation at each aging step. Furthermore, the use of thermal aging to simulate the effect of real world long term aging in exhaust environments, is justified.

2.3 Investigations of Barium in LNT Catalysts

Previously identified literature has shown LNT catalysts can effectively store and reduce NO_x in lean/rich environments [6]. Barium addition can change the nature of catalysts for both NO oxidation and NO_x storage. The first complete storage mechanism proposed shows only a basic understanding of Pt/Ba LNT catalysts [20]. The storage mechanism was based upon uptake experiments conducted in 500 PPM NO/7% O_2 in N_2 and NO_x storage increased with temperature up to 350ºC. Nearly twice as much storage occurred with NO_2 in the inlet. The NO_x storage mechanism including both NO and NO_2 is hypothesized as:

$$NO + Pt \leftrightarrow NO - Pt$$

$$NO_2 + Pt \leftrightarrow NO_2 - Pt$$

$$O_2 + 2Pt \leftrightarrow 2\,O - Pt$$

The above equations represented adsorption of individual species to available metallic Pt. The following equations represented the storage mechanism on BaO species:

$$BaO + 2NO - Pt + 3O - Pt \leftrightarrow Ba\,(NO_3)_2 + Pt$$

$$BaO + 2NO_2 - Pt + O - Pt \leftrightarrow Ba\,(NO_3)_2 + Pt$$

Two types of storage were also hypothesized. Storage which occurred on Ba sites directly adjacent to Pt and those Ba sites far away from Pt.

The Ba NO_x storage mechanism was expanded upon by the identification of the ba nitrite intermediate [21]. Observations of the FT-IR spectra for $Pt/Ba/Al_2O_3$ LNT's showed formation of both bridged nitrite, as well as monodenate and linear nitrite after NO_x storage experiments at low temperatures (150ºC). These peaks were virtually eliminated at storage temperatures above 300ºC. At moderate storage temperatures the nitrite peak was replace by the nitrate predicted by the above NO_x storage mechanism. It was also observed that substantial amounts of NO are formed during the initial breakthrough of long term NO_x storage experiments which indicates the production of NO is a byproduct of storage at intermediate storage times; this was not predicted by the original storage mechanism. NO_x is most available on $Pt/Ba/Al_2O_3$ catalysts as compared to Pt/Al_2O_3 and BaO/Al_2O_3 catalysts via NO_2-TPD.

A comprehensive investigation via FT-IR of NO_x storage with time and temperature over Pt/Al_2O_3 and BaO/Al_2O_3 and $Pt/Ba/Al_2O_3$ helped to elucidate the functionality of each component in the NO_x storage process [22]. It was shown that NO/NO_2 can be stored on Al_2O_3 without any catalyst present. While the storage amount is small, this observation confirms the assertion that Al_2O_3 supports enhance NO_x storage via interaction with the supported catalytic material. At low temperatures in NO/O_2 environments the nitrite is favored for all the catalysts tested. The lack of nitrate formation is due to the decreased NO oxidation that occurred at low temperatures. At the same temperatures in the NO_2/O_2 environments nitrates were observed. NO_x adsorption over LNT catalyst with high barium loadings was shown to continue for extended periods even after the initial breakthrough of NO_x. NO oxidation was shown to be an important step in NO_x storage. Furthermore, barium nitrite was identified as a potential

precursor and/or the final adsorbed phase depending upon adsorption condition. Finally, longtime storage occurred without the formation of bulk $Ba(NO_3)_2$ in the less than 10 minute uptake regime.

With the nitrite species identified as a precursor to the stable nitrate formed during NO_x storage under oxidizing conditions and at temperatures above 200ºC a mechanism had yet to be proposed that included this step. NO_x uptake experiments after reduction in complex gas environments including CO_2 and H_2O showed that in addition to the nitrite intermediate multiple Ba sites were available for NO_x storage [23]. It was shown that significant H_2O and CO_2 production will occur under lean conditions during NO_x uptake indicating that all three species BaO, $Ba(OH)_2$, and $BaCO_3$ are active for NO_x uptake. Where the order of activity is as follows $BaO>Ba(OH)_2>BaCO_3$. The mechanism proposed incorporates the active barium forms as well as the nitrite precursor:

$$O_2 + 2Pt \leftrightarrow 2\,O - Pt$$

$$BaO + O - Pt + 2NO \leftrightarrow Ba(NO_2)_2$$

$$Ba(OH)_2 + O - Pt + 2NO \leftrightarrow Ba(NO_2)_2 + H_2O$$

$$Ba(NO_2)_2 + 2O - Pt \leftrightarrow Ba(NO_3)_2$$

$$NO + \frac{1}{2}O_2 \rightarrow NO_2$$

$$BaO + 2NO_2 + O - Pt \leftrightarrow Ba(NO_3)_2$$

$$Ba(OH)_2 + 2NO_2 + O - Pt \leftrightarrow Ba(NO_3)_2 + H_2O$$

$$2NO_2 \leftrightarrow N_2O_4$$

$$2BaO + N_2O_4 \leftrightarrow Ba(NO_2)_2 + Ba(NO_3)_2$$

$$2BaO + N_2O_4 \leftrightarrow Ba(NO_2)_2 + Ba(NO_3)_2$$

$$2Ba(OH)_2 + 2N_2O_4 \leftrightarrow Ba(NO_2)_2 + Ba(NO_3)_2 + 2H_2O$$

The above mechanism does not include the barium carbonate species as the authors assume that relative to the hydroxide and oxide forms of barium in the storage process the carbonate is significantly less active.

Another extension to the NO_x storage mechanism was proposed when the production of NO during initial NO_x storage was validated [24]. It was shown that NO_2 is consumed at a 3:1 ratio to NO produced during storage over BaO/Al_2O_3 catalysts. The mechanism for NO production was proposed as:

$$BaO + 3NO_2 \rightarrow Ba(NO_3)_2 + NO$$

NO production did not occur in as high a ratio over catalysts which included a noble metal component or in environments when H_2O was present. This suggests that while the NO_2 decomposition method of adsorption is likely to occur, it is only partially facilitated in more complex environments and must be considered in addition to the proposed traditional mechanisms of NO_x storage.

Epling et al. gave the first description of the NO_x uptake profile with time which clearly defined the three stages of NO_x uptake [25]. Extended time NO_x uptake profiles were shown to have three distinct regimes. The first was identified as the "complete uptake" defined as the regime where all inlet NO_x is adsorbed by the catalyst and none is present in the outlet. This regime was associated with Ba which is directly adjacent to Pt particles and can participated

directly in the NO oxidation and spill-over mechanism. The second regime "rapid NO_x uptake" was characterized by the drastic change in uptake with time. Ba associated with the rapid regime was the Ba with surface storage availability but not adjacent to the Pt particles requiring surface diffusion from the noble sites to the available NO_x storage sites. The third and final regime was the "slow but significant uptake", this was associated with diffusion into the bulk storage material. The authors admit there was insufficient evidence to completely define the long term uptake profiles observed, however substantial insight was gained. There were also important findings with regard to complex inlet gas compositions including H_2O and CO_2. Others have found the addition of H_2O to have mixed effects on NO_x adsorption with temperature [23]. The addition of H_2O was shown at both low and high temperatures to negatively affect NO_x uptake. Furthermore, at high NO_x storage temperatures, the addition of H_2O to a lean gas environment already containing CO_2 did not significantly impact the NO_x uptake profile. This justified modeling uptake system using only CO_2 to accurately approximate NO_x uptake profiles on pre-reduced catalysts.

To this point in the literature, Ba content had been varied only slightly between 16-22% loadings. A comprehensive investigation of the effect of barium loading on the catalytic activity helped elucidate the role of barium loading in generating effect NO_x storage material [26]. A number of important effects are observed with varying Ba loading. Platinum particle size, catalyst pore volume and surface area decreased with Ba addition. Bulk barium carbonate was not substantially formed until 23% Ba loading. This showed the bulk carbonate transition occurred between Ba loading of 16-23%. The carbonate transition also coincided with the maximum NO_x uptake achieved, as well as the largest percentage of barium involved in NO_x storage. These findings were the first critical steps in understanding the types of barium involved

in the NO_x storage reaction and the functionality of the "high barium loading" NO_x storage catalyst.

Investigations of NO_x storage with Ba loading also identified various phases present in high Ba loading LNT's [27]. "Low temperature" (LT) and "high temperature" (HT) $BaCO_3$ species were identified via TPD. LT-$BaCO_3$ species were identified as the Ba species active for NO_x storage. TPD experiments showed decomposition and CO_2 desorption at temperatures below 800ºC for LT-$BaCO_3$. The LT Ba was only shown to form after 16 wt% loadings, above which HT-$BaCO_3$ was formed. HT-$BaCO_3$ was shown to be the non-participatory $BaCO_3$ species. While NO_x uptake experiments were not presented, the idea of multiple phases is important when investigating aging of LNT catalysts. Furthermore the concept that the bulk $BaCO_3$ does not participate in NO_x storage is important when analyzing degradation via XRD. An investigation into the effects of changes in barium loading on various supports including CeO_2, ZrO_2, and SiO_2 show a substantial effect on the barium phase present [28]. It was shown that increased support basicity resulted in increased LT-$BaCO_3$ formation at lower loadings. While the effects of CeO_2 addition will be discussed later, it is important to note that even in earlier investigations CeO_2 is found to have a positive effect on NO_x uptake.

Studies investigating thermal aging in air resulted in very little change in XRD spectra all the way up to 1000ºC with catalyst loading below 20 wt% Ba [29]. Both aging temperature and time had little effect on the Ba morphology where nearly all loaded Ba existed in the BaO form. When loading was increased to 20 wt%, significant $BaAl_2O_4$ (barium aluminate) formation was observed at temperatures as low as 800ºC. While this preliminary work does not include complex systems such as the addition of Pt in the catalyst formulation, and does not report on the

NO_x storage capacity of the affected catalyst, it suggests that mixed metal oxide formation can be a major issue for thermally aged LNT catalysts.

While groups have identified $BaAl_2O_4$ formation as a possible mechanism for thermal degradation of LNT catalysts, there still remains a number of possibilities for the deterioration of NO_x storage. Kim et al showed that while $BaAl_2O_4$ can occur at temperatures as low as 850ºC, the degradation in NO_x storage correlated more closely to platinum particle size [30]. A lack of Pt-Ba adjacency was identified as the major contributor to the degradation in NO_x storage. The degradation was also in part attributed to the deep oxidation that can occur on Pt particles aged in air at elevated temperatures. While these conclusions have merit based on the previously reported NO_x storage mechanism, to this point there has been no definitive investigation of the changing NO_x uptake profiles of thermally aged catalyst where the aging resulted in mixed metal oxide formation. Because long term NO_x uptake profiles show all three uptake regimes, the variation in uptake with storage regime will help elucidate which mechanism contributes the most to NO_x storage degradation.

The above literature review has shown barium is an effective catalyst for NO_x storage when loaded on a variety of substrates. Loading above 16 wt% is required to achieve high percentages of Ba active for NO_x uptake described as LT-$BaCO_3$. It has also been shown that thermal degradation of LNT catalyst in air can cause the formation of mixed metal oxides such as $BaAl_2O_4$ and some have debated whether the formation of the aluminate or the reduction in platinum particle size is the main reason for the reduction in NO_x storage performance. The mechanism of storage degradation is critical to effective implementation of LNT catalysts and, as such, has been a major focus of investigation within this dissertation

Literature has also shown that in comparison to Al_2O_3, CeO_2 supports are more likely to form mixed metal oxides under thermal aging in air and thermal aging has the potential to produce $BaCeO_2$ (barium cerates) at temperatures as low as 773K [31]. The following section will address the benefits associated with cerium addition including, promotion of platinum dispersion, increased NO_x storage capacity and increased sulfur tolerance in cycling environments.

2.4 Investigations of Cerium in LNT Catalysts

Cerium is an extremely common additive to TWC catalysts. It has been shown in low loadings to promote noble metal activity, but is most commonly used to increase oxygen storage capacity (OSC) of TWC's, as well as promote noble metal dispersion and has been most recently investigated for its use in applications for LNT catalysts [32, 33]. Ceria has the ability to uptake measurable quantities of NO_x in lean environments. Also ceria can facilitate the water gas shift (WGS) reaction to produce H_2 for help in desulfation, where barium has been shown to undergo deep sulfation in the form of $BaSO_4$ under moderate concentrations of sulfur in the model exhaust gas streams [34, 35]. Additional benefits of ceria during sulfation have been shown as ceria can serve as an alternate uptake site to prevent deep sulfation of the storage component. Where Kim et al. have reported reduction in BaS after regeneration when ceria is used as the catalyst support material [36]. Easterling et al confirmed the use of Ce as an additive reduces the effect of sulfur poising where low amounts of cerium addition were found to optimize NO_x storage both pre and post sulfur deactivation [37]. With the benefits to platinum reactivity identified in the previous section as well as the positive regeneration characteristics and NO_x storage uptake impacts, the addition of cerium in LNT catalysts has become attractive in recent years.

Damyanova et al. showed that Ce addition had a significant effect on Pt in the Pt/Al_2O_3 system for oxidation reactions [38]. H_2 uptake and oxidation reactivity in the presence of Ce were improved, however, the improvement was dependent upon ceria loading. Loading of 1 wt% Ce was found to be optimum for CH_4 and CO oxidation reactions. XPS studies showed that the OSC and electronic interaction with Pt caused particle oxidation to occur more readily with higher cerium loadings. Oxidation of Pt particles was identified as the reason for the reduction in catalytic activity at higher cerium loadings. This investigation, combined with the previous studies, showed that ceria impacts Pt particle size changes under sintering conditions through noble metal anchoring. This provides evidence that ceria can have positive effects on LNT catalysts. However, an optimum Ce loading exists where by oxidation promotion effects, OSC and NO_x storage benefits are optimized.

While there are positive effects identified with the addition of cerium in traditional LNT formulations, Casapu et al. found when comparing Pt/Ba catalysts supported on Al_2O_3 and CeO_2 that the alumina supported catalyst performed better in NO_x storage and regeneration activity [39]. The reduction in activity was attributed to decreased surface are of the CeO_2 support as well as an increase in the stable or HT-$BaCO_3$ form of the storage material. In the investigations reported previously on the LT-$BaCO_3$ /HT-$BaCO_3$ transition with barium loading, it is shown that transition from LT to HT-CO_3 occurs at lower loadings for CeO_2 supported LNT catalysts. Therefore, Ce does not have the same optimal Ba loading because of the rapid transition from LT to HT $BaCO_3$, this leads to difficulties when comparing the two support materials at identical loadings.

The impact of ceria on the morphology and NO_x storage characteristics of $aPt/Ba/Al_2O_3$ catalyst was studied by Infantes et al. [40]. The addition of Ce resulted in little to no observable

changes in the catalysts morphology. However, additional XPS measurements showed the Ce did affect the Pt-Al_2O_3 interaction. NO_x storage was shown to be promoted by the addition of Ce to the support. Reduction of stored NO_x was also shown to slightly increase where NO_x reduction favored the production of N_2 over NH_3 when compared to the Al_2O_3 only catalysts. The following study reports different results when comparing the addition of Ce to traditionally formulated catalysts. The lack of continuity illustrates the importance of continuing investigations into Ce addition, and the investigation of degradation mechanism has potential to further the understanding of the impacts of this important additive.

Say et al. shows the importance of thermal degradation and the effect of Ce addition are at the forefront of the current literature [41]. The authors report XRD spectra in-situ FT-IR and several other surface and bulk characterization techniques to compare Pt/BaO/Al_2O_3 catalysts to the Pt/BaO/CeO_2/Al_2O_3 catalysts. However, they find mixed metal oxide formation ($BaAl_2O_4$) begins for both Al_2O_3 an CeO_2/Al_2O_3 at the same calcination temperature 873K, this is in contrast to previous literature which show $BaAl_2O_4$ is observed to form at lower calcination temperatures with cerium addition [31]. This may be due to the higher Ce loadings used in the Say investigations where Ce loadings generally vary from 1-5wt% due to the observed reduction in catalytic benefits from higher loadings that have been reported. The authors report the only benefit to Ce addition in the current investigation is the promotion of NO_x reduction and selectivity to N_2 over NH_3.

2.5 Summary

While many authors attempt to connect surface morphology and adsorbed species to changes under thermal aging, they often do not report NO oxidation or NO_x storage data for any

of the catalysts given. Conversely, those that report on catalytic activity changes with catalyst formulation or aging, do not connect the observed changes to catalyst characterization. This is an important gap in the reported literature and must be addressed for effective LNT implementation. Investigations of degradation effects on NO oxidation, and NO_x storage, with constant reaction conditions, catalysts loadings, and preparation conditions as a standalone study is important to advance current literature in the $Pt/Ba/CeO_2/Al_2O_3$ arena. Those studies coupled with a comprehensive investigation of Pt/Al_2O_3, $Pt/Ba/Al_2O_3$ and $Pt/Ba/CeO_2/Al_2O_3$ catalysts using the same conditions for operation and aging is required to further the understanding of the addition of these components in the LNT catalysts system. Furthermore, the studies of long term uptake, while not fully representative of the rapid cycling LNT system, have significant merit as tools in understanding uptake mechanism and interactions with the multiple adsorption sites associated with the high Ba loading LNT catalysts. As such, the following work presents investigations of lean phase operation after inflicted thermal degradation for a range of LNT catalysts. An understanding of thermal degradation in the Pt/Al_2O_3 catalyst system has been applied to adaptive kinetic modeling. The study of the effects of thermal degradation in NO oxidation has been extended to the fully formulated catalyst systems $Pt/Ba/Al_2O_3$ and $Pt/Ba/Ce/Al_2O_3$. The effects of thermal degradation of $Pt/Ba/CeO_2$ was then extended to NO_x storage, where long term NO_x uptake profiles have been connected to both bulk and surface properties as thermal aging is induced. Finally, the established experimental set-up has been employed to investigate a Pt-free LNT catalyst for stability, NO_x storage, and reduction capacity in the lean/rich cycling LNT system.

2.6 Reference

1. Miyoshi, N., et al., *Development of new concept three-way catalyst for automotive lean-burn engines*. 1995, SAE Technical Paper.
2. Dawody, J., et al., *Role of Pt-precursor on the Performance of Pt/BaCO3/Al2O3.NOx Storage Catalysts.* Journal of Molecular Catalysis A: Chemical, 2005. **225**: p. 259-269.
3. Epling, W., et al., *Overview of the Fundamental Reactions and Degradation Mechanism of NOx Storage/Reduction Catalysts.* Catalysis Reviews, 2004. **46**(2): p. 163-245.
4. Hauff, K., et al., *Reaction Kinetics of Aged NO x Storage Catalysts.* Industrial & Engineering Chemistry Research, 2013. **52**(25): p. 8399-8409.
5. Nguyen, H., M.P. Harold, and D. Luss, *Spatiotemporal behavior of Pt/Rh/CeO 2/BaO catalyst during lean–rich cycling.* Chemical Engineering Journal, 2015. **262**: p. 464-477.
6. Takahashi, N., et al., *The new concept 3-way catalyst for automotive lean-burn engine: NOx storage and reduction catalyst.* Catalysis Today, 1996. **27**(1–2): p. 63-69.
7. E. Xue, K.S., J. Ross, *Roles of support, Pt loading and Pt dispersion in the oxidation of NO to NO2 and of SO to SO2.* Applied Catalysis B, 1996. **11**: p. 65-79.
8. Lee, J.-H. and H. Kung, *Effect of Pt dispersion on the reduction of NO by propene over alumina-supported Pt catalysts under lean-burn conditions. .* Catalysis Letters, 1998. **51**(1): p. 1-4.
9. Olsson, L., et al., *A Kinetic study of Oxygen adsorpion/desorption and NO oxidation over Pt/Alumina catalysts.* J. Physical Chemistry, 1999. **103**: p. 10433-10439.
10. Huang, H.Y., R.Q. Long, and R.T. Yang, *The Promoting Role of Noble Metals on NOx Storage Catalyst and Mechanistic Study of NOx Storage under Lean-Burn Conditions.* Energy & Fuels, 2001. **15**(1): p. 205-213.
11. Salasc, S., M. Skoglundh, and E. Fridell, *A comparison between Pt and Pd in NOx storage catalysts.* Applied Catalysis B: Environmental, 2002. **36**(2): p. 145-160.
12. Olsson, L. and E. Fridell, *The influence of Pt oxide formation and Pt dispersion on the reactions NO2 <-> NO+1/2 O-2 over Pt/Al2O3 and Pt/BaO/Al2O3.* Journal of Catalysis, 2002. **210**(2): p. 340-353.
13. Despres, J., et al., *Catalytic oxidation of nitrogen monoxide over Pt/SiO 2.* Applied Catalysis B: Environmental, 2004. **50**(2): p. 73-82.
14. Mulla, S., et al., *Reaction of NO and O 2 to NO 2 on Pt: Kinetics and catalyst deactivation.* Journal of Catalysis, 2006. **241**(2): p. 389-399.
15. Hauptmann, W., et al., *Inverse hysteresis during the NO oxidation on Pt under lean conditions.* Applied Catalysis B: Environmental, 2009. **93**(1): p. 22-29.
16. Bradley Shumbera, R., H.H. Kan, and J.F. Weaver, *Oxidation of Pt(1 0 0)-hex-R0.7° by gas-phase oxygen atoms.* Surface Science, 2007. **601**(1): p. 235-246.
17. Weaver, J.F., J.-J. Chen, and A.L. Gerrard, *Oxidation of Pt(1 1 1) by gas-phase oxygen atoms.* Surface Science, 2005. **592**(1–3): p. 83-103.
18. Smeltz, A.D., W.N. Delgass, and F.H. Ribeiro, *Oxidation of NO with O2 on Pt (111) and Pt (321) Large Single Crystals†.* Langmuir, 2010. **26**(21): p. 16578-16588.
19. Auvray, X., et al., *The effect gas composition during thermal aging on the dispersion and NO oxidation activity over Pt/Al2O3 catalysts.* Applied Catalysis B-Environmental, 2013. **129**: p. 517-527.
20. Mahzoul, H., J. Brilhac, and P. Gilot, *Experimental and mechanistic study of NOx adsorption over NOx trap catalysts.* Applied Catalysis B: Environmental, 1999. **20**(1): p. 47-55.
21. Fridell, E., et al., *The mechanism for NOx storage.* Catalysis Letters, 2000. **66**(1-2): p. 71-74.
22. Westerberg, B. and E. Fridell, *A transient FTIR study of species formed during NOx storage in the Pt/BaO/Al2O3 system.* Journal of Molecular Catalysis A: Chemical, 2001. **165**(1–2): p. 249-263.

23. Lietti, L., et al., *NO x Storage Reduction over Pt □ Ba/γ-Al 2 O 3 Catalyst.* Journal of catalysis, 2001. **204**(1): p. 175-191.
24. Cant, N.W. and M.J. Patterson, *The storage of nitrogen oxides on alumina-supported barium oxide.* Catalysis Today, 2002. **73**(3): p. 271-278.
25. Epling, W.S., et al., *Further evidence of multiple NO x sorption sites on NO x storage/reduction catalysts.* Catalysis Today, 2004. **96**(1): p. 21-30.
26. Castoldi, L., et al., *Study of the effect of Ba loading for catalytic activity of Pt–Ba/Al 2 O 3 model catalysts.* Catalysis Today, 2004. **96**(1): p. 43-52.
27. Piacentini, M., M. Maciejewski, and A. Baiker, *Pt-Ba/alumina NO x storage-reduction catalysts: Effect of Ba-loading on build-up, stability and reactivity of Ba-containing phases.* Applied Catalysis B: Environmental, 2005. **59**(3): p. 187-195.
28. Piacentini, M., M. Maciejewski, and A. Baiker, *Supported Pt-Ba NO x storage-reduction catalysts: Influence of support and Ba loading on stability and storage efficiency of Ba-containing species.* Applied Catalysis B: Environmental, 2006. **66**(1): p. 126-136.
29. Szailer, T., et al., *Effects of Ba loading and calcination temperature on BaAl 2 O 4 formation for BaO/Al 2 O 3 NO x storage and reduction catalysts.* Catalysis today, 2006. **114**(1): p. 86-93.
30. Kim, D.H., et al., *Relationship of Pt Particle Size to the NO x Storage Performance of Thermally Aged Pt/BaO/Al2O3 Lean NO x Trap Catalysts.* Industrial & engineering chemistry research, 2006. **45**(26): p. 8815-8821.
31. Casapu, M., et al., *Formation and stability of barium aluminate and cerate in NO x storage-reduction catalysts.* Applied Catalysis B: Environmental, 2006. **63**(3): p. 232-242.
32. Koltsakis, G. and A. Stamatelos, *Catalytic Automotive Exhaust Aftertreatment.* Progress in Energy and Combustion Science, 1997. **23**(1): p. 1-39.
33. Kašpar, J., P. Fornasiero, and M. Graziani, *Use of CeO2-based oxides in the three-way catalysis.* Catalysis Today, 1999. **50**(2): p. 285-298.
34. Rohart, E., et al., *Ceria-Based Materials for DeNOx Catalysts Efficient at Low Temperature and with Improved Sulphur Tolerance*. 2008, SAE Technical Paper.
35. Ji, Y., T.J. Toops, and M. Crocker, *Effect of Ceria on the Sulfation and Desulfation Characteristics of a Model Lean NO x Trap Catalyst.* Catalysis letters, 2009. **127**(1-2): p. 55-62.
36. Kim, D.H., et al., *Characteristics of Desulfation Behavior for Presulfated Pt-BaO/CeO2 Lean NOx Trap Catalyst: The Role of the CeO2 Support.* The Journal of Physical Chemistry C, 2009. **113**(50): p. 21123-21129.
37. Easterling, V., et al., *Effect of ceria on the desulfation characteristics of model lean NO x trap catalysts.* Catalysis Today, 2010. **151**(3): p. 338-346.
38. Damyanova, S. and J.M.C. Bueno, *Effect of CeO2 loading on the surface and catalytic behaviors of CeO2-Al2O3-supported Pt catalysts.* Applied Catalysis A: General, 2003. **253**(1): p. 135-150.
39. Casapu, M., et al., *Comparative study of structural properties and NO x storage-reduction behavior of Pt/Ba/CeO 2 and Pt/Ba/Al 2 O 3.* Applied Catalysis B: Environmental, 2008. **78**(3): p. 288-300.
40. Infantes-Molina, A., et al., *Characterization and reactivity of Ce-promoted PtBa lean NOx trap catalysts.* Catalysis Today, 2012. **197**(1): p. 178-189.
41. Say, Z., et al., *Influence of ceria on the NOx reduction performance of NOx storage reduction catalysts.* Applied Catalysis B: Environmental, 2013. **142–143**: p. 89-100.

Chapter 3: Materials and Methods

The following chapter outlines the materials and methods used in the production and analysis of the LNT degradation studies. The chapter will cover catalyst production methods, reactor set-up including system design and data acquisition, as well as reaction conditions for all three of the major reaction chapters. Reaction conditions will be described for NO oxidation, NO_x storage, and Lean/Rich cycling. The first section covered will be catalyst production methods.

3.1 Catalyst production

Catalysts have been produced via the incipient wetness impregnation method. The amount of catalyst precursor was measured for the desired catalysts loading and dissolved in deionized (DI) water. The water volume was measured to precisely the pore volume of the material to be impregnated. In the case of multiple impregnation steps BET was used to determine the pore volume of intermediate catalysts loading steps. For the three catalysts, produced, the loading weight ratios can be found in Table 3-1.

Table 3-1: list of catalysts names formulation and weight ratio of loading

Catalyst Name	Formulation	Weight Ratio
PA	Pt/Al_2O_3	1/100
PBA	$Pt/Ba/Al_2O_3$	1/20/100
PBCA	$Pt/Ba/CeO_2/Al_2O_3$	1/20/5/100

The catalyst precursor and support material were kept consistent for each of the alumina supported catalysts. All precursors were loaded on a high surface area γ-Al_2O_3 support provide by Strem Chemicals (97%). The precursor salts for each of the loaded metals were platinum diammine nitrite (Strem Chemicals 5 wt% in ammonium hydroxide), barium acetate (Strem Chemicals 99%), and cerium nitrate (Strem Chemicals 99.9%). In the case of barium impregnation, multiple impregnation steps were required to achieve the weight loading necessary. Barium acetate was used in place of the more common precursor barium nitrate due to its higher solubility in DI water. The barium acetate precursor also allowed for a reduction in the number of successive impregnation steps required for barium impregnation.

When successive impregnation was required (both the PBA and PBCA catalysts), separate production conditions were used for the catalyst prepared for NO oxidation experiments (condition 1) and for the NO_x storage experiments (condition 2). The preparation sequence can be found in Table 3-2. Thermal aging has been conducted in a Thermolyne 46100 high temperature furnace equipped with a Eurotherm 2408 temperature controller. All aging steps were conducted with a 1ºC/min ramp rate to the specified aging temperature and held for 8 hours under stagnant air.

Table 3-2: Impregnation steps for conditions 1 and 2

Condition 1	Condition 2
Cerium impregnation (PBCA only)	Cerium impregnation (PBCA only)
Drying 120ºC for 24hr	Drying 120ºC for 24hr
Sintering in stagnant air 800ºC for 8hr	Sintering in stagnant air 500ºC for 8hr
Barium impregnation	Barium impregnation

Drying 120ºC for 24hr	Drying 120ºC for 24hr
Sintering in stagnant air 800ºC for 8hr (repeat to desired barium loading)	Sintering in stagnant air 500ºC for 8hr (repeat to desired barium loading)
Platinum impregnation	Platinum impregnation
Drying 120ºC for 24hr	Drying 120ºC for 24hr
Aging at varying temperatures (500-800ºC)	Aging at varying temperatures (500-800ºC)

For the perovskite production, the EDTA/Citrate complexation method was used. Precursor salts and complexation material are as follows: lanthanum nitrate (Strem Chemicals 99.9%), strontium nitrate (Strem Chemicals 99+%), cobalt nitrate (Strem Chemicals 99%), citric acid (Alfa Aesar 99%), ethylene diaminetetraacidic Acid (EDTA) (Strem Chemicals 99.4%). EDTA was dissolved in an ammonia solution (28-30 wt%) at 70ºC. The citric acid was then added to the EDTA-NH_3-H_2O solution followed by the metal nitrates in the correct ratios, to generate a perovskite of the form $La_{.8}Sr_{.2}CoO_x$. EDTA, citric acid, and metal nitrates were added in a 1-1-1.5 molar ratio. pH was measured by a Fischer Scientific pH/Ion 510 bench pH meter. The solution pH was adjusted to a pH of 8 via the addition of additional ammonia solution. The solution was then evaporated down to a gel with stirring and continuous heating at 70ºC. The gel was then dried further in a muffle furnace at 120ºC for 24 hours and the black precursor material was obtained. The precursor was then calcined at 800ºC for 8 hours with a 1ºC/min ramp rate to obtain the perovskite material. The perovskite material was than ground and sieved to <50μm particle size.

3.2 Catalyst characterization

A number of catalyst characterization techniques have been employed to measure catalyst reactivity and morphology. The techniques described in this section are those broad heterogeneous catalysis characterization techniques employed to characterize the LNT catalysts. Techniques which are specific to NO_x catalysts, such as NO_x storage and NO oxidation, will be described in the reactor design and set-up sections.

3.2.1 CO chemisorption/TPR

CO – chemisorption, and hydrogen temperature programed reduction (H_2 – TPR) experiments were conducted using an Autochem 2910 equipped with thermal conductivity detector (TCD). CO pulsed experiments were conducted using a 0.247ml injection loop employing 10.05% CO in Ar. CO was pulsed over the sample and outlet concentration was measured via TCD. Pulses were continued until the sample was saturated (defined as three consecutive pulses with identical peak areas). Pt particle size was calculated based upon the amount of CO adsorbed to the sample. A CO-Pt ratio of 1-1 was used and the assumption of hemispherical particles. H_2 – TPR was conducted prior to CO-chemisorption, where 5% H_2 in Ar was passed over the catalyst as temperature was ramped at a rate of 5ºC/min. Changes in H_2 concentration with temperature were measured by the TCD detector and output to the peak analysis software.

3.2.2 Scanning Electron Mircoscopy (SEM) and Transmission Electron Microscopy (TEM)

All imaging of LNT catalysts was performed by the Microscopy and Analytical Imaging (MAI) Laboratory at the University of Kansas. Imaging was conducting by a Carl Zeiss Leo 1550 field emission scanning electron microscope (High vacuum with a schottky field emitter operating at voltages from 200V to 30kV) and an FEI Tecnai F20 XT transmission electron

microscope (200kV electron source – Schottky field emitter, with high tension values of 20, 40, 80, 120, 160 and 200kV). In the case of PBCA catalysts, it was not possible to determine Pt particles size through CO chemisorption due to cerium uptake of CO; Hence Pt particle size was estimated by an average of observed Pt particles under TEM.

3.2.3 Fourier transform infrared spectroscopy (FT-IR)

FT-IR spectra of the used NO_x storage catalysts were collected on a Varian 600 series equipped with a GladiATR^{TM} from PIKE technologies operated at a constant temperature of 105ºC. Measured absorbance spectra were taken as the average of 254 consecutive scans collected from 500 to 4000 cm^{-1} with a resolution sensitivity of 8 cm^{-1} and 4 cm^{-1}, at the respective ends of the absorbance measured.

3.2.4 Brunauer-Emmett-Teller (BET) analysis

BET analysis was conducted on a Quantachrome NOVA 2200e. Samples were degassed under vacuum at 120ºC for one hour. A seven point adsorption isotherm was measured from 0 kPa to ambient at liquid nitrogen temperatures (77K) to determine catalyst surface area in m^2/g.

3.3 Quartz tube reactor system

The reactor system was fed by pure component gases provide by Matheson. The gases used in the mixing system consisted of argon (HP). Reductant gases consisted of 5.00% H_2 in argon or 5.00% CO_2/.90% CO/2.10% H_2 in argon, 1000 PPM NO in argon, and either 10% O_2 in argon or 10.00% O_2 /10.00% CO_2 in argon. The percentage of each component in the reaction gas will be specified in the experimental section for each of the NO_x experiments later in the chapter. The gases were then sent to a ¼ inch stainless steel mixing system shown in Figure 3-1.

After the mixing system in Figure 3-1, the reactant gas was sent to a two position, 6-way switching valve (Valco Instrument Company Incorporated). The 6-way actuator was connected to a USB computer interface emulating a COM port. The COM port emulation was linked to a Labview program "6-way switching valve" capable of manual switching as well as timed switching modes, where the switch timings are variable in any increment of one second. Smaller switching windows are achievable but have not been implemented.

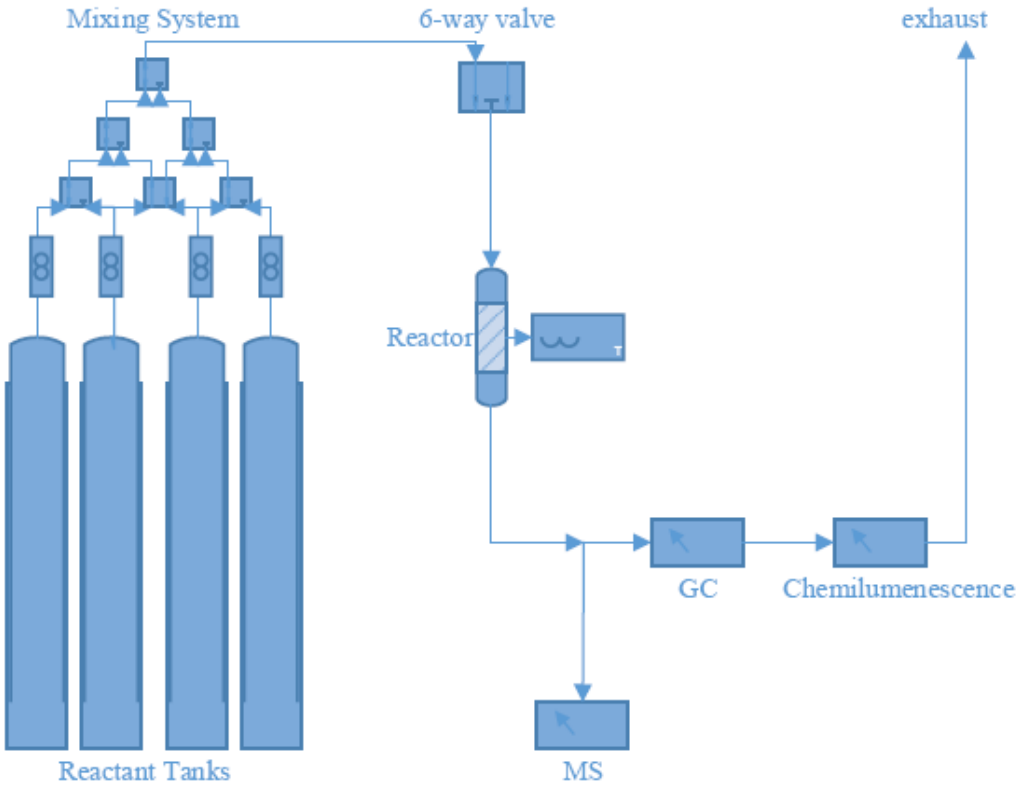

Figure 3-1: Outline of full quartz tube reactor system set-up

After passing through the 6-way valve the gas enters the quartz tube reactor system shown in Figure 3-2. The reactor temperature was controlled by an Omega CN6000 PID

controller connected to a K-type thermocouple inserted directly adjacent to the catalyst bed within the heating zone. The controller was used to control a ceramic resistive heating furnace. Reactor inlets were wrapped in resistive heating tap and continuously heated above 100ºC when water was present in the inlet gas. Water was added to the inlet gas by a Kent Scientific genie plus syringe pump. The syringe pump used a 1ml Hamilton gas tight syringe with a 4.61mm ID syringe body. The catalyst bed consisted of the required amount of catalytic material inserted in a 12.75mm OD (10.5mm ID) quartz tube held in place by quartz wool plugs inserted into both the top and bottom of the quartz tube reactor system. The catalyst was further stabilized in place by use of an internal quartz tube "prop" sized to hold the reactor bed up directly in the center of the resistive heating furnace heating area. The catalyst bed length of 2 cm and reactor tube ID of 10.5mm, coupled with the required reactant gas flow rate of >450 ml/min, achieved a resonance time of 40,000 hr^{-1} for NO_x storage and lean rich cycling experiments. For NO oxidation experiments gaseous flow rates were 260 ml/min which resulted in a resonance time of 59,000 hr^{-1}.

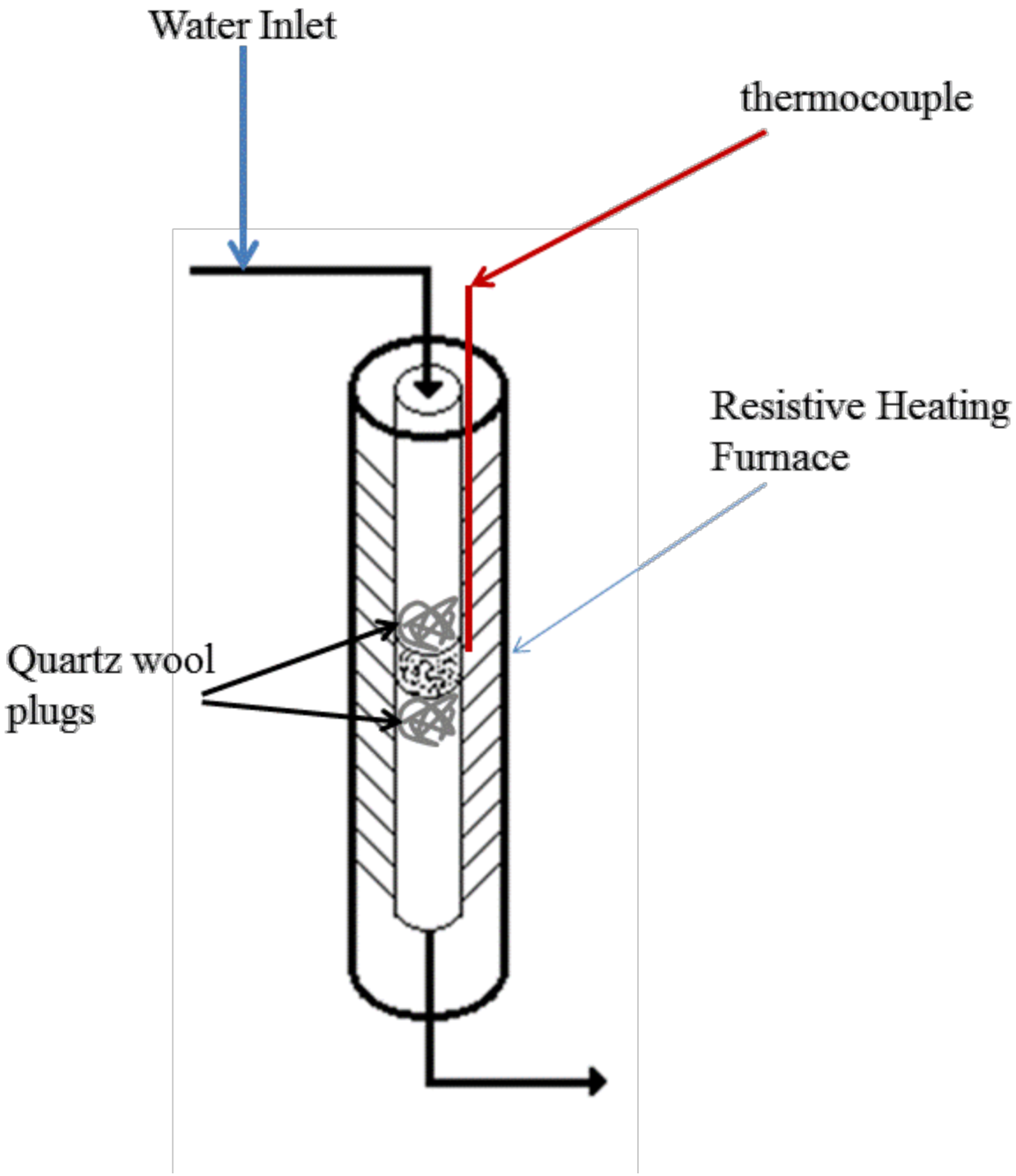

Figure 3-2: Quartz tube reactor system

The outlet of the reaction system was sent to a chemiluminescence detector HCLD600 series from California Analytical Instruments. It is possible to measure NO_x in the range of 0-3000 PPM and the current analyzer has been factory calibrated for the 0-1000 PPM range. The

chemiluminescence detector is capable of operating in three modes: NO_x, NO, or NO/NO_x switching mode. NO and NO_x mode are continuous sampling modes. NO mode measured NO by reacting inlet NO with ozone which produces light. The luminescence is detected and reported as a PPM value based on calibration. In NO_x mode, the inlet gas is sent over a catalyst to reduce NO_2 to NO and the reduced NO_2 and remaining NO are measured. Because the NO_2 has been pre-reduced, the measurement represents the total NO_x in the measured gas stream. Switching mode allows the device to measure both NO and NO_x over ten second intervals. The difference between total NO_x and NO is NO_2. Therefore, switching mode is capable of measuring $NO/NO_2/NO_x$. The limitation of switching mode is the individual component measurements are taken over 10 second intervals, and each NO_x measurement is taken only every ten seconds.

The detector outputs NO_x concentration measurements as voltages in the range of 0-10 volts where the variation in voltage is linearly dependent upon the PPM value. The voltages are read by a National Instruments NI-1620 16 Input Data Acquisition (DAQ) module and relayed to the laboratory computer via USB output. The data is read into Labview via the DAQmx Labview drivers. The program "NOx Data Acquisition" acquires the voltage measurements and uses a calibration to translate voltages into PPM values. The PPM values are then sent to a GUI and saved to assigned files names.

3.4 NO Oxidation Conditions

After the catalyst was initially loaded into the quartz tube reactor the system, the catalyst was heated to 400ºC in Ar and reduced for 15 minutes in 5% H_2/Ar. The reactor was then cooled to 50ºC in Ar and re-heated to the starting temperature for the isothermal NO oxidation reactions at 200ºC. The system was held at each NO oxidation temperature for 1 hr. After 1 hr, the

reaction temperature was increased by 50ºC at a rate of 5ºC/min to the next reaction temperature. This was continued at each reaction temperature up to the maximum measured temperature of 500ºC.

$$NO\ conversion = \frac{(Average\ NO_x\ outlet\ concentration) - (Average\ NO\ outlet)}{Average\ NO_x\ outlet\ concentration} \quad 3.1$$

NO conversion is calculated by averaging the final 10 minutes of NO and Total NO_x concentration at each of the isothermal NO oxidation temperatures. NO average is then subtracted from the total NO_x outlet and divided by average total NO_x. The reaction conditions for NO oxidation were 608 PPM NO/3.7% O_2 in argon with the residence time of 59,000hr^{-1}.

3.5 NO_x Storage Conditions

NO_x storage experiments were conduct in the quartz tube reactor system previously described. For the lean NO_x storage experiments, gas concentrations consisted of 577 PPM NO/4.7%O_2/4.7%CO_2 with the remainder argon. The NO_x inlet step change was facilitated by a switching program controlling the two position 6-way valve located inline directly prior to the quartz tube/reactor bed system. Total NO_x storage was calculated by calculating the difference between the step change inlet and measured NO_x outlet and integrating over the time of operation. NO_x storage calculation is given by

$$NO_x\ storage = \int (NO_x inlet - NO_x\ outlet)dt \quad 3.2$$

Further separation of the data was conducted by separating the uptake measurements into three distinct regimes described in Table 3-3:

Table 3-3: Defines integration conditions for total NO_x uptake in each of the three operating regimes

Regime	NO_x Outlet Condition
Complete Uptake	Outlet < 3ppm
Rapid Uptake	3ppm< Outlet Concentration Change averages < 0.1ppm over 10 seconds
Diffusive Uptake	Outlet > all time greater than the rapid uptake condition

3.6 Lean/Rich oscillating reaction conditions

Cycling experiments have been conducted using the cycling program and the two position 6-way valve described above. Cycling operation consisted of three minutes of lean phase and one minute of rich phase. Gas compositions and space velocities for each phase are given in Table 3-4.

Table 3-4: lean/rich cycling gas compositions

Gas	Lean	Rich
H_2	-	2.1%
CO	-	0.9%
NO	577PPM	-
CO_2	4.7%	5.0%
H_2O	5.0%	10.0%
Space Velocity	40,000 hr^{-1}	58,000 hr^{-1}

Cycling experiments were conducted at a constant 350ºC with no prior catalyst reduction. In contrast to the continuous NO_x measurements taken for the previous two reactions, NO_x

measurements were taken in cycling mode. As a result, NO/NO_2 and total NO_x were measured during cycling. Due to time delay of measurement, real time NO_x measurements are used to compare NO_x uptake and reduction to the inlet compositions.

Table 3-4 shows there is a difference in space velocity between lean and rich operating conditions. Discontinuous residence times are not representative of real world LNT conditions and should be addressed for future work. The difference is due to the capabilities of the gas mixing system and number of available mass flow controllers. For future work, it is suggested that an additional mass flow controller be added for mixing the rich phase gas stream. The additional controller would allow the mass flow of both the lean and rich streams to be equal resulting in more representative residence times.

Chapter 4: NO Oxidation Experimental and Modeling

The following chapter is a complete publication that has been submitted for review in *Reaction Kinetics, Mechanisms and Catalysis*. As this publication is a combination of multiple authors' efforts, this paragraph briefly outlines my contribution to the work. As the first author of the publication, I have contributed in both the modeling and data sections of the work. I produced all of the steady state isothermal NO oxidation data used for calibration of the model as well as for comparison of the models' validity over the range of temperatures and noble metal particle sizes measured. I conducted all of the aging and characterization experiments including, CO-chemisorption, TEM/EDAX, and BET surface area analysis. I contributed to the global rate expression development, as well as the literature review associated with the model development and developed the expressions for variation of desorption activation energy and oxygen adsorption activation energy for inclusion in the global kinetic model. Finally, I developed the discussion relating the model performance relative to the produced data and contributed to the conclusions established based on model performance development and application.

4.1 Abstract

The oxidation of nitric oxide (NO) is a critical step in the operation of Lean NO_x Trap (LNT) catalysts; hence, it is important to understand the fundamental reaction mechanism. An understanding of the detail reaction mechanism allows for determination of an appropriate global reaction rate expression for numerical simulation efforts in the automotive field. This work succinctly reviews the literature in this area and derives a global expression for NO oxidation from stoichiometry using the detailed reactions steps. In this version, the parameters used to simulate the global expression are derived from the kinetic theory of gases and the detailed study of each NO reaction step; ensuring the correct functional dependency of each reaction parameter. Moreover, the global model is adapted to simulate different surface morphologies. The effect of temperature and surface changes (dispersion, particle size) are included while determining the parameters, so that the same variables can be effectively used over wide range of LNT catalysts. This work summarizes the literature of experimental NO oxidation findings in terms of surface coverage, species concentration dependency, and temperature variation. Finally, the authors verify the global model by simulating experimental data obtained for different particle size catalysts. As a result, the adaptive global model predicts NO oxidation conversion with varying surface morphologies with greater than 93% accuracy of the experimental data taken.

4.2 Introduction

In today's society, there is a significant need to decrease fuel consumption while reducing dependency on fossil fuels. This has led to an increase in demand for compression ignition (CI) and gasoline direct injected (GDI) engines because of their increased fuel economy relative to stoichiometric engines. However, current and future regulations on nitrogen oxides (NO_x) emissions are particularly challenging to meet, for these lean-burning engines [1-4]. Under the

traditional stoichiometric operating conditions of a port fuel injected gasoline engine, carbon monoxide (CO), hydrogen (H_2) and hydrocarbon (HC) emissions exist in sufficient quantities to reduce NO_x emissions from the engine over a traditional three way catalyst (TWC). However, the lean exhaust of CI and GDI engines contains mainly oxygen (O_2) and nitrogen monoxide (NO) without any other reducing species in adequate amounts to react over the TWC. Since NO_x decomposition is difficult to facilitate in oxygen rich environments, a low cost solution for conversion of NO_x to N_2 and O_2 is required.

In order to overcome this issue, various indirect catalyst approaches have been studied for NO_x reduction. The most common approaches are through Selective Catalytic Reduction (SCR) and Lean NO_x Traps (LNTs). While SCR devices have largely become the automotive industry standard, the prospect of LNTs operating without a secondary fueling infrastructure (i.e., Diesel Exhaust Fluid) make them an attractive option. LNTs operate in two phases; a lean phase is used for storing NO_x, whereas a rich phase provides regeneration of the catalyst to reduce the stored NO_x. Since LNTs prefer the storage of nitrogen dioxide (NO_2) as compared to NO, the oxidation of NO is a critical step during LNT operation [5-7].

Even though LNTs are commercially produced, one can still improve their operation by reducing the amount of precious metals while increasing their NO_x conversion. In this area, various researchers have investigated NO oxidation over Pt/γ-alumina catalysts while describing detailed and global reaction mechanisms [7-20]. However, while review of the NO oxidation mechanism has been accomplished [12, 21], further depth and understanding is needed. Hence, this work summarizes the literature findings for the detailed reaction mechanism. Moreover, only a few papers discuss the global reaction mechanism for NO oxidation [7, 13, 14, 22-25]. This kinetic modeling option is a definite need in the automotive industry for computationally fast

catalyst simulation tools [26]. While some efforts use a power law expression, only Bhatia et al. provided a global mechanism for NO oxidation and modeled the system using the same reaction rate expression [25]. The following global reaction rate derivation differs from the Bhatia version as it takes NO oxidation as written in equation (1). The half order oxygen reaction rate dependence has been shown by a number of groups [27-30]. A simplified overall reaction rate expression based upon this global reaction by Sampara et al achieved acceptable results modeling NO oxidation for diesel oxidation catalysts (DOC)[30]:

$$NO + 0.5O_2 \underset{k_{-1}}{\overset{k_1}{\rightleftarrows}} NO_2 \qquad (4.1)$$

There is no consensus in the literature with respect to the various parameters to be used in the reaction mechanism, such as surface coverage of O_2 and NO_2, or how the various parameters might change with temperature or catalyst surface properties (e.g., dispersion or particle size). As a result, this work aims to fill in the gaps in the literature by providing experimental conversion data for catalysts with different dispersion and particle sizes at the same reaction conditions (ie space time, oxygen, and NO concentrations) along with a global reaction rate expression and corresponding parameter values. Finally, a novel approach to simulated aging within the global kinetic frame work is established wherein noble metal particle size and reaction temperatures are used to described changes in the catalyst surface and atomic surface coverages resulting from the aforementioned thermal aging and operating temperature variation.

This adaptive approach for determining parameters expands the use of a global reaction rate expression for different catalyst morphologies, and aging conditions [31, 32]. Furthermore, these values were derived from catalyst fundamentals, resulting in parameter changes that can be interpreted based upon the observed physical changes. Of note, both experimental and simulation efforts were performed in the absence of additional species like water and carbon dioxide in

order to focus on the main goal of an NO oxidation study. First, in order to understand NO oxidation in more detail, a succinct historical account is provided.

4.3 Historical Review

Work on NO oxidation began in the 1980's and it has undergone substantial research since then [33, 34]. The reaction was found to be equilibrium limited with NO_2 production peaking around 623 to 643K [10, 12]. This presence of NO_2 inhibits the reaction [23] and it was found that the rate is structure sensitive; it rises with an increase in platinum particle size (i.e., a decrease in Pt dispersion) [10, 12, 35, 36]. In addition, the NO oxidation rate will increase with platinum loading up to 2-4% [37]. Finally, there is no definitive consensus in the literature on whether the reaction follows a Langmuir Hinshelwood (L-H) or Eley-Rideal (E-R) reaction mechanism [7, 8, 11-15, 22, 23, 25].

With respect to the individual steps of the detailed mechanism, NO adsorbs molecularly on the platinum particle with nitrogen attaching to the platinum and its dissociation is substantially reduced in presence of oxygen [38-40]. Both oxygen and nitrogen dioxide adsorb dissociatively on platinum within the range of reaction temperatures studied [41, 42]. Nitrogen dioxide is a strong sintering agent as compared to NO, which in turn is stronger than oxygen [43]. Oxygen tends to desorb above 650K and desorption temperature decreases with increased platinum particle size. On the other hand, surface coverage of oxygen increases with temperature from 300 to 650K [41]. Nearly all researchers agree on the following steps of NO oxidation given below.

$$NO + Pt \underset{k_{-2}}{\overset{k_2}{\rightleftarrows}} Pt \cdot NO \qquad (4.2)$$

$$\frac{1}{2}O_2 + Pt \underset{k_{-3}}{\overset{k_3}{\rightleftarrows}} Pt \cdot O \quad (4.3)$$

$$Pt \cdot NO + Pt \cdot O \underset{k_{-4}}{\overset{k_4}{\rightleftarrows}} Pt \cdot NO_2 + Pt \quad (4.4)$$

$$Pt \cdot NO_2 \underset{k_5}{\overset{k_{-5}}{\rightleftarrows}} NO_2 + Pt \quad (4.5)$$

.

Although, there is debate in literature with respect to the L-H or the E-R reaction mechanism, in this effort the authors observe that L-H is the preferred method for NO oxidation over the E-R mechanism [7, 44]. This is because NO_2 requires two sites to dissociate; hence, the forward reaction of NO oxidation should follow accordingly [7, 10, 39]. In addition, the literature suggests that surface coverage of both NO and oxygen contribute to variations observed in the NO oxidation rate, further suggesting the L-H pathway [10, 14, 25, 28]. Finally, most researchers working in the field of NO oxidation and storage support the same pathway for generation of the global reaction rate expression [12, 14-16, 18, 19, 22, 25, 28].

Based upon the presented detailed reaction mechanism, the global reaction mechanism is developed in a latter part of this paper. In order to calibrate the kinetic parameters of this global mechanism, a Pt/γ-alumina catalyst was prepared and packed bed experiments were conducted.

4.4 Nomenclature

Variable	Description	Units
A	Adsorption pre-exponential	[atm^{-1}]
A_{Pt}	Area of platinum site	[m^2 $site^{-1}$]
α	Constant of calibration	[-]
β	Constant of calibration	[-]
$\overline{C}$	Molar species concentration	[mol m^{-3}]
d	Particle size	[nm]
D	Gas diffusivity	[m^2 s^{-1}]
E	Activation energy	[J mol^{-1}]
G_a	Geometric surface area per	[m^2 m^{-3}]

	unit volume	
G_{ca}	Catalytic surface area per unit volume	[m^2 m^{-3}]
$\bar{h}$	Molar specific enthalpy	[J mol^{-1}]
ΔH	Heat of adsorption	[J mol^{-1}]
k	Reaction kinetics pre-exponential	[mol m^{-2} s^{-1}]
K	Adsorption equilibrium	[atm^{-1}]
m_a	Mass of molecule	[kg]
N_A	Avogadro's number (6.02214179×10^{23})	[mol^{-1}]
ν	Frequency of collision	[s^{-1}]
$Pt \cdot O$	Adsorbed atomic oxygen on platinum	[-]
$Pt \cdot NO$	Adsorbed NO on platinum	[-]
$Pt \cdot NO_2$	Adsorbed NO_2 on platinum	[-]
p	Pressure	[atm]
r	Forward or reverse reaction rate	[varies]
$\bar{R}$	Molar gaseous reaction rate	[mol m^{-2} s^{-1}]
R_u	Universal gas constant	[J mol^{-1} K^{-1}]
S	Sticking coefficient	[-]
S^0	Initial sticking coefficient	[-]

4.5 Experimental

4.5.1 Catalyst samples:

High surface area γ-alumina (Strem Chemicals) was conditioned by sintering at 1073K for 24 hours and sieved to a particle size <100 μm. The conditioned γ-alumina was impregnated with an aqueous solution of the Pt precursor (platinum diammine nitrite 5 wt% in ammonia hydroxide, Strem Chemicals). Catalysts were produced using the incipient wetness impregnation technique. The Pt precursor was diluted to a solution volume equivalent to the total pore volume of the support. $Pt/\gamma\text{-}Al_2O_3$ was produced to contain a 1/100 ratio respectively by weight. The catalyst was dried at 393K for 24 hours and sintered at temperatures between 873-1073K in order to obtain varying catalyst dispersion and particle size.

Catalyst sintering was carried out in a Thermolyne 46100 muffle furnace controlled by a Eurotherm 2408 temperature controller. During each of the sintering steps the ramp rate for heating was 1K/min and the cooling rate was 5 K/min. Catalysts were held at the specified sintering temperature for 8 hours. Sintering was conducted in a stagnant air environment.

4.5.2 Flow reactor set up:

NO oxidation experiments were carried out in a quartz tube reactor of 6.35 mm OD, ID of 4 mm, and a length of 2 cm. Catalyst powder was inserted into the tube held in place by quartz wool packing on both the top and bottom of the vertical tube. Flow rates of the inlet gasses were set by Porter mass flow meters and controlled by a Porter four-channel mass flow controller. Reactor temperature was controlled by an Omega CN6000 PID controller connected to a K-type thermocouple inserted directly adjacent to the catalytic bed within the heating zone.

4.5.3 Catalyst Characterization:

A Micromeritics Autochem 2920 catalyst characterization system was used to perform pulsed CO chemisorption to determine platinum dispersion. CO chemisorption was performed at 323K and a CO/Pt ratio of 1 was assumed in the calculation of dispersion and subsequent particle size calculation. Transmission electron microscopy (TEM) and energy-dispersive x-ray (EDX) analysis were performed on an FEI Tencai F20 XT microscope using a Schottky field emitter electron source.

4.5.4 Steady state experiments:

The catalyst was initially reduced in 5% H_2/Argon mixture for 15 minutes at 673K [8, 45, 46]. The catalyst was then conditioned in NO/O_2 environment (608 ppm/3.7% vol., respectively)

with argon balance at 313K at a space velocity of 59,000 hr^{-1} [8]. The flow conditions for the experiments are based on typical LNT catalyst studies [47].

To obtain steady state NO oxidation conversions, the reactor was ramped to temperature and held for 1 hour at each steady state temperature. The conversion was measured in the range of temperatures from 473-773K with 50K temperatures increments. Pseudo-steady state profiles were obtained successively starting from the lowest temperature of 473K. Following the 1 hour steady state measurement, the reactor was then ramped at 10 K/min to the next temperature set point through the full temperature range.

4.6 Modeling

4.6.1 Global Kinetic Mechanism

Bhatia et al. proposed a global reaction model similar to this effort and proved that oxygen adsorption is the rate determining step using a micro-kinetic parametric study (validated by other groups [14-16, 18, 19, 28, 48]). Given the previously identified half order oxygen concentration dependence of NO oxidation, a new global reaction rate expression is derived here based upon the reaction mechanism in equations (4.1-4.5).

The first step indicates that NO adsorption and desorption occurs with the forward and reverse rates equal to:

$$R_2 = k_2 p_{NO} \theta_{Pt} \tag{4.5}$$

$$R_{-2} = k_{-2} \theta_{Pt \cdot NO} \tag{4.6}$$

As oxygen adsorption is the rate determining step, these reactions are assumed to be in equilibrium, where the equilibrium constant equals:

$$K_{NO} = k_2 / k_{-2} \tag{4.7}$$

At the same time, dissociative oxygen adsorption and desorption on platinum occurs with the forward and reverse rates expressed as:

$$R_3 = k_3 p_{O_2}^{1/2} \theta_{Pt} \tag{4.8}$$

$$R_{-3} = k_{-3} \theta_{Pt\cdot O} \tag{4.9}$$

Literature review has already shown oxygen adsorption to be the RDS therefore, the RDS is written as:

$$R_1 = R_{NO} = k_3 p_{O_2}^{1/2} \theta_{Pt} - k_{-3} \theta_{Pt\cdot O} \tag{4.10}$$

The third step of the reaction is the L-H oxidation reaction between adsorbed NO and atomic oxygen combined with the reverse reaction which is the dissociation of NO_2:

$$R_4 = k_4 \theta_{Pt\cdot NO} \theta_{Pt\cdot O} \tag{4.11}$$

$$R_{-4} = k_{-4} \theta_{Pt\cdot NO_2} \theta_{Pt} \tag{4.12}$$

with the equilibrium constant for the L-H step set as:

$$K_{LH} = k_4 / k_{-4} \tag{4.13}$$

In the next step, molecular nitrogen dioxide adsorption and desorption on platinum occurs with the forward and reverse rates expressed as:

$$R_5 = k_5 p_{NO_2} \theta_{Pt} \tag{4.14}$$

$$R_{-5} = k_{-5} \theta_{Pt\cdot NO_2} \tag{4.15}$$

Where the equilibrium constant expressed as:

$$K_{NO_2} = k_5 / k_{-5} \tag{4.16}$$

Solving Eqn. (4.6-4.8), (4.12-4.17), results in:

$$\theta_{\mathrm{Pt\cdot O}} = \frac{K_{\mathrm{NO_2}} p_{\mathrm{NO_2}} \theta_{\mathrm{Pt}}}{K_{\mathrm{LH}} p_{\mathrm{NO}} K_{\mathrm{NO}}} \tag{4.17}$$

Literature review illustrates that under most conditions, the surface is primarily covered with atomic oxygen and NO, leaving negligible vacant sites. As a result, $1 = \theta_{\mathrm{Pt\cdot NO}} + \theta_{\mathrm{Pt\cdot O}}$ and NO_2 and O_2 surface coverage fractions are negligible. This outcome, combined with Eqns. (4.6), (4.7), and (4.18), results in the following expression for the available surface sites of Pt:

$$\theta_{\mathrm{Pt}} = \frac{1}{\left(\frac{K_{\mathrm{NO_2}} p_{\mathrm{NO_2}}}{K_{\mathrm{LH}} p_{\mathrm{NO}} K_{\mathrm{NO}}} + p_{\mathrm{NO}} K_{\mathrm{NO}} \right)} \tag{4.18}$$

Substituting Eqn. (4.18) and (4.19) into Eqn. (4.11) finds:

$$R_{\mathrm{NO}} = \left(k_3 p_{\mathrm{O_2}}^{1/2} - k_{-3} \frac{K_{\mathrm{NO_2}} p_{\mathrm{NO_2}}}{K_{\mathrm{LH}} p_{\mathrm{NO}} K_{\mathrm{NO}}} \right) \theta_{\mathrm{Pt}} \tag{4.19}$$

Furthermore, incorporation of Eqn. (4.19) into Eqn. (4.20) results in:

$$R_{\mathrm{NO}} = \frac{\left[\begin{matrix} k_3 p_{\mathrm{O_2}}^{1/2} \left(K_{\mathrm{LH}} p_{\mathrm{NO}} K_{\mathrm{NO}} \right) \\ -k_{-3} \left(K_{\mathrm{NO_2}} p_{\mathrm{NO_2}} \right) \end{matrix} \right]}{\left[K_{\mathrm{NO_2}} p_{\mathrm{NO_2}} + \left(p_{\mathrm{NO}} K_{\mathrm{NO}} \right)^2 K_{\mathrm{LH}} \right]} \tag{4.20}$$

However, writing the global reaction rate as above does not account for the equilibrium limiting conditions at higher temperatures. Recalling the governing global reaction, Eqn. (4.1), the forward and reverse reactions are

$$R_1 = k_1 p_{\mathrm{NO}} p_{\mathrm{O_2}}^{1/2} \tag{4.21}$$

$$R_{-1} = k_{-1} p_{\mathrm{NO_2}} \tag{4.22}$$

At equilibrium, the forward and backward rates are equal giving

$$k_1 p_{\mathrm{NO}} p_{\mathrm{O_2}}^{1/2} = k_{-1} p_{\mathrm{NO_2}}, \tag{4.23}$$

where the equilibrium constant that can be calculated from Gibbs Free Energies equals:

$$K_{eq} = k_1 / k_{-1} \tag{4.24}$$

Substituting Eqn. (4.24) into (4.25) recovers:

$$K_{eq} p_{NO} p_{O_2}^{1/2} = p_{NO_2} \tag{4.25}$$

However, instead of substituting back the equilibrium constant from Eqn. (4.26) directly in to the NO oxidation reaction rate expression Eqn. (4.21), Eqn. (4.26) can be modified using the properties of equilibrium for each detailed reaction step as proposed by Bhatia et al. [25]. The equilibrium constant for overall NO oxidation can be deduced as:

$$K_{eq} = K_{LH} \frac{K_{NO} K_{O_2}}{K_{NO_2}} \tag{4.26}$$

This can be modified as

$$\frac{K_{NO_2}}{K_{O_2}} = \frac{K_{LH} K_{NO}}{K_{eq}} \tag{4.27}$$

As a result, Eqn. (4.21) can be written as:

$$R_{NO} = \frac{k_3 \left[p_{O_2}^{1/2} \left(K_{LH} p_{NO} K_{NO} \right) - \frac{K_{NO} K_{LH} p_{NO_2}}{K_{eq}} \right]}{\left[K_{NO_2} p_{NO_2} + \left(p_{NO} K_{NO} \right)^2 K_{LH} \right]} \tag{4.28}$$

Where equation (4.29) is the derived global reaction rate expression for NO oxidation with the adsorption of oxygen as the Rate Determining Step.

4.1 Kinetic Parameter Values

The equilibrium constants used in Eqn. (4.29) are derived from the kinetic theory of gases [7, 8, 31, 49, 50]. For NO adsorption-desorption this is given as

$$K_{\mathrm{NO}} = \left[\begin{array}{l} \dfrac{N_A A_{\mathrm{Pt}} S^0_{\mathrm{NO}}}{\nu_{\mathrm{NO}} \left(2\pi W_{\mathrm{NO}} R_u T_m\right)^{1/2}} \\ \cdot \exp\left(-\dfrac{E_2 - E_{-2}}{R_u T_m} \right) \end{array} \right] \tag{4.29}$$

whereas, for NO_2 adsorption-desorption it is given by

$$K_{\mathrm{NO_2}} = \left[\begin{array}{l} \dfrac{N_A A_{\mathrm{Pt}} S^0_{\mathrm{NO_2}}}{\nu_{\mathrm{NO_2}} \left(2\pi W_{\mathrm{NO_2}} R_u T_m\right)^{1/2}} \\ \cdot \exp\left(-\dfrac{E_5 - E_{-5}}{R_u T_m} \right) \end{array} \right] \tag{4.30}$$

However, for L-H reaction, the equilibrium constant is modified as

$$K_{\mathrm{LH}} = A_{LH} \exp\left[-\frac{\left(E_4 - E_{-4}\right)}{R_u T_m} \right] \tag{4.31}$$

Of note, the pre-exponential factor for the L-H reaction step A_{LH} depends on the surface coverage of NO and atomic oxygen along with their proximity with respect to each other. Since the surface coverage and proximity depends on temperature, dispersion, etc., it cannot be directly determined from kinetic theory and is therefore calibrated.

The equilibrium constant for overall NO oxidation (K_{eq}) is derived from the Gibbs free energy at the catalyst temperature. The reaction rate coefficient for oxygen adsorption is modeled by the Arrhenius rate expression, where the pre-exponential factor is calculated from the kinetic theory of gases:

$$k_3 = A_3 \exp\left(-\frac{E_3}{R_u T_m} \right), \text{ with}$$

$$A_3 = \frac{N_A S^0_{\mathrm{O_2}}}{\left(2\pi W_{\mathrm{O_2}} R_u T_m\right)^{1/2}} p^{1/2} \tag{4.32}$$

Of note, in the above equation, the value of A_3 is multiplied by the square root of the inlet pressure in order to ensure correct units for this parameter in the overall rate expression.

For Eqns. (4.30) through (4.33), values for the ideal gas constant, Avogadro's number, and molecular weight are commonly available in literature. The remaining parameters are evaluated based upon a literature review and their dependence on temperature and catalyst formulations (i.e., dispersion). Parameters that are taken to be independent of temperature and the catalytic surface are given in Table 4-1.

Table 4-1: Values of Constant Parameters.

Parameters	**Units**	**Values**
A_{Pt}	[m^2 $site^{-1}$]	8×10^{-20} [51]
S_{NO}^0	[-]	0.9
ν_{NO}, ν_{NO_2}	[s^{-1}]	1×10^{16}
E_2, E_5	[kJ mol^{-1}]	0.00
$S_{NO_2}^0$	[-]	1
E_4	[kJ mol^{-1}]	101
E_{-4}	[kJ mol^{-1}]	51

The sticking coefficient of NO is 0.9 which matches closely to 0.92 given by Olsson et al [7, 8]. Bhatia et al. provided a sticking coefficient value at 0.85, Hauptman et al. indicated its value at 0.87 [14, 25], and Rankovic et al. used 0.88 [18, 19]. The sticking coefficient of NO_2 matches values given by Olsson et al. and Crocoll et al. and is close to the Rankovic et al. and Hauptman et al. value of 0.97 [7, 13, 14, 18, 19, 28].

The oxygen sticking coefficient depends upon temperature and surrounding species. Hence, Campbell et al. is followed and the sticking coefficient is defined as [31, 52]

$$S_{O_2}^0 = S_{O_2} \exp\left(-\frac{E_{S,O_2}}{R_u T_m}\right) \tag{4.33}$$

where S_{O_2} is 1.166×10^{-2} [-] and E_{S,O_2} is -4.029 [kJ mol^{-1}]

The desorption frequency (ν_{NO}) of NO matches the value given by Olsson et al., Crocoll et al., Hauptman et al., Bartram and Gorte [7, 8, 13, 14, 38, 39]. Also, desorption frequency (ν_{NO_2}) of NO_2 is in line with Olsson et al. and Hauptmann et al.; however, it deviates from the 10^{13} value given by Crocoll et al. and Bartram et al. [7, 8, 13, 14, 39]. Adsorption activation energy for both NO and NO_2 is negligible as indicated by the literature [7, 8, 13-16, 18, 25].

The activation energy for the L-H reaction ranges from 101 to 124 kJ mol^{-1} in the literature apart from Crocoll et al. whom provide a low value of 35 kJ mol^{-1} [7, 13, 16-19, 25]. Hauptman et al. suggest the dependence of this activation energy on surface coverage of NO and oxygen; however, the authors have written the activation energy without surface coverage dependence in which is in agreement with the majority of previous studies [16, 17]. The value chosen of 101 kJ mol^{-1} is close to that of Olsson et al. and Rankovic et al. and not too dissimilar from Hauptman et al. if one neglects surface coverage effects [7, 16-19]. The activation energy of 51 kJ mol^{-1} for NO_2 decomposition (backward L-H reaction) is in line with 52.5 kJ mol^{-1} provided by Olsson et al. and 56 kJ mol^{-1} provided by Hauptman et al. after neglecting surface coverage effects [7, 8, 16, 17]. However, it is slightly higher than the Rankovic et al. value of 36.9 kJ mol^{-1} [18, 19]. The value chosen matches Crocoll et al. but they support the E-R mechanism [13].

Apart from the previously mentioned variables, there are three major parameters left to discuss: activation energy for desorption of NO and NO_2 and activation energy for oxygen adsorption. Literature illustrates that these three parameters depend on surface coverage and, in turn, on temperature and catalyst surface morphology. Hence, these parameters have been chosen to incorporate a functional dependency representative of the physical dependence on catalyst morphology.

NO adsorbs at room temperature [13], starts desorbing at 500K, and near 550-600K, desorbs completely [9, 25, 39]. At relatively high temperatures (> 450K), NO_2 dissociates promoting the formation of NO [13, 39]. This increases the surface coverage of NO, which reduces the activation energy of NO desorption [16]. Furthermore, the activation energy of NO desorption decreases with increasing oxygen surface coverage [13, 16]. It is commonly observed that NO_2 dissociation promotes a growth in oxygen surface coverage beyond oxygen self-promotion [8, 17, 24]. In the absence of NO_2 dissociation oxygen tends to desorb readily at high temperatures. In the case of oxygen surface coverage promotion by NO_2 dissociation oxygen coverage increases relative to the higher temperature dissociation observed in the absence of reaction. This results in a reduction of the activation energy of NO desorption [53, 54]. The claim of a relative increase in surface coverage of oxygen with respect to temperature is independently supported by Wang and Yeh [41].

It is well known that the lack of surface species increases the activation energy of desorption of that respective species [8, 16, 17, 38, 39]. As discussed prior, increasing the catalyst temperature decreases NO availability on the surface and some authors have even taken surface species coverage to be zero at high temperature. However, the literature review illustrates that oxygen surface coverage promotes NO desorption [13, 16, 17, 38, 39]. Hence, at high

temperatures, the effect of desorption promotion by oxygen overtakes the decrease in desorption due to lack of species, subsequently promoting NO desorption (and lowering NO desorption activation energy).

When incorporating surface coverage effects most authors write desorption activation energy as a function of surface coverage. However, this is not possible for a global reaction mechanism without modeling surface coverages independently; therefore, temperature is used as a proxy for surface coverage based on the earlier discussion. Literature suggests that NO desorption activation energy is in the range of 90 to 140 kJ mol^{-1} [7-9, 11, 13, 14, 17, 25, 28]. Based on this information, the expression for NO desorption activation energy is formulated as:

$$E_{-2} = 115 - \alpha T_m \quad (34)$$

where α is a constant used for calibration. Writing the activation energy in this manner will predict the highest activation energy for desorption at low temperatures which favors NO surface coverage and NO oxidation. Furthermore, at high temperatures, decreased desorption activation energy will increase the probability of desorption without reaction, helping to satisfy the equilibrium condition. Finally, the calibrated parameter α directly serves as an indicator of the relative effect of the adapted parameter, where a larger α indicates increased importance of the surface coverage dependence term.

For the activation energy of NO_2 desorption, at low temperatures (< 500K), NO_2 decomposition is slower than NO oxidation and NO_2 desorption; thus, promoting NO_2 formation [7, 10, 13]. However, at higher temperatures (> 550-600K), the decomposition of NO_2 is preferred over desorption [13, 39]. In addition, around this temperature range, NO desorption is preferred over NO oxidation; thus, promoting decomposition of adsorbed NO_2 [39]. However, if the NO_2 decomposition is preferred and NO desorption is fast, than surface oxygen species

should increase. This scenario is consistent with Hauptmann et al finding an increase in PtO via the NO_2 dissociation reaction at temperatures >550K [7, 8]. As temperature increases, NO desorbs from the surface and reduces the possibility of NO_2 formation [39]. With a high decomposition rate and low surface concentrations of NO_2, it can be theorized that the decrease in observed surface NO_2 is a function of increased decomposition rate and an increase of NO_2 desorption activation energy is a function of the decrease in other surface species concentrations (change in surface concentrations of O_2 will be discussed later).

Therefore, this summary indicates that as the temperature increases, NO_2 struggles to form as a result of strong adsorption and decomposition as well as changing surface coverage fraction of other components. This is represented by an increase NO_2 desorption activation energy modeled here as:

$$E_{-5} = 95 + \beta T_m \tag{4.35}$$

where β is a constant used for calibration. In the literature, the activation energy of desorption is between 95 and 120 kJ/mol; hence, the authors have chosen the same range for the indicated expression [7, 8, 14, 16-19, 25].

Most important is the dependence of oxygen adsorption on catalyst morphology. Wang et al show a direct correlation between heat of adsorption of oxygen and platinum particle size on alumina supported catalysts**.** It has also been shown that NO conversion is significantly increased with platinum particle size [41, 55]. This justifies the prior findings of higher NO conversions over larger platinum particles and the proposed correlation between oxygen adsorption and O_2 adsorption activation energy [7, 10, 13, 17, 18, 25]. Olsson et al., Bhatia et al., and Rankovic et al. all suggest the value of 30.4 kJ mol^{-1} that is used here with a slight

modification [7, 18, 19, 25]. The particle size dependence of oxygen adsorption is included in the activation energy expression as such:

$$E_3 = 30.4 - \left(\frac{d_{\mathrm{Pt}} - 5.9}{d_{\mathrm{Pt}}} \right) \chi \tag{4.36}$$

where the reference particle size of 5.9 nm is used based on Bhatia et al.'s findings [25].

4.6.2 Packed Bed Reactor Model:

Since the measurement of conversion took place at pseudo-steady state conditions, only the chemical species equation needs to be modeled for the packed bed reactor. Of note, the authors simulated a temperature ramp experiment after the kinetic model was calibrated and no difference was seen in the results.

Based on prior efforts of the third author [56], the chemical species equation for a packed bed simulation is equal to:

$$\varepsilon u_s \frac{\partial \bar{\mathbf{C}}}{\partial z} = \mathbf{D}^{eff} \frac{\partial^2 \bar{\mathbf{C}}}{\partial z^2} - G_{ca} \bar{\mathbf{R}} \tag{4.37}$$

where the left hand side represents the advection of the molar species concentration $\left(\bar{\mathbf{C}}\right)$ as a function of the superficial velocity (εu_s). Indicated species concentrations include a combination of the two phases (surface and gas). The first term on the right hand side is the effective diffusivity that includes the porosity of the medium. The last term on the right hand side includes the influence of the reaction rates $\left(\bar{\mathbf{R}}\right)$ on the surface along with a catalytic surface area per unit volume term (G_{ca} – m^2 m^{-3}) in order to ensure the reaction rate expression (Eqn. (4.29) is in the correct units. This is used as an additional calibration variable since it cannot be readily measured.

4.7 Results and Discussion

Figure 1 shows the NO oxidation conversion profile with varying catalyst sintering temperatures. Conversion with sintering temperature varies substantially at temperatures below that which equilibrium conversion is reached. Above 604K, all catalysts demonstrate less than a 1.2% variation in total conversion with the standard deviation averaging 0.9%. These results illustrate that changing sintering conditions at these higher temperatures results in no significant change in conversion. This finding is further confirmed by prior literature findings; i.e., above 604K, NO oxidation follows the equilibrium conversion curve and is independent of the catalyst aging conditions.

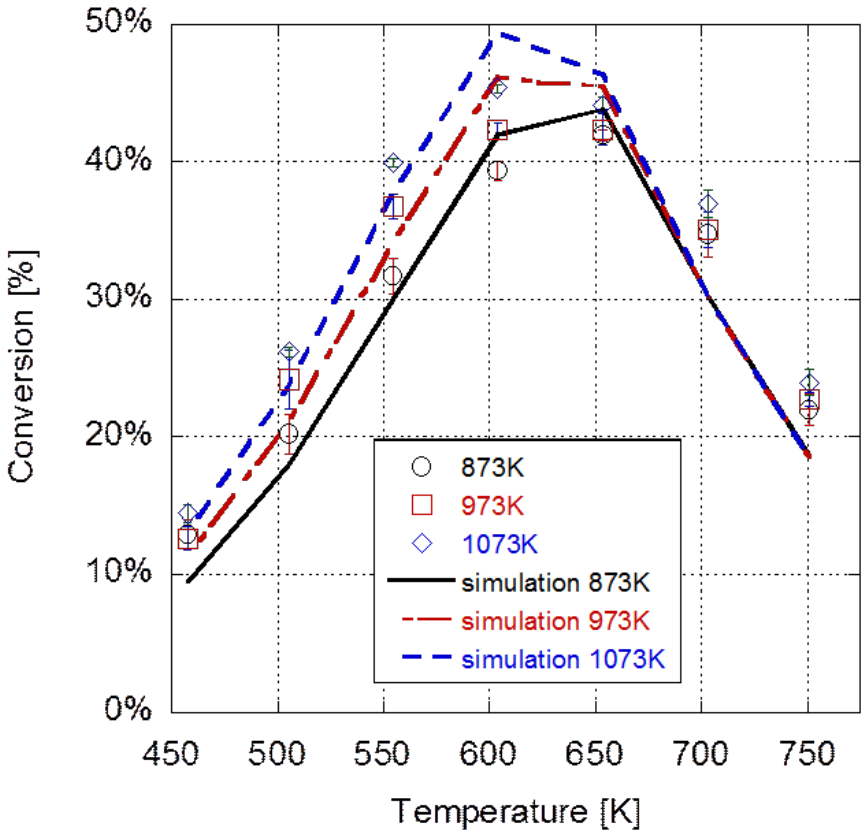

Figure 4-1: Pseudo-steady state NO oxidation conversion versus temperature (both model and experimental) at isothermal conditions with varying catalyst sintering temperatures indicated (Model 1)

Figure 4-1 also presents the results of the simulation efforts employing the adaptive kinetics model. Calibration of model parameters was accomplished using the Matlab *fmincon* routine while minimizing the least-squared curve-fit between the simulation results and the experimental data at each pseudo-steady state temperature. The model is able to capture both the trends with temperature and dispersion with the model parameters given in Table 4-2. Furthermore, the equilibrium temperature limitation is accurately represented in the results.

Table 4-2: Surface properties of the Pt/Alumina catalyst

Sintering Temp.	Dispersion	Pt Particle Size
800°C	11.0%	10.23nm
700°C	17.9%	6.33nm
600°C	42.6%	2.65nm

Table 4-2 shows the platinum particle size for each of the sintered catalysts, as sintering temperature is increased from 873K to 1073K platinum particle size is increased from 2.65 to 10.24 nanometers. As shown in Figure 4-1, the increase in particle size results in higher NO oxidation conversion rates across all temperatures while the temperature of maximum conversion decreases with dispersion. For example, a maximum conversion of 45.3% is achieved at 604K over the catalyst sintered at 1073K; whereas, the catalyst with the smallest platinum particle size only achieved 41.9% conversion at 654K. This result is consistent with the literature for NO oxidation under oxidizing conditions; i.e., larger platinum particles have higher conversion rates [10, 14, 25, 28, 35].

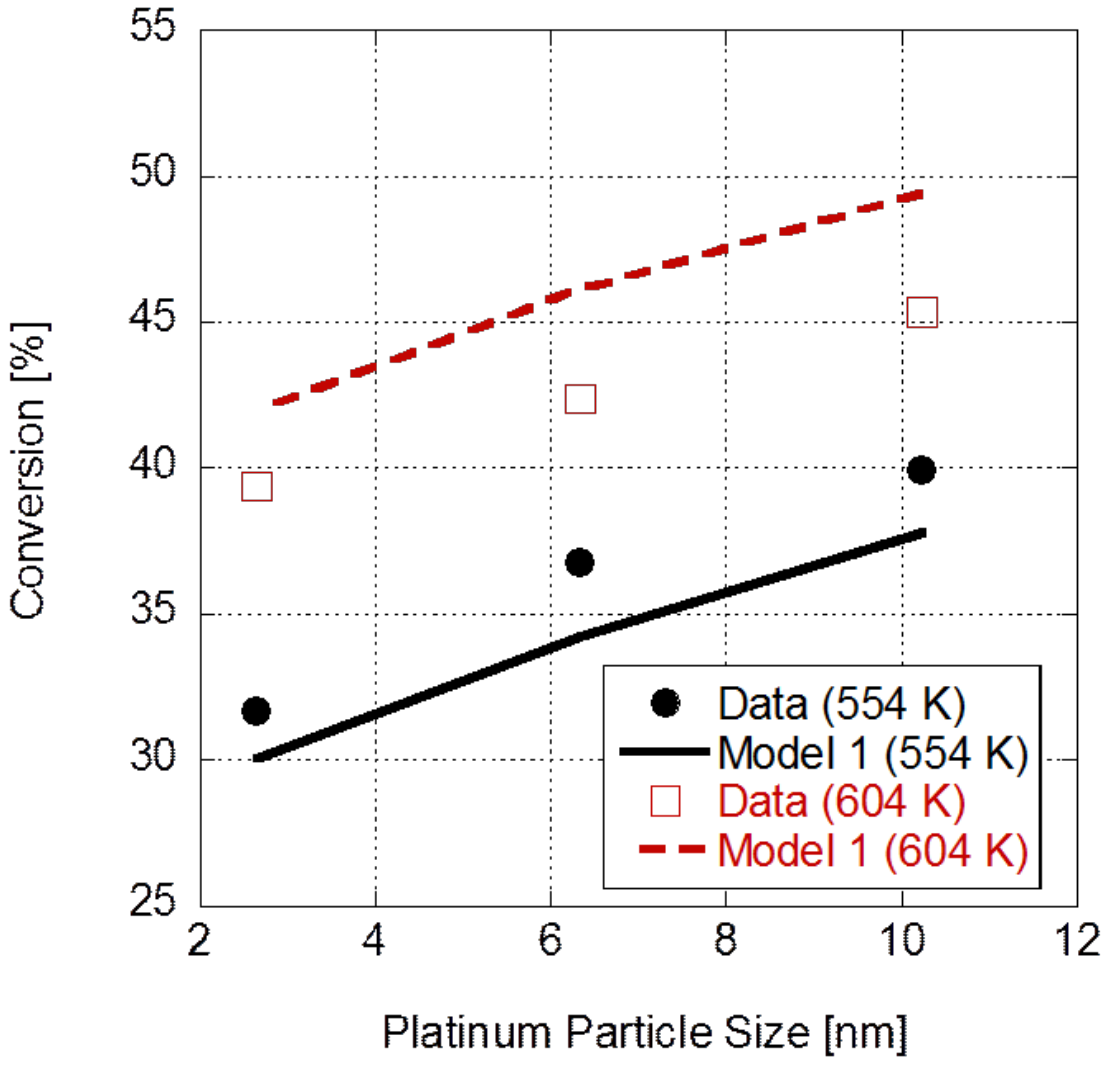

Figure 4-2: Pseudo-steady state NO oxidation conversion versus particle size (both model and experimental) at isothermal conditions • 554K □604K.

For NO oxidation below the equilibrium conversion temperatures, the change in conversion as a function of platinum particle size at each isothermal operating temperature is significant. Figure 4-2 shows the impact of particle size on conversion at two individual isothermal operating temperatures (554K and 604K) for both experimental data and those predicted by Model 1. The maximum variation in conversion with particle size is observed at 554K, with an 8.2% increase in conversion. Increasing the isotherm temperature to 604K did not

change the observed trend, but did results in a slight reduction of the percent increase in conversion to 5.9%. While the trend of increasing conversion with particle size is accurately captured by Model 1, the absolute value of the conversion at each particle size deviates. This deviation is maintained through the range of reaction temperatures.

Table 4-3: Model 1 parameters specified or determined through calibration

Variable / Parameter	Value
Packed bed particle dia. [μm]	0.0436
Bed pore diameter [μm]	0.0101
Packed bed void fraction [-]	0.4
Diffusivity model	Parallel pore
A_{LH} [-]	8.913×10^{-9}
G_{ca} [$m^2\ m^{-3}$]	8.913×10^{-12}
χ [-]	1.603
α	0.030
β	0.030

In comparison to previous literature modeling results, this simulation effort accurately portrays an increased maximum conversion while the temperature at which maximum conversion is achieved decreases as platinum particle size grows. These results support Bhatia et al.'s claim that surface coverage of NO has to be included in a global model for higher accuracy at lower temperatures [25]. Moreover, the results presented support the idea that oxygen adsorption is the rate determining step and that particles size effects must also be included in the expressions for desorption activation energy of NO and NO_2. The new expression was developed based upon the premise that adjacently adsorbed species affect the adsorption and desorption of NO and NO_2 substantially, where O_2 dominates the surface in the kinetically

limited regime. Based upon this assumption the authors used the changes in O_2 desorption profile with particle size as the basis for the model modification given in equation 39:

$$T_d = 476 + \frac{51}{D_{pt}} \tag{4.39}$$

T_d modifies both the NO and NO_2 desorption activation energy expression as such

$$E_{-2} = 115 - \alpha(T_m - T_d) \text{ where } T_d > 0 \tag{4.40}$$

$$E_{-2} = 95 + \beta(T_m - T_d) \text{ where } T_d > 0 \tag{4.41}$$

The expression in equation (4.39) has been developed based upon literature desorption profiles of oxygen, with surfaces coverages in the range of 0.5 - 0.7ML over platinum single crystals where representative facets of platinum have been used to approximate well dispersed and non-dispersed platinum particles. In the case of well dispersed platinum, O_2-TPD from the Pt(100) surface shows an increased temperature of desorption, this is justified by the propensity of small platinum particles to undergo oxidation and subsequently have stronger Pt-O bonding [57]. To represent the non-dispersed platinum case, the authors reference O_2 –TPD from the Pt(111) facet by Weaver et al. On these surfaces, oxygen desorption occurs at the lowest temperature where desorption begins at 476K [58]. The expressions defined in equation 40 and 41 vary with temperature to approximate surface coverage effects, and are further modified by the platinum particle size effect incorporation defined by equation (4.39). It should be noted that no additional calibrated parameters are introduced with the adapted activation energy equations. Also, the particle size dependence of the oxygen adsorption activation energy is retained from equation (4.37). The results from the modified version of model 1 identified hence forth as

Model 2 are presented in Figure 4-3. The calibrated model parameters are presented in Table 4-3.

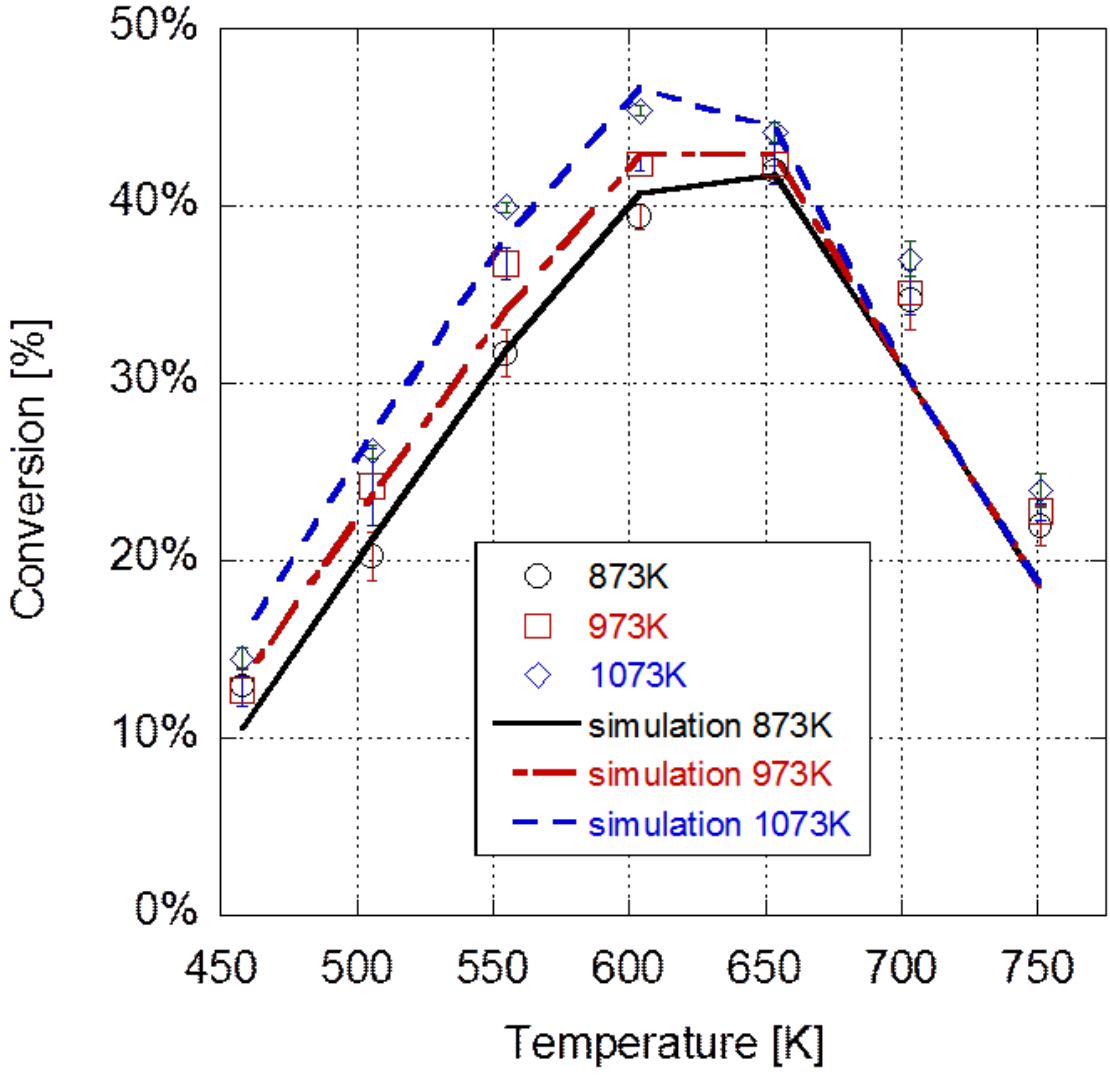

Figure 4-3: Pseudo-steady state NO oxidation conversion versus temperature (both model and experimental) at isothermal conditions with varying catalyst sintering temperatures indicated (Model 2)

Model 2 shows substantial improvement over Model 1, evident in the LSQ value (Model 1 LSQ of 10.19, Model 2 LSQ of 4.85). The model accurately represents the trend of decreasing maximum conversion temperature with increased platinum particle size. Figure 4-4 shows the

change NO oxidation conversion for both Model 1 and Model 2 as well as the experimental data at the 554K pseudo-steady state operating temperature.

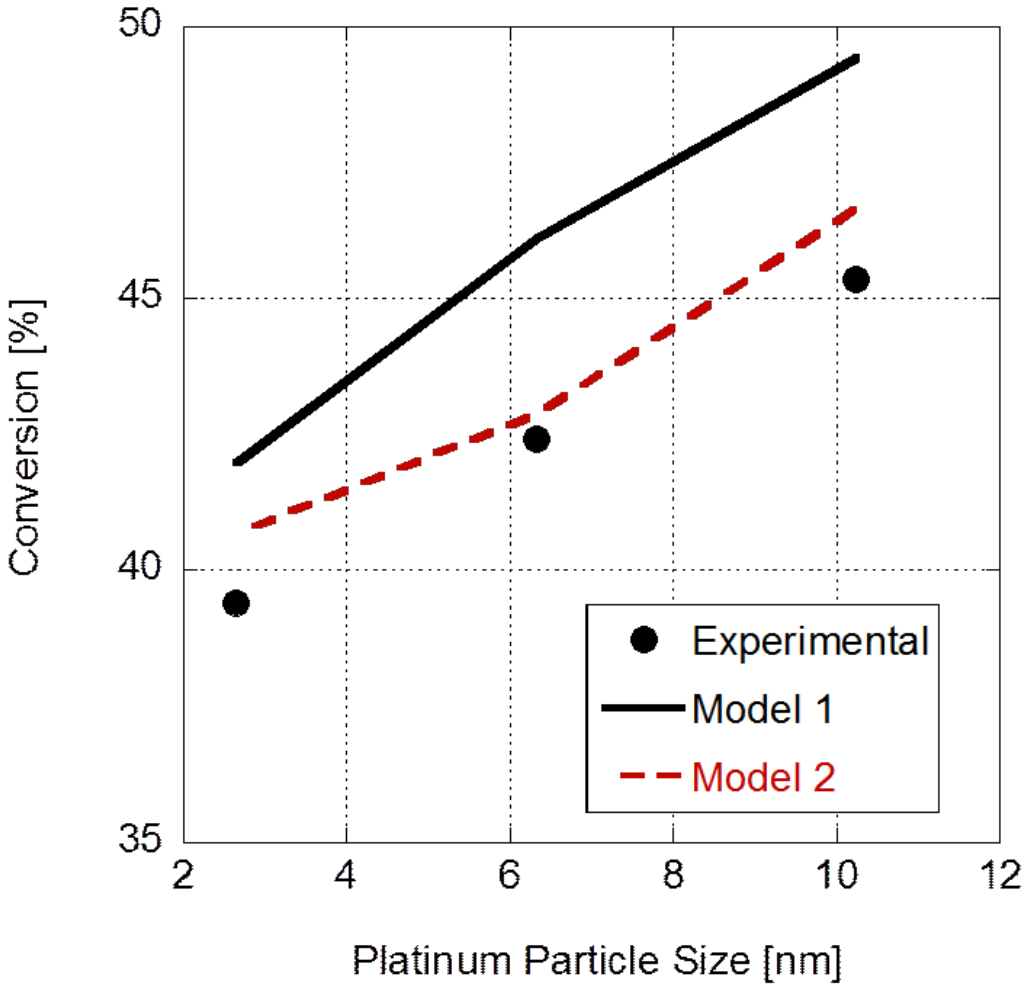

Figure 4-4: Pseudo-steady state NO oxidation conversion versus particle size (both model and experimental) at 604K

It can be seen in Figure 4-4 that model 2 more accurately predicts the NO oxidation conversion at each of the platinum particle sizes. Model 2 also shows similar accuracy to Model 1 with respect to the relative change from the smallest to the largest particle size (slope of the line).

Table 4-4: Model 1 parameters specified or determined through calibration

Variable / Parameter	Value
Packed bed particle dia. [μm]	0.0436
Bed pore diameter [μm]	0.0101
Packed bed void fraction [-]	0.4
Diffusivity model	Parallel pore
A_{LH} [-]	4.996×10^{-11}
G_{ca} [$m^2\ m^{-3}$]	5.767×10^{-12}
χ [-]	1.993
α	0.0175
β	0.0175

While detailed kinetics including surface coverage effects will more accurately simulate the conversion rate, the choice of modeling these effects through temperature dependencies provides a good compromise for a global kinetic approach. The kinetic parameters are within the range provided in the literature. Furthermore, the same kinetic parameters are used for multiple surface chemistries making the model truly global. This is important, because Stewart et al. have demonstrated that there is significant change in prediction of conversion curves for different global models when compared to various surface morphologies [59].

Further improvements in the kinetic constants can be accomplished with additional experiments employing different inlet conditions (including water and other chemical species) and particle sizes. In addition, the global kinetics formulation presented can be utilized in a predictive manner prior to experimentation in order to help guide efforts.

4.8 Conclusion

Here in, an updated global kinetic model for NO oxidation is provided. The majority of kinetic parameters are evaluated based on kinetic theory of gases; however, a select few are calibrated to fit experimental results for different catalyst morphologies. The values of the kinetic parameters all fall within previously reported in the literature values. The results illustrate the necessity of including NO surface coverage in the model (via a temperature analog) to simulate NO oxidation conversion at lower temperatures. The modification of the original modeling efforts clearly illustrate platinum particle size effects must be included to capture the effects of changing surface coverage with particle size.

The developed model accurately reflects that within the kinetic region, NO oxidation conversion increases with a decrease in dispersion (increase in platinum particle size) and, in the equilibrium region, NO oxidation conversion follows the equilibrium condition irrespective of the catalyst surface morphologies. Both of these results are consistent with the literature. Overall, the developed model predicts NO oxidation as a function of platinum particle size well. Substantial improvement is achieved when the model is modified to include particle size effects on energies of desorption of NO and NO_2. The model is applicable for pre-reduced surfaces only. However, for an actual LNT device, NO oxidation occurs on the pre-reduced surface because of the previous regeneration event due to lean-rich cycling operation. Hence, the model provided is suitable for including in the simulation of an LNT.

5 Acknowledgement

This material is based upon work supported by the National Science Foundation under Award No. EPS-0903806 and matching support from the State of Kansas through Kansas Technology Enterprise Corporation. Financial support was also provided by the NSF IGERT C-CHANGE program at the University of Kansas.

4.9 Reference

1. Zelenka, P., *Worldwide Diesel Emission Standards, Current Experiences and Future Needs.* Applied Catalysis B, 1996. **10**(1): p. 3-28.
2. Koltsakis, G. and A. Stamatelos, *Catalytic Automotive Exhaust Aftertreatment.* Progress in Energy and Combustion Science, 1997. **23**(1): p. 1-39.
3. Chorkendorff, I. and J. Niemantsverdriet, *Concepts of Modern Catalysis and Kinetics*. 2 ed. Vol. 1. 2007: Wiley-VCH.
4. Johnson, T., *Diesel Engine Emissions and Their Control.* Platinum Metal reviews, 2008. **52**(1): p. 23-37.
5. Erkfeldt, S., E. Jobson, and M. Larrson, Topics in Catalysis, 2001. **16/17**(1-4).
6. Epling, W.S., et al., Catalysis Reviews, 2004. **46**(2).
7. Olsson, L., et al., *A Kinetic Study of NO Oxidation and NOx Storage on Pt/Alumina and Pt/BaO/Alumina.* J. Physical Chemistry, 2001. **105**: p. 6895-6906.
8. Olsson, L., et al., *A Kinetic study of Oxygen adsorpion/desorption and NO oxidation over Pt/Alumina catalysts.* J. Physical Chemistry, 1999. **103**: p. 10433-10439.
9. Bourane, A., et al., *Heats of Adsorption of Linear NO Species on a Pt/Alumina Catalyst Using in Situ Infrared Spectroscopy under Adsorption Equilibrium* Journal of Catalysis, 2001. **204**(1): p. 77-88.
10. Olsson, L. and E. Fridell, *The Influence of Pt Oxide Formation and Pt Dispersion on the Reactions of NO2<-> NO +1/2 Oxygen over Pt/Alumina and Pt/ BaO/Alumina* Journal of Catalysis, 2002. **210**: p. 340-353.
11. Crocoll, M. and W. Weisweiler, *Kinetische Untersuchungen Zur Pt-Katalysierten Oxidation von NO: Modellierung und Simulation.* Chemie Ingenieur Technik, 2004. **76**(10): p. 1490-1494.
12. Epling, W., et al., *Overview of the Fundamental Reactions and Degradation Mechanism of NOx Storage/Reduction Catalysts.* Catalysis Reviews, 2004. **46**(2): p. 163-245.
13. Crocoll, M., S. Kureti, and W. Weisweiler, *Mean Field Modelling of NO Oxidation Over Pt/Alumina Catalyst Under Oxygen Rich Conditions.* Journal of Catalysis, 2005. **229**: p. 480-489.
14. Hauptmann, W., et al., *Global Kinetic Models for the Oxidation of NO on Platinum under Lean Conditions.* Topics in Catalysis, 2007. **42-43**: p. 157-160.
15. Kromer, B., et al., *Modeling of NO Oxidation and NOx Storage on Pt/BaO/Alumina NOx Traps.* Catalysis Today, 2008. **136**(1): p. 93-103.
16. Hauptmann, W., et al., *Inverse Hysteresis During the NO Oxidation on Pt Under Lean Conditions.* Applied Catalysis B, 2009. **93**(1): p. 22-29.
17. Hauptmann, W., et al., *A Fast Approach to Predicitve Models: NO-Oxidation in Exhaust Gas Aftertreatment Systems.* Topics in Catalysis, 2009. **52**: p. 1925-1928.
18. Rankovic, N., et al., *Extension of a Kinetic Model for NO oxidation and NOx Storage to fixed-Bed Pt/Ba/Alumina Catalysts.* Catalysis Communications, 2010. **12**(1): p. 54-57.
19. Rankovic, N., A. Nicolle, and P. Da Costa, *Detailed Kinetic Modeling Study of NOx Oxidation and Storage and Their Interactions Over Pt/Ba/Alumina Monolith Catalysts.* J. Physical Chemistry C, 2010. **114**: p. 7102-7111.

20. Sharma, H. and A. Mhadeshwar, *A Detailed Microkinetic Model for Diesel Engine Emissions Oxidation on Platinum Based Diesel Oxidation Catalysts (DOC).* Applied Catalysis B 2012. **127**: p. 190-204.
21. Roy, S. and A. Baiker, *NOx Storage-Reduction Catalysis: From Mechanim and Materials Properties to Storage-Reduction Performance.* Chemical Reviews, 2009. **109**: p. 4054-4091.
22. Marques, R., et al., *Kinetics and Mechanisms of Steady-State Catalytic NO+O2 Reactions on Pt/SiO2 and Pt/CeZrO2.* Journal of Molecular Catalysis A: Chemical, 2004. **221**: p. 127-136.
23. Mulla, S.S., et al., *NO2 Inhibits the Catalytic Reaction of NO and Oxygen over Pt.* Catalysis Letters, 2005. **100**(3-4): p. 267-270.
24. Mulla, S., et al., *Reaction of NO and Oxygen to Nitrogen Dioxide on Pt: Kinetics and Catalysts Deactivation.* Journal of Catalysis, 2006. **241**: p. 389-399.
25. Bhatia, D., et al., *Experimental and Kinetic Study of NO oxidation on model Pt Catalysts.* Journal of Catalysis, 2009. **266**(1): p. 106-119.
26. Depcik, C. and D. Assanis, *One-Dimensional Automotive Catalyst Modeling* Progress in Energy and Combustion Science 2005. **31**: p. 308-369.
27. Wang, T.J., S.W. Baek, and J.-H. Lee, *Kinetic Parameter Estimation of a Diesel Oxidation Catalyst under Actual Vehicle Operating Conditions.* Industrial & Engineering Chemistry Research, 2008. **47**(8): p. 2528-2537.
28. Olsson, L., R. Blint, and E. Fridell, *Global Kinetic Model for Lean NO Traps.* Industrial and Engineering Chemistry Research, 2005. **44**(9): p. 3021-3032.
29. Kim, Y.-D. and W.-S. Kim, *Re-evaluation and Modeling of a Commercial Diesel Oxidation Catalyst.* Industrial & Engineering Chemistry Research, 2009. **48**(14): p. 6579-6590.
30. Sampara, C.S., E.J. Bissett, and M. Chmielewski, *Global Kinetics for a Commercial Diesel Oxidation Catalyst with Two Exhaust Hydrocarbons.* Industrial & Engineering Chemistry Research, 2008. **47**(2): p. 311-322.
31. Depcik, C., et al., *Adaptive Global Carbon Monoxide Kinetic Mechanism over Platinum/Alumina Catalysts.* Catalyst, 2013. **3**(2): p. 517-542.
32. Konstantas, G.S. and A.M. Stamatelos, *Modelling Three-Way Catalytic Converters: An Effort to Predict the Effect of Precious Metal Loading*, in *Proc. IMechE* 2007. p. 355-373.
33. Cooper, B. and J. Thoss, *Role of NO in Diesel Particulate Emission Control.* Society of Automotive engineers, 1989(890404): p. 171-183.
34. Gohndrone, J. and R.I. Masel, *A TPD Study of Nitric Oxide Decomposition on Pt(100), Pt(411) and Pt(211).* Surface Science, 1989. **209**(1-2): p. 44-56.
35. E. Xue, K.S., J. Ross, *Roles of support, Pt loading and Pt dispersion in the oxidation of NO to NO2 and of SO to SO2.* Applied Catalysis B, 1996. **11**: p. 65-79.
36. Lee, J.-H. and H. Kung, *Effect of Pt dispersion on the reduction of NO by propene over alumina-supported Pt catalysts under lean-burn conditions. .* Catalysis Letters, 1998. **51**(1): p. 1-4.
37. Xue, E., K. Seshan, and J.R.H. Ross, *Roles of supports, Pt loading and Pt dispersion in the oxidation of NO to NO2 and of SO2 to SO3.* Applied Catalysis B-Environmental, 1996. **11**(1): p. 65-79.

38. Gorte, R.J. and L.D. Schmidt, *Binding States and Decomposition of NO on Single Crystal Planes of Pt.* Surface Science, 1981. **109**(2): p. 367-380.
39. Bartram, M., R. Windham, and B. Koel, *The Molecular Adsorption of Nitrogen Dioxide on Platinum Studied by TPD and Vibrational Spectroscopy.* Surface Science, 1987. **184**(1): p. 57-74.
40. Ovesson, S., et al., *NO Oxidation Properties of Pt(111) revealed by AB INITIO kinetic Simulations.* Physical Review B, 2005. **71**: p. 115406-115410.
41. Wang, C.-B. and C.-T. Yeh, *Effects of Particle Size on the Progressive Oxidation of Nanometer Platinum by Dioxygen.* Journal of Catalysis, 1998. **178**(2): p. 450-456.
42. Gland, J., *Molecular and Atomic Adsorption of Oxygen on the Pt(111) and Pt(S)-12(111)x(111) Surfaces.* Surface Science, 1980. **93**: p. 487-514.
43. Loof, P., et al., *Rapid Sintering in NO of Nanometre-Sized Pt Particles on Alumina Observed by CO Temperature-Programmed Desorption and Transmission Electron Microscopy.* Journal of Catalysis, 1993. **144**(1): p. 60-76.
44. H. Mahzoul, J.B., P. Gilot, *Experimental and mechanistic study of NOx adsorption over NOx trap catalysts.* Applied Catalysis B, 1999. **20**: p. 47-55.
45. Despress, J., et al., *Catalytic Oxidation of Nitrogen Monoxide Over Pt/Silica.* Applied Catalysis B, 2004. **50**: p. 73-82.
46. Dawody, J., et al., *Role of Pt-precursor on the Performance of Pt/BaCO3/Al2O3.NOx Storage Catalysts.* Journal of Molecular Catalysis A: Chemical, 2005. **225**: p. 259-269.
47. Clayton, R., et al., *Pt Dispersion Effects During NOx Storage and Reduction on Pt/BaO/Al2O3 Catalysts.* Applied Catalysis B: Environmental 2009. **90**: p. 662-676.
48. Liu, G. and P.-X. Gao, *A Review of NOx Storage/Reduction Catalysts: Mechanism, Materials and Degradation Studies* Catalysis Science and Technology, 2011. **1**: p. 552-568.
49. Vannice, *A. Kinetics of Catalytic Reactions*. 2005, New York, NY, USA: Springer.
50. White, M., *Heterogeneous Catalysis*. 1990, Upper Saddle River, NJ, USA: Prentice Hall.
51. Anderson, J.R., *Structure of Metallic Catalysts*. 1975, London. U.K.: Academic Press.
52. Campbell, C.T., et al., *A Molecular-Beam Investigation of the Interactions of CO with a Pt(111) Surface.* Surface Science, 1981. **107**: p. 207-219.
53. Elg, A.-P., f. Eisert, and A. Rosen, *The Temperature Dependence of the Initial Sticking Probability of Oxygen on Pt(111) Probed with Second Harmonic generation* Surface Science, 1997. **382**(1): p. 57-66.
54. Tieber, W., W. Athenstaedt, and M. Leisch, *3D-Atom Probe Study of Oxygen Adsorpion on Stepped Platinum Surfacea.* Fresenius Journal of Analytical Chemistry, 1997. **358**: p. 116-118.
55. Benard, S., et al., *Supported Platinum Catalysts for NO Oxidation Sensors.* Applied Catalysis B, 2005. **55**(1): p. 11-21.
56. Srinivasan, A. and C. Depcik, *One-Dimensional Pseudo-Homogeneous Packed-Bed Reactor Modeling: I. Chemical Species Equation and Effective Diffusivity.* Chemical Engineering & Technology, 2013. **36**(1): p. 22-32.
57. Bradley Shumbera, R., H.H. Kan, and J.F. Weaver, *Oxidation of Pt(1 0 0)-hex-R0.7° by gas-phase oxygen atoms.* Surface Science, 2007. **601**(1): p. 235-246.

58. Weaver, J.F., J.-J. Chen, and A.L. Gerrard, *Oxidation of Pt(1 1 1) by gas-phase oxygen atoms.* Surface Science, 2005. **592**(1–3): p. 83-103.
59. Stewart, J., et al., in *International Powertrains, Fuels & Lubricants Meeting*. 2012, SAE.

Chapter 5: Effect of catalyst degradation on NO oxidation

In the previous chapter it was shown that NO oxidation can change greatly with catalyst morphology. An understanding of the morphology changes in the Pt/Al_2O_3 catalyst improved the reliability of a global kinetic model with respect to thermal aging of Pt. Fully formulated LNT catalysts have additional metals such as the alkali earth component for NO_x uptake and the Ce promoter for additional NO_x storage, improvements in sulfur tolerance, and preventing metal sintering. However, the impact of catalyst aging on the properties of the promoters and the ultimate morphology of the catalyst in unknown. As such, the study of NO oxidation with thermal aging has been extended to the fully formulated LNT catalysts $Pt/Ba/Al_2O_3$ and $Pt/Ba/CeO_2/Al_2O_3$.

Lean phase NO_x uptake begins by the catalytic oxidation of NO to NO_2. A comprehensive literature review has identified a number of critical factors influencing NO oxidation over LNT catalysts [1-5]. Important factors include support material, catalyst formulation, metal precursor selection, reductant concentrations, and lean phase gas concentrations. More specifically, metal interactions are the best way to characterize the changes in NO oxidation with changing catalysts parameters. Pt particle size, Pt-Ba adjacency, and Pt-Ce interactions can be interpreted by H_2 - TPR to determine the effects of these parameters on the NO oxidation reaction. It has been shown in the previous chapter, that platinum particle size has a major impact on NO conversion in Pt/Al_2O_3 catalysts. It is also known that the loading of additional catalyst components can affect both the platinum particle size and the morphology of the catalyst surface [6]. Subsequent investigations have proposed that the Pt-Ba and Pt-Ce adjacency can affect the ability of Pt to catalyze the reaction [6, 7].

While many studies have identified the effects of metals additions on the NO oxidation reaction, an accurate comparison of the catalysts is often not possible due to changing operating conditions, production conditions, and reactor configurations. The effect of degradation is even more difficult to interpret across literature sources as nearly every investigation induces catalyst degradation differently. Examples include thermal, chemical aging (such as SO_2), or long term learn/rich cycling. All of the examples listed contain within them even more variables that can be changed, making comparison of catalyst degradation across literature sources exponentially more difficult. The goal of this chapter is to systematically evaluate the effects of thermal degradation on NO oxidation as new support materials are incorporated into the catalyst formulation. To effectively compare the degradation effects across catalyst formulations, experimental conditions have been kept as constant as possible. Each catalyst has been characterized by H_2-TPR, TEM/EDAX, BET, and CO-chemisorption. Isothermal steady state NO oxidation conversion has been determined in the range of temperatures from 250 – 500ºC. Additional information regarding production conditions, reaction conditions, and analytical techniques are available in Chapter 3: Materials and Methods.

5.1 Physical characterization of all catalysts

Physical characterization of all catalysts analyzed are presented in Table 5-1. Metal loadings have been confirmed by both EDAX and ICP-OES for selected catalysts. Platinum particle size increases with increasing sintering temperature for all three catalysts. However, the trend with metal addition varies. Catalysts are labeled such that the metals contained within the sample are identified by a single letter (i.e., $Pt/Ba/Al_2O_3$ would be PBA) followed by the temperature at which the catalysts was aged (i.e. PBA aged at 600ºC would be PBA600). PA catalysts have the highest surface area which results in highly dispersed Pt particles. When Ba is added to the

catalyst formulation, platinum particle size decreases for all sintering temperatures relative to the PA samples. Cerium exhibits the Pt "anchoring" effect that was identified in the literature review [8]. As a result, Pt particle size decreases relative to the PBA catalysts at all sintering temperatures and the PBCA catalysts also exhibit slightly smaller Pt particle sizes when compared to the PA samples with identical sintering conditions.

Table 5-1: Weight percent loading, Pt particle size, % dispersion, and surface area of all Pt based LNT catalysts

Sample Title	Pt (%)	Ba (%)	Ce (%)	Pt Size (nm)	Pt Disp. (%)	Surface Area (m^2/g)
PA500	1	0	0	-	-	182.15
PA600	1	0	0	2.65	42.6	167.95
PA700	1	0	0	6.33	17.9	154.75
PA800	1	0	0	10.23	11.0	144.93
PBA500	0.82	16.5	0	2.62	43.7	118.82
PBA600	0.82	16.5	0	5.60	22.4	102.17
PBA700	0.82	16.5	0	10.11	11.4	101.85
PBA800	0.82	16.5	0	19.87	5.7	102.57
PBCA500	0.8	15.9	4	1.7	70.6	93.824
PBCA600	0.8	15.9	4	2.3	50.8	90.293
PBCA700	0.8	15.9	4	4.8	24.1	88.720
PBCA800	0.8	15.9	4	7.6	15.1	79.129

Although it may appear that the loading parameters changed as the catalyst formulation changed, the metals loading was maintained at a constant weight ratio to the alumina support. The weight ratios for the three catalysts respectively are Pt/Al_2O_3 – 1/100, $Pt/Ba/Al_2O_3$ – 1/20/100, and $Pt/Ba/CeO_2/Al_2O_3$ – 1/20/5/100.

5.2 Pt/Al_2O_3 characterization and reactivity

In the case of the PA catalysts, H_2 – TPR is an indicator of reactivity and availability of Pt sites. The temperature at which the maximum H_2 consumption is observed is representative of

the activity of the catalyst. If H_2 consumption occurs at a lower temperature, the catalyst is more easily reduced (less thermal energy is required for hydrogen to reduce the surface). The size of the peak is representative of the amount of catalytic material available for reduction. The larger the area under the curve, the more H_2 molecules that are consumed, and the consumed hydrogen is equivalent to the amount of Pt reduced. .

The TPR profiles presented in Figure 5-1 confirm the reduction trends identified by previous groups where thermal sintering of Pt/Al_2O_3 catalysts is employed. As Pt particle size is increased, the reduction peak shifts from the minimum temperature peak at 175ºC for the PA500 catalysts to the highest temperature of reduction (nearly 315ºC), which is achieved over the PA800 catalyst. The reduction peaks also show a decrease in size with increasing thermal aging temperature. The decrease in size indicates that less Pt is being reduced and thus, less Pt is available for reaction. This data will be a critical component in comparing the TPR profiles of the more complex catalysts. It is also relevant when analyzing the steady state NO oxidation profiles of the Pt/Al_2O_3 catalysts.

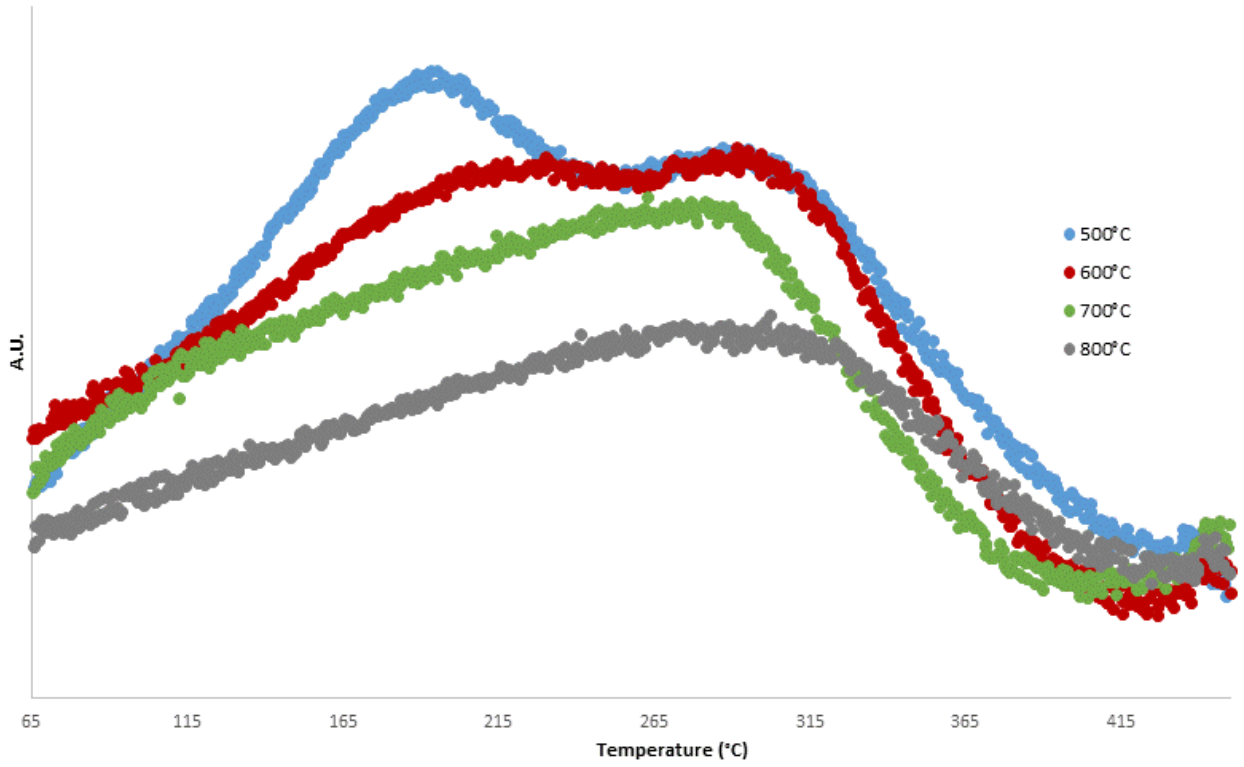

Figure 5-1: H_2 – TPR of Pt/Al_2O_3 catalyst with varying sintering temperatures from 500-800°C

The steady state NO oxidation conversion profiles for the aged PA catalysts are presented in Figure 5-2. The data is presented similarly to the previous chapter, where Figure 5-2 presents PA conversion profiles as a standalone without the overlay of the modeling efforts that were the focus of the previous chapter. Figure 5-2 shows that as sintering temperature is increased, the maximum conversion increases and the maximum conversion temperature decreases. These results are expected as Table 5-1 shows that the particle size increases with increasing sintering temperature, and literature has shown that NO is more easily oxidized over larger platinum particles on the Al_2O_3 support.

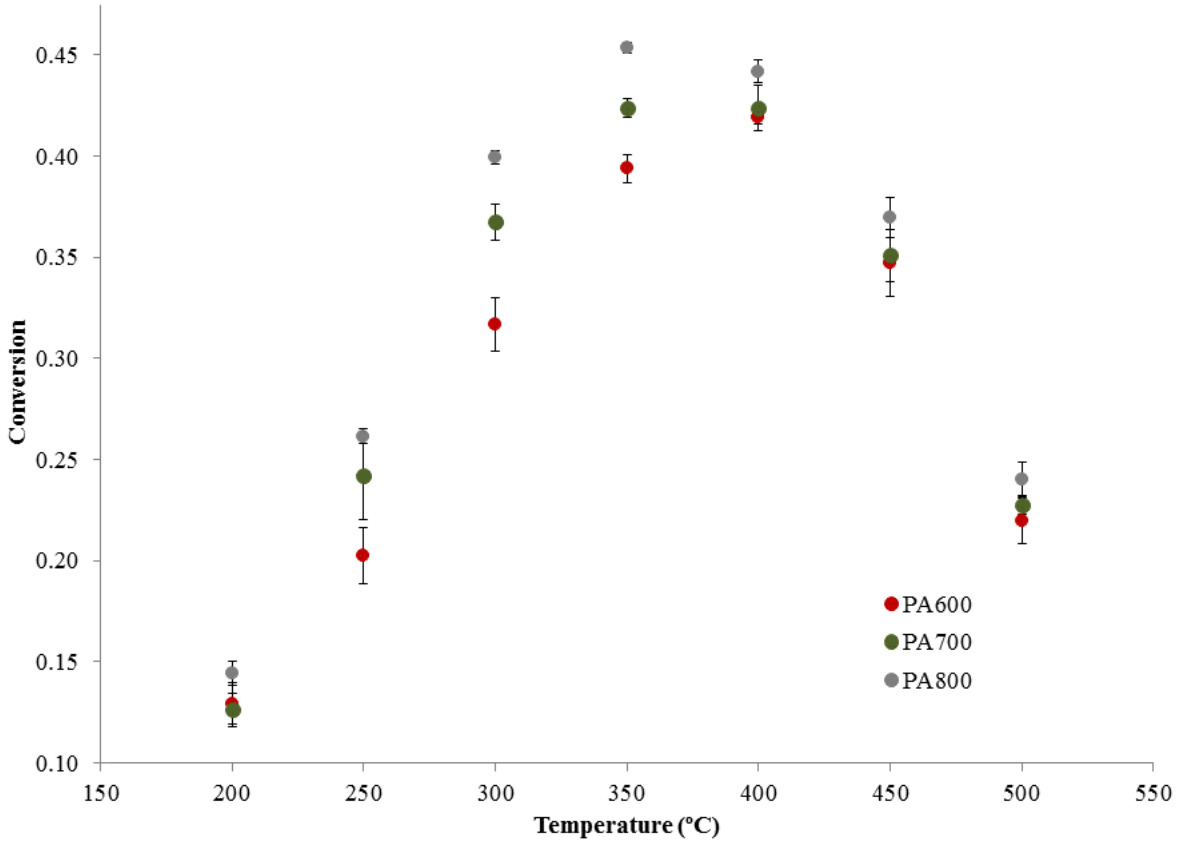

Figure 5-2: Isothermal steady state NO oxidation conversion for PA catalysts with varying sintering temperatures over the temperature range of 200-500ºC

5.3 Pt/Ba/Al_2O_3 catalyst characterization and reactivity

Ba as a storage component is an integral part of the LNT formulation. Therefore, it is necessary to include Ba in the catalyst formulation when investigating thermal degradation of LNT catalysts. TPR profiles presented in Figure 5-3 show two distinct H_2 consumption peaks. The first peak observed in the 100-150ºC range is associated with reduction of platinum. The second larger peak, beginning at 350ºC, is associated with the reduction of the storage component, barium. Similar to the PA catalyst, as sintering temperature is increased, the H_2-TPR peak associated with Pt decreases and shifts to higher temperatures. At the 800ºC catalyst

sintering temperature, the Pt reduction peak has nearly disappeared and shifted to a maximum of 145ºC. Again, this is due to the increase in particle size which impacts the availability of Pt for reduction. When comparing the Pt reduction peaks to those observed for the PA catalysts in Figure 5-1, the larger platinum particles found in the PBA catalysts have a narrow band of reduction and a reduced peak size relative to the PA catalysts sintered at the same temperature. This indicates a reduction in the amount of catalyst available, which is confirmed by the Pt particles size calculated by CO-chemisorption.

The peaks associated with Ba reduction show a similar trend to the Pt reduction peaks, shifting to higher temperatures and reducing in size. The start of the Ba reduction peak is shifted nearly 50ºC from 350ºC for the PBA600 catalyst to 400ºC for both the PBA700 and PBA800 catalysts.

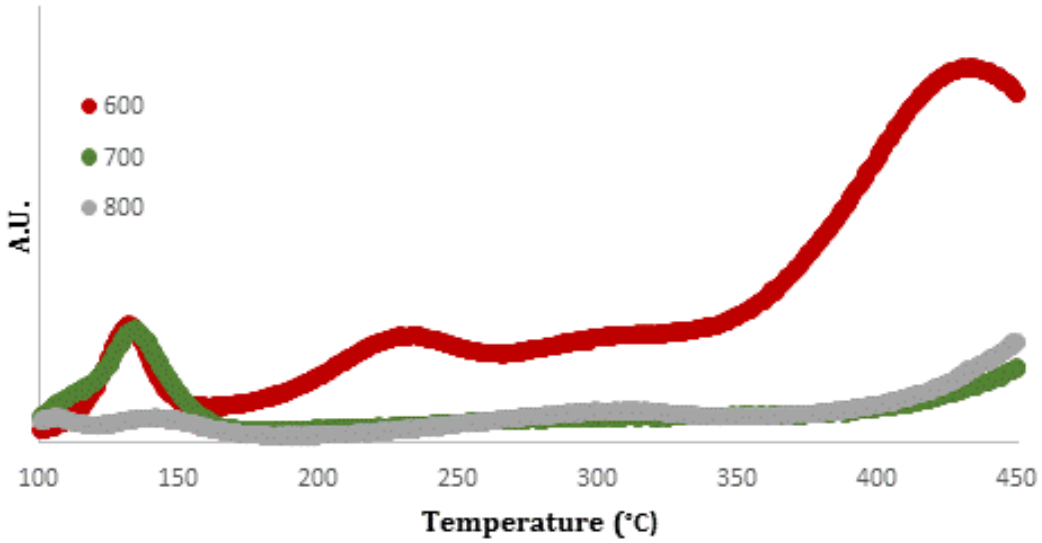

Figure 5-3: H_2 - TPR of Pt/Ba/Al_2O_3 with varying sintering temperature from 600 - 800ºC

The change in catalytic activity with sintering temperature after the addition of barium can be seen in the steady state NO oxidation profiles. Figure 5-4 shows the conversion of NO over the $Pt/Ba/Al_2O_3$ catalysts produced with varying sintering temperatures. As sintering temperature increases, maximum conversion decreases and the temperature at which maximum conversion is reached shifts to higher temperatures. The observed trend in NO conversion with sintering temperature is the opposite of that shown for the PA catalysts. Increasing sintering temperature, while not significantly impacting surface area of the PBA catalyst does result in an increase in the Pt particle size (Table 5-1) from 5.6nm at 600 to 19.87nm at 800. When comparing the PBA to PA catalyst it can be seen that Pt particle size is higher for all PBA catalysts relative to the identical aging condition in the PA catalysts. However, the Pt particle size of the PBA600 and PBA700 material is within the range of particle sizes observed for the PA catalysts. Recalling that the NO conversion increased with increasing particle size for the PA catalyst, the decreasing CO conversion trend in the PBA catalyst with increasing sintering temperature indicates that other factors are impacting the NO conversion over the PBA catalyst.

The addition of the barium has been shown to facilitate the oxidation of Pt in an oxidizing environment. The increase in Pt oxide formation has been attributed to a difference in the nature of Al_2O_3 supports relative to the BaO material. Where Al_2O_3 is electronphilic drawing electrons away from the Pt which are required for PtO formation, alkaline Ba decreases this effect which intern allows increased oxidation of Pt particles [9]. Furthermore, surface oxygen is more available in when BaO is added to the catalyst formulation additionally increasing oxidation of Pt during the NO oxidation reaction. This oxidation of the Pt would result in a reduction in the amount of Pt available for the conversion of NO. Thus, even though the Pt particles on the PBA600 and PBA700 are still within the range of Pt particle sizes for the PA catalyst, the

oxidation state of the Pt maybe very different in the barium containing materials. This change in oxidation state of the metal could result in the decreased activity observed with increased sintering temperature.

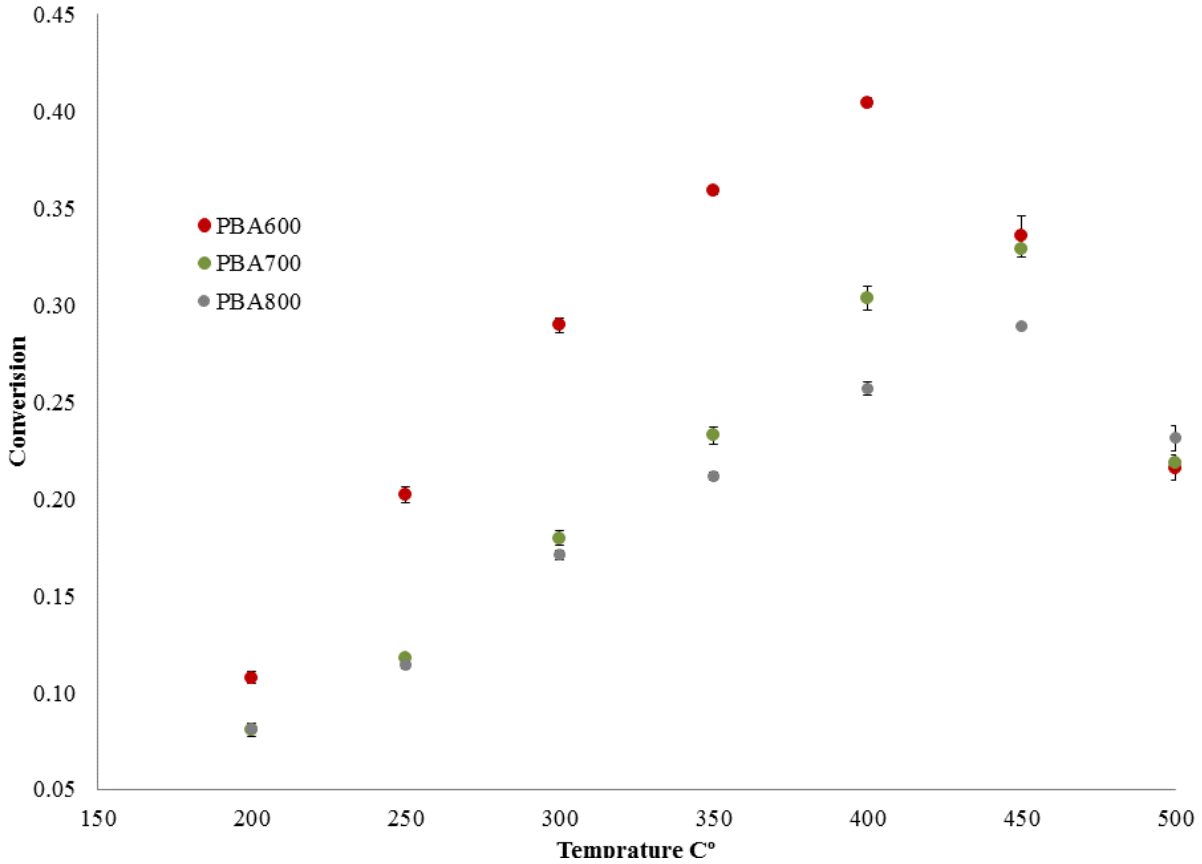

Figure 5-4: Isothermal NO oxidation conversion with temperature for PBA catalyst with varying sintering temperature from 600-800°C

5.4 $Pt/Ba/CeO_2/Al_2O_3$ catalyst characterization and reactivity

Ce addition has been shown to increase NO_x storage, abate degradation due to sulfation and decrease Pt particle size growth under aging conditions. As such, Ce is an important promoter in the LNT catalyst formulation [8, 10, 11]. An investigation of NO oxidation over LNT catalysts would not be complete without extending the investigation to include this promoting additive. Figure 5-5 shows the H_2-TPR profiles of the $Pt/Ba/CeO_2/Al_2O_3$ catalyst. H_2 uptake can be observed from 150 – 450ºC. The low temperature uptake peak associated with Pt reduction is the largest for the PBCA500 catalyst; however, the peak maximum occurs at the highest temperature 247ºC. The low temperature reduction peak is reduced for catalysts with increasing sintering temperature and the peak maximum decreases with sintering temperature. This is opposite to the trend observed for both the PA and PBA catalysts. The high temperature reduction peak associated with Ba reduction is apparent for all four catalyst sintering temperatures. The largest reduction peak occurs for the lowest sintering temperature PBCA500 and reduction peak size decreases with sintering temperature for all catalysts. Furthermore, the peak maximum is shifted to higher temperatures with increasing catalyst sintering temperature.

The trends in reduction in peak size and temperature of maximum reduction for barium indicate that as sintering temperature is increased, surface barium species become both less available and more stable based upon both the size of the reduction peak as well as the temperature at which reduction occurs. While the size of the low temperature reduction peak appears to indicate significant Pt reduction, it is important to note that Ce reduction is also possible during the TPR experiments, and could contribute to overall H_2 consumption and the peak sizes observed. The actual Pt reduction and thus, available noble metal is likely lower.

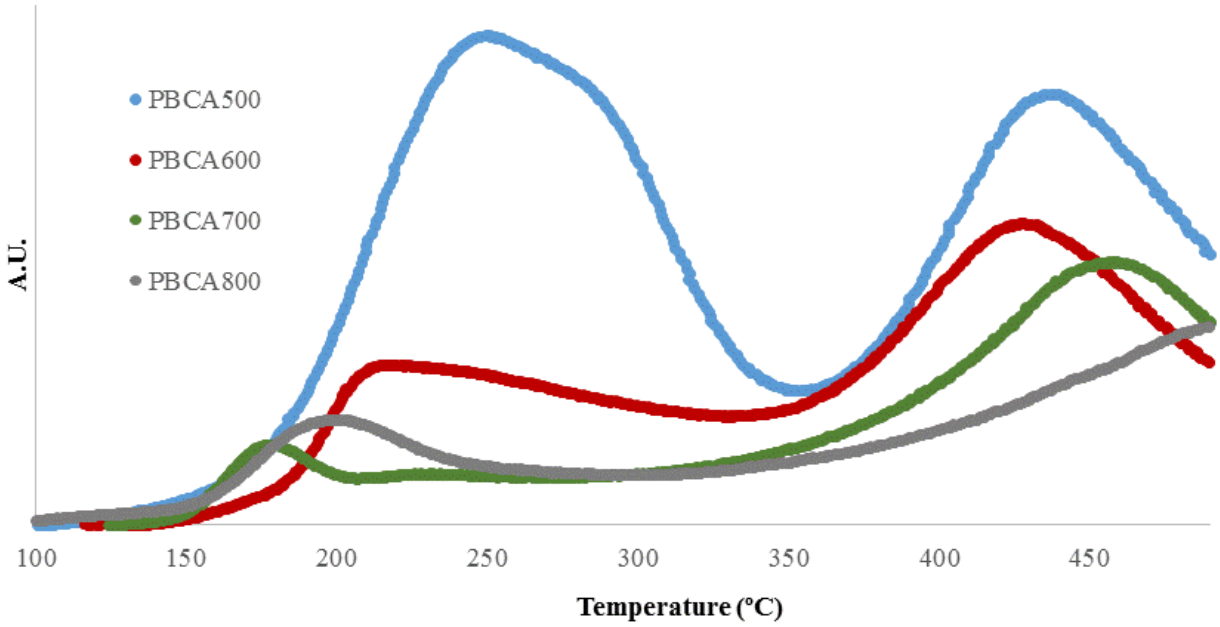

Figure 5-5: H_2 - TPR of PBCA catalysts with sintering temperature varying from 500-800°C

The isothermal steady state NO oxidation profiles in Figure 5-6 show similar trends with sintering temperature to the PBA profiles in Figure 5-4. The PBCA catalyst shows that as sintering temperature increased, a decrease in maximum conversion and an increase in the temperature at which maximum conversion is achieved is observed. The measured Pt particle sizes on the PBCA catalysts are within the range of Pt particle sizes observed over the PA catalyst.

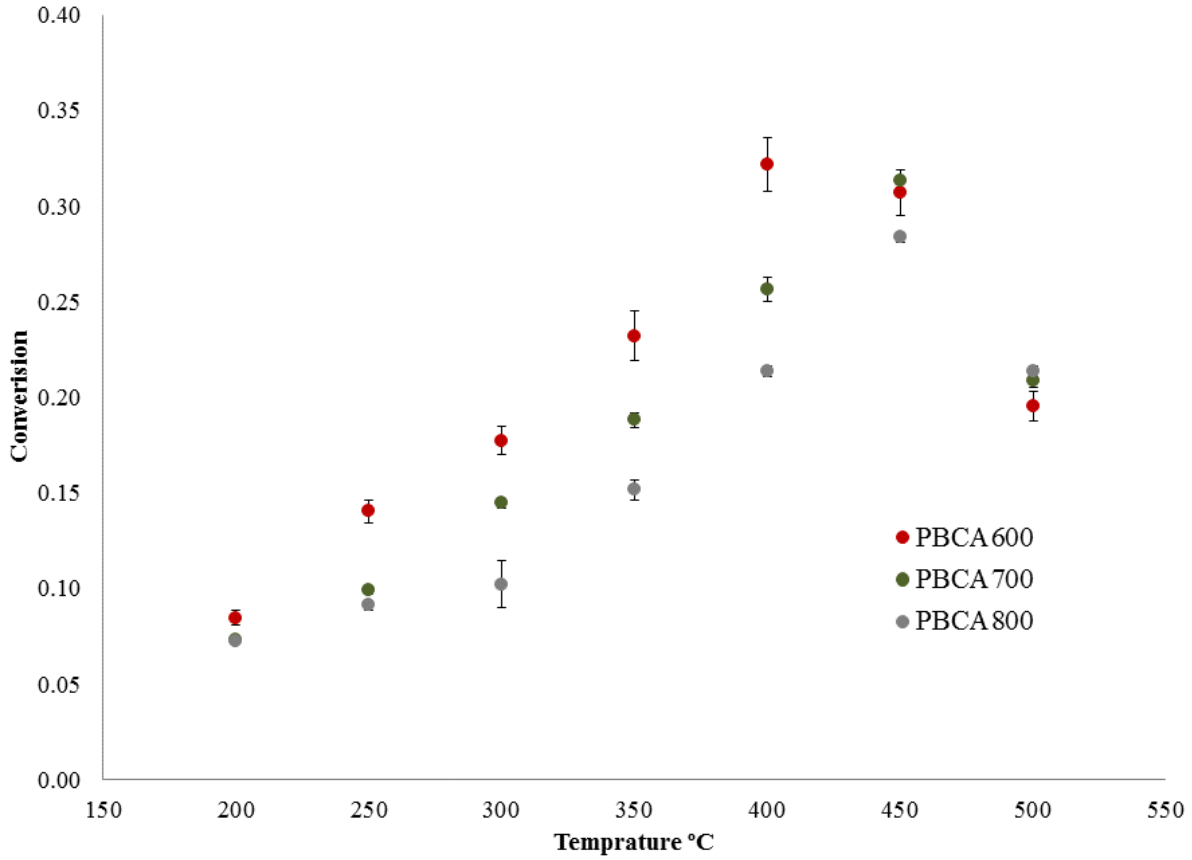

Figure 5-6: Isothermal SS NO oxidation over PBCA catalysts with varying sintering temperature 600-800°C

Therefore, the changes in NO oxidation conversion profile are again a function of more than just the morphology of the noble metal. Given that the incorporation of Ba in the formulation resulted in similar trends in NO conversion with increasing sintering temperature, it is reasonable to ascribe the trends observed in Figure 5-6 to the Pt-Ba interaction. However, a closer comparison of the catalysts at similar sintering temperatures shows the presence of ceria plays a critical role.

Figure 5-7 shows the NO oxidation profiles for the PA600, PBA600, and PBCA600 catalysts. The PA catalyst has the highest maximum conversion. The conversion of NO over the

PBA catalyst is only slightly lower than the PA catalysts. However, the PBCA600 shows substantially decreased conversion over the entire kinetic regime and a depression in the 250-350ºC temperature range.

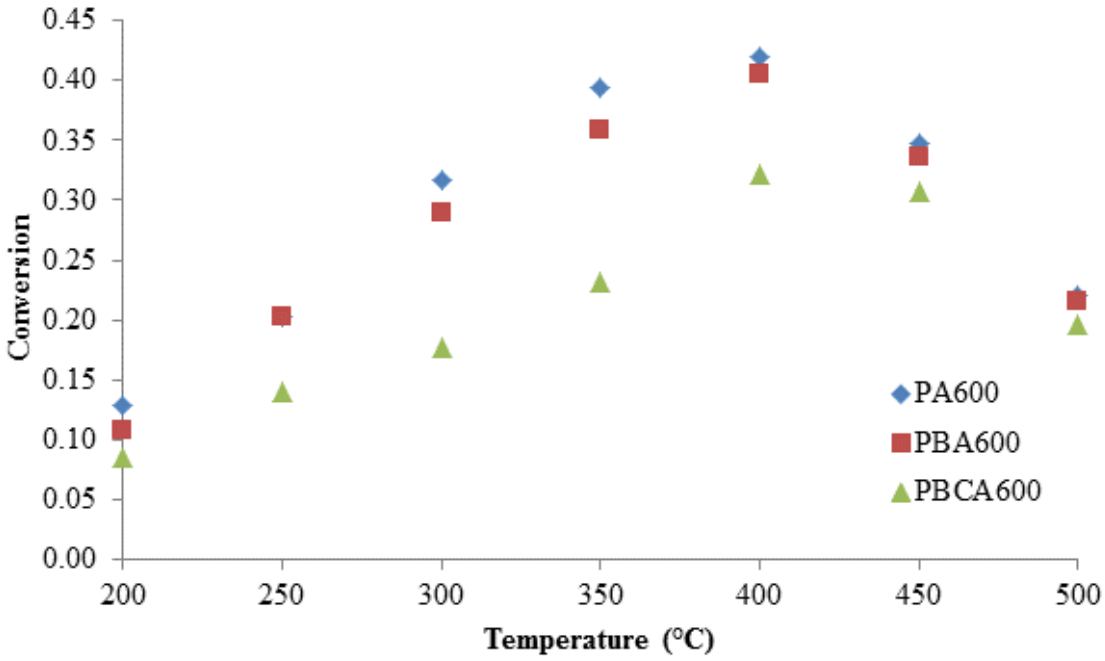

Figure 5-7: Isothermal SS NO oxidation over PA, PBA and PBCA catalysts at the 600ºC sintering temperature

It has already been established that the NO conversion trends with increasing sintering temperature are different for the PBA and PBCA catalysts compared to the PA catalyst. The oxidation state of Pt may play a key role in understanding these differences. Small Pt particles on the PA catalysts are readily oxidized and, thus, NO oxidation occurs more readily on larger particles which resist oxidation in the oxidative environment of lean phase LNT operation. The PBA catalysts have larger particles, but an increased affinity to oxidize as a result of the Pt interaction with alkaline Ba. It is well known that ceria has high oxygen storage and release

capacity [12, 13], which again could significantly impact oxidation state of Pt and thus, the reactivity of Pt for NO conversion.

Figure 5-8 shows a comparison of the PBA800 and PBCA800 catalysts. In contrast to what was observed after sintering at 600ºC, the PBCA800 had a higher conversion at all temperatures between 200ºC and 500ºC compared to the PBA800 catalyst. Thus, the addition of Ce resulted in improved performance at the highest sintering temperatures. Comparison of the catalyst properties shows that the Pt particles size is increased substantially in the PBA catalyst. PBA800 shows that largest Pt particles at nearly 20nm, while the PBCA800 catalyst shows an increase in Pt particle size to only 7nm. While the addition of Ce initially serves to decrease conversion by facilitating the oxidation of Pt particles, it appears that at higher sintering temperatures the Ce anchoring effect may help to reduce the impact of thermal aging on NO conversion.

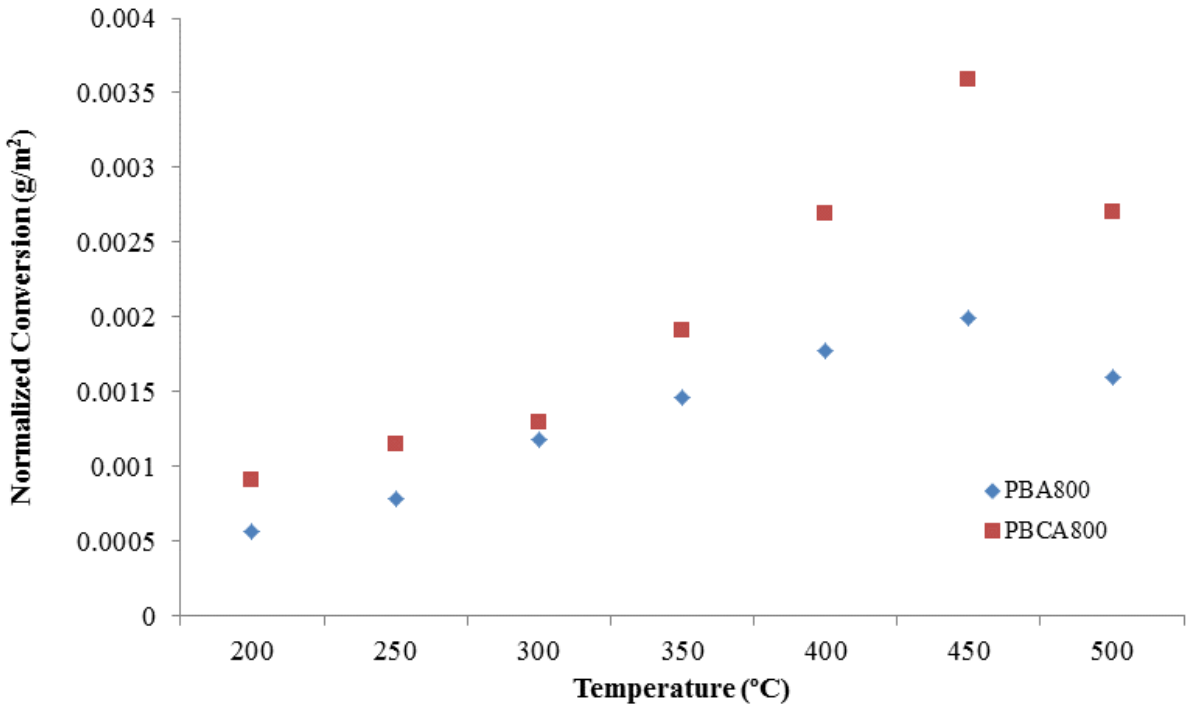

Figure 5-8: Isothermal SS NO oxidation over PA, PBA and PBCA catalysts at the 600ºC sintering temperature

To further illustrate that dynamics of Pt particles size changes and Pt particle oxidation in each of three catalysts formulations, Table 5-2 shows each of the effects proposed and the contribution of these effects to each catalyst formulation. The PA catalyst shows a substantial increase in activity with particle size, no Ba interaction and a minimal effect due to the decrease in available particles with increased Pt particle size due to high Pt particle activities. PBA shows no observable increase in activity with particle size due to the other two effects, decrease in available metallic sites due to Ba addition, and decrease in available sites due to substantial increases in Pt size with thermal aging. Finally, the PBCA catalyst shows no observable increase due to Pt particle size growth as a result of the two additional effects. A decrease in metallic sites due to the oxidation of Pt particles (this is increased due to Ce addition), and a decrease in available Pt due to particle size growth (this is decreased relative to PBA due to the Ce addition).

The change in particle size growth for the PBA and PBCA catalyst are highlighted because this effect is important in understand the changes observed from Figure 5-7 to Figure 5-8. While Ce promotes oxidation and results in the decreased NO oxidation observed in Figure 5-7, the anchoring effect of Ce upon thermal aging reduces the sintering effect of aging and cause the PBCA catalyst to outperform the PBA catalyst upon aging at 800ºC, which is shown in Figure 5-8.

Table 5-2: Effects of catalyst formulation on the NO oxidation reaction

Effect	(Increase in Activity)	(Decrease in available metallic sites)	(Decrease in available sites)
Change	Pt Particle Size increase	Pt Oxidation due Ba interaction	Pt particle size increase
Catalyst			
PA	yes, substantial	No	Yes, minimal (high activity)
PBA	Not observable due to substantial decrease in available sites	Yes, Substantial	Yes, substantial
PBCA	Not observable due to substantial decrease in available sites	Yes, Substantial (additional deactivation due to Ce)	Yes, minimal (Ce anchoring)

5.5 Conclusions

The data presented indicates there is a substantial change in the NO oxidation profiles of LNT catalyst with varying support materials. In addition, the change in catalysts morphology and NO oxidation with thermal degradation is different for all three catalysts formulations. The traditional Al_2O_3 support shows the trend most commonly observed in the literature where reduction of the noble metal is more easily facilitated with smaller platinum particles. The NO oxidation reaction is facilitated better over larger platinum particles.. However, the observation of increased NO oxidation with particle size holds for only the Al_2O_3 supported material. For both the BaO/Al_2O_3 and the $BaO/CeO_2/Al_2O_3$ supports, as platinum particle size increases the

NO oxidation conversion decreases. Thus, the NO oxidation conversion trend with catalyst degradation depends on more than just platinum particle size when other metals are present. Furthermore, the reducibility of the Pt can be eliminated as the cause of the changes in NO oxidation because the TPR profiles for all the catalysts exhibit the same trend. As Pt particle size is increased, the H_2 consumption peak is decreased for all catalysts. It is shown that oxidation state of Pt is the property that dictates NO oxidation for all three of the catalysts. The oxidation state is affected by a number of factors as increasing complexity; however, the NO oxidation conversion profile can be interpreted in terms of Pt oxidation state in all three catalysts.

5.6 References

1. Mahzoul, H., J. Brilhac, and P. Gilot, *Experimental and mechanistic study of NOx adsorption over NOx trap catalysts.* Applied Catalysis B: Environmental, 1999. **20**(1): p. 47-55.
2. Fridell, E., et al., *The mechanism for NOx storage.* Catalysis Letters, 2000. **66**(1-2): p. 71-74.
3. Olsson, L., et al., *A Kinetic Study of NO Oxidation and NOx Storage on Pt/Alumina and Pt/BaO/Alumina.* J. Physical Chemistry, 2001. **105**: p. 6895-6906.
4. Olsson, L. and E. Fridell, *The influence of Pt oxide formation and Pt dispersion on the reactions NO2 <-> NO+1/2 O-2 over Pt/Al2O3 and Pt/BaO/Al2O3.* Journal of Catalysis, 2002. **210**(2): p. 340-353.
5. Epling, W., et al., *Overview of the Fundamental Reactions and Degradation Mechanism of NOx Storage/Reduction Catalysts.* Catalysis Reviews, 2004. **46**(2): p. 163-245.
6. Infantes-Molina, A., et al., *Characterization and reactivity of Ce-promoted PtBa lean NOx trap catalysts.* Catalysis Today, 2012. **197**(1): p. 178-189.
7. Damyanova, S. and J.M.C. Bueno, *Effect of CeO2 loading on the surface and catalytic behaviors of CeO2-Al2O3-supported Pt catalysts.* Applied Catalysis A: General, 2003. **253**(1): p. 135-150.
8. Nagai, Y., et al., *Sintering inhibition mechanism of platinum supported on ceria-based oxide and Pt-oxide–support interaction.* Journal of Catalysis, 2006. **242**(1): p. 103-109.
9. Olsson, L. and E. Fridell, *The Influence of Pt Oxide Formation and Pt Dispersion on the Reactions of NO2<-> NO +1/2 Oxygen over Pt/Alumina and Pt/ BaO/Alumina* Journal of Catalysis, 2002. **210**: p. 340-353.
10. Easterling, V., et al., *Effect of ceria on the desulfation characteristics of model lean NO x trap catalysts.* Catalysis Today, 2010. **151**(3): p. 338-346.
11. Ji, Y., T.J. Toops, and M. Crocker, *Effect of Ceria on the Sulfation and Desulfation Characteristics of a Model Lean NO x Trap Catalyst.* Catalysis letters, 2009. **127**(1-2): p. 55-62.
12. Santos, A.C.S.F., et al., *The effect of ceria content on the performance of Pt/CeO2/Al2O3 catalysts in the partial oxidation of methane.* Applied Catalysis A: General, 2005. **290**(1–2): p. 123-132.
13. Pereda-Ayo, B., et al., *Influence of ceria loading on the NO x storage and reduction performance of model Pt–Ba/Al 2 O 3 NSR catalyst.* Catalysis Today, 2015. **241**: p. 133-142.

Chapter 6: Effects of Thermal Degradation on NO_x Storage over $Pt/Ba/CeO_2/Al_2O_3$ Catalysts

The previous chapter identified the changes in the catalysts' physical characteristics, as well as the ability of these catalysts to oxidize NO. It has been shown that NO oxidation conversion varies substantially with thermal oxidation of all catalysts formulations [1, 2]. It is also clear that while NO oxidation is the initial step in the storage of NO_x the mechanism of storage varies with formulation [3]. Literature has not definitively established the effect of catalyst aging on NO_x uptake and the NO_x, uptake mechanism over $Pt/Ba/CeO_2/Al_2O_3$. To determine the effect of aging on NO_x uptake, long term storage experiments have been conducted. Long term refers to 1 hr storage times, as this is much longer than the typical lean phase, which generally operates between 1 and 3 minutes.

In Chapter 2: Overview of LNT Catalysis, it has been established that long term storage occurs in three stages or regimes. The regimes have been explained previously but are visually presented in Figure 6-1.

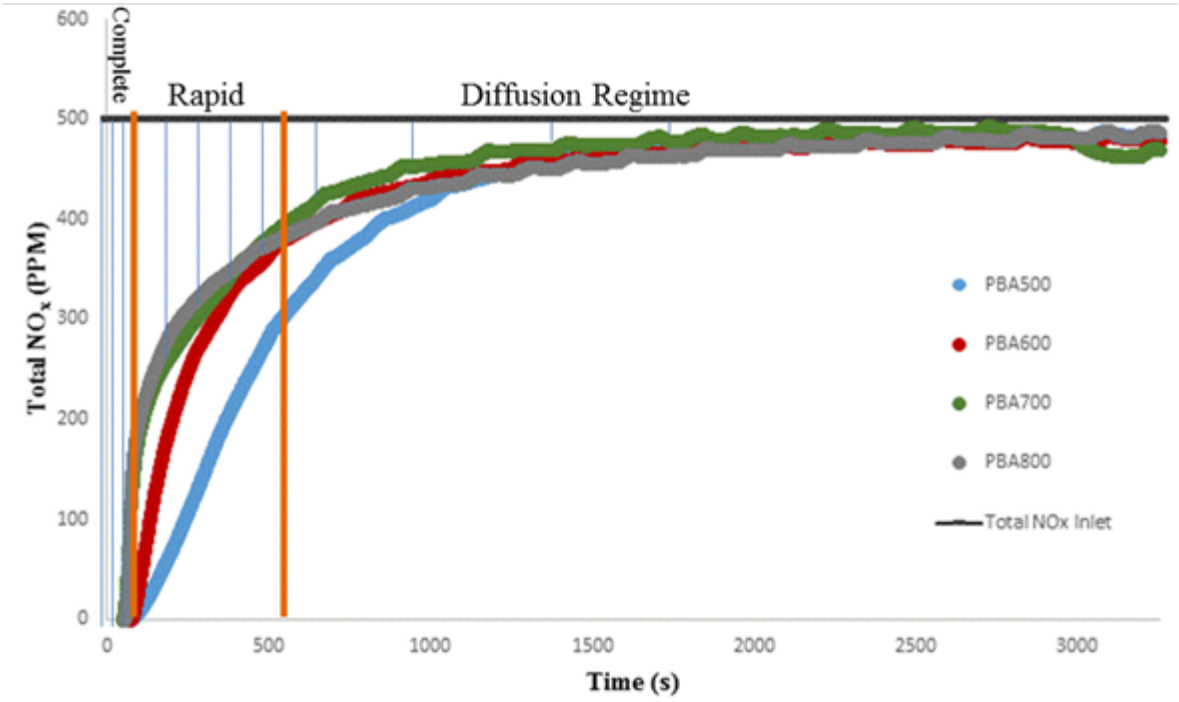

Figure 6-1: NO_x uptake profile at 350ºC of PBA catalysts with varying sintering temperature from 500-800ºC

Figure 6-1 shows the NO_x uptake profile of the PBA catalysts produced using production condition 1 as described in Chapter 3: Materials and Methods. The barium impregnation step was conducted at a calcination temperature of 800ºC. With the high intermediate calcination temperature, the storage component was sintered such that uptake was hindered substantially. This is evidenced by the fact that nearly no complete uptake is observed. PBA600-800 show only nominal rapid uptake. Rapid uptake is associated with active barium far away from Pt-Ba adjacent sites. Condition 1 is ideal for negating the effect of storage material sintering on the noble metal (where noble metal sintering is the focus of the previous chapter). However, condition 1 is not ideal for the investigation of thermal degradation on NO_x storage. Because barium can sinter substantially a high intermediate calcination temperatures, storage degradation

must be evaluated via thermal aging under condition 2. Furthermore, XRD confirms the formation of barium aluminate ($BaAl_2O_4$). $BaAl_2O_4$ is significantly less active than LT-$BaCO_3$ (XRD can be found in appendix I).

Literature has shown thermal degradation of $Pt/Ba/Al_2O_3$ catalyst can have a significant impact on catalyst morphology and NO_x uptake [4]. In Chapter 5: Effects of thermal degradation on NO oxidation, the addition of cerium has been shown to affect LNT catalyst performance under thermal degradation. Cerium has also been shown to promote mixed metal oxides in aged LNT catalysts [5]. It is therefore, extremely important to understand the impacts of thermal aging on NO_x uptake in Ce containing LNT catalysts.

6.1 NO_x Storage over $Pt/Ba/CeO_2/Al_2O_3$ at 250ºC

NO_x storage can occur over a range of temperatures in real world exhaust. The following study has been conducted over a range of uptake temperatures and exhaust conditions. At temperatures 200ºC and below NO_x storage has been shown to proceed via a mechanism that does not include NO oxidation. Also the ideal operating conditions for $Pt/Ba/CeO_2/Al_2O_3$ catalysts has been shown to be between 250-350ºC [5]. Understanding how storage changes with degradation in the ideal operating range will be most useful for real world applications. As such, the starting point for NO_x uptake has been chosen as 250ºC.

Figure 6-2 shows NO_x uptake profiles at 250ºC for the PBCA catalysts. The dark grey lines outlining each of the labeled NO_x uptake profiles are error bars for each point calculated by the standard deviation of runs performed in triplicate. The complete uptake regime is short for all four catalysts at the lowest uptake temperature. It can be seen in Figure 6-3 that complete uptake represents no more than 8.8% of any catalysts' total uptake. PBCA600 shows the longest

and most substantial instance of rapid uptake followed by PBCA700 and PBCA500. Thermal degradation impacts the PBCA800 catalyst the most where very little complete uptake is observed and the slow uptake regime is reached quickly. The PBCA600 catalyst achieves the highest total storage capacity followed by the PBCA500 catalyst. The change in transition from rapid to slow uptake can be observed for the PBCA700 catalysts where there is a clear distinction between rapid and slow uptake at 230 seconds. Slow uptake for the PBCA700 catalysts is more substantial when compared to the PBCA800 material.

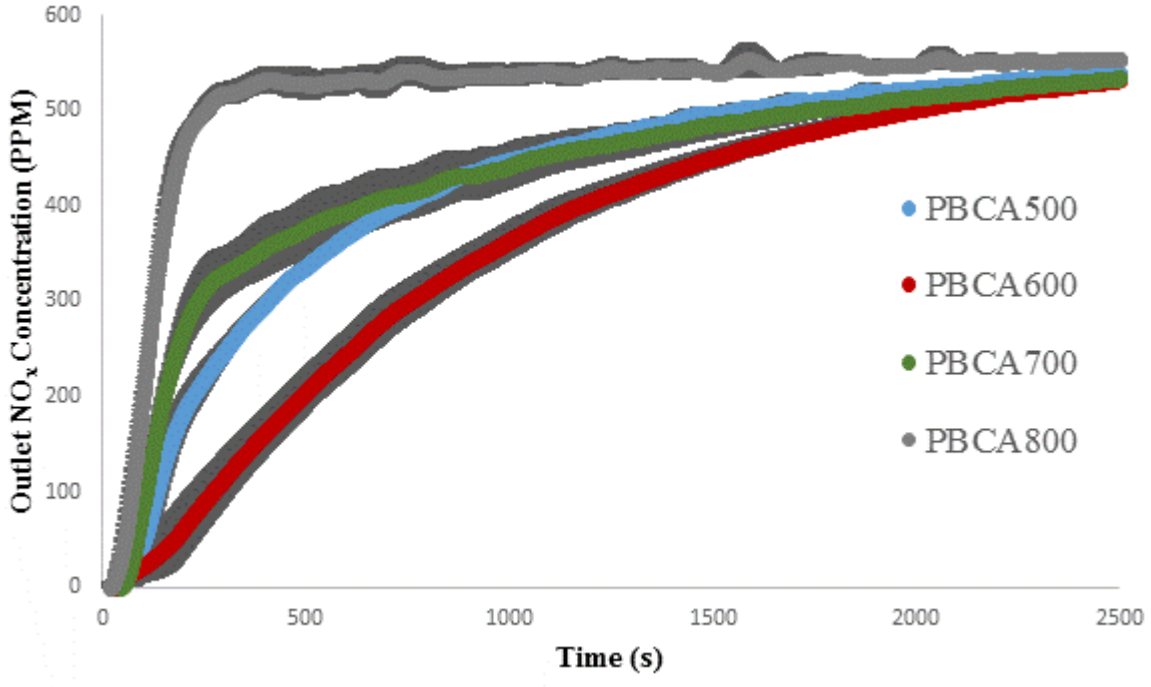

Figure 6-2: NO_x Uptake Profile at 250°C for $Pt/Ba/CeO_2/Al_2O_3$

Figure 6-3 shows a bar graph of the total NO_x uptake by catalyst and uptake regime. Uptake is calculated as the integrated area between the NO_x inlet step change and the observed outlet concentrations as illustrated by light blue lines where the orange lines indicate regime distinctions in Figure 6-1. The comparison of each of the calculated uptake amounts clearly

elucidates the differences in total uptake for each of the regimes with catalyst aging. The rapid uptake regime represents the largest portion of the total uptake for all catalysts, where the only aged catalyst which has significant uptake during the diffusion limited regime is the PBCA700 catalyst. The difference in diffusion/rapid uptake regimes for the PBCA700 catalyst may be due to the calculation definition for the rapid-diffusion transition. While the 0.1PPM/10 seconds variation has been shown to be an accurate transitional definition for all other catalysts temperatures and aging conditions, the stark transition from rapid to the slow "diffusion" regime for the PBCA700 catalyst at the 250ºC uptake temperature may be less accurate.

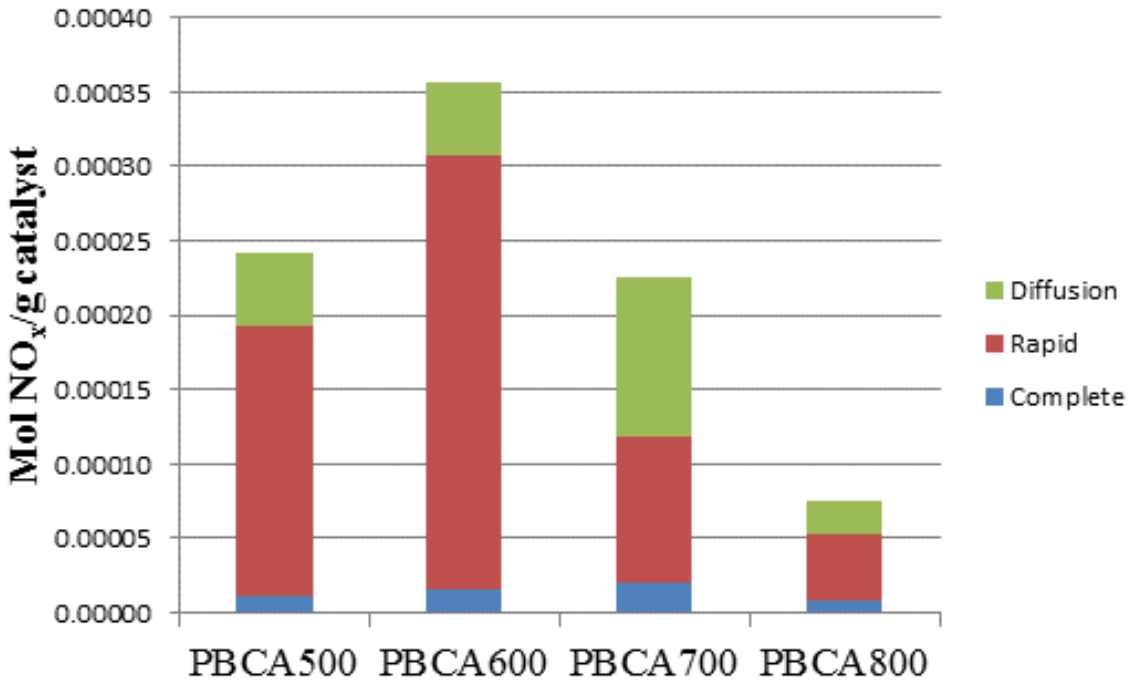

Figure 6-3: Total NO_x Storage at 250ºC separated by uptake regime for PBCA catalysts with varying sintering temperature

The NO_x storage experiments at 250ºC show that thermal aging induces substantial variations in total uptake at low temperatures. It is hypothesized that the increase in conversion observed with sintering temperature from PBCA500 to PBCA600 is due to the mechanism of

$BaAl_2O_4$ formation. Literature describes the formation of LT-$BaCO_3$ and HT-$BaCO_3$ where the LT carbonate forms on top of a more stable HT carbonate base layer[6]. As a result, the Ba form with the most Ba-Al adjacency is HT-$BaCO_3$. Because of the Ba-Al adjacency, the first species to transition to the $BaAl_2O_4$ form is the HT-$BaCO_3$. Literature has also shown that while HT-$BaCO_3$ is inactive for NO_x storage, $BaAl_2O_4$ has some activity for storage[5, 6]. Surface characterization shown in Figure 6-8 confirms that $BaAl_2O_4$ does have some activity for surface adsorption. Therefore, moderate amounts of $BaAl_2O_4$ formation may in fact promote NO_x - storage as in the case of the increased NO_x storage observed in the PBCA600 at 250ºC. Also, due to the reduction in storage capacity of $BaAl_2O_4$ with decreased storage temperature, as storage temperature is increased the effect of $BaAl_2O_4$ formation is likely to be decreased.

6.2 NO_x Storage over Pt/Ba/CeO_2/Al_2O_3 at 300ºC

The 300ºC uptake temperature is the intermediate storage temperature studied to bridge the gap between the differences observed at the low and high uptake temperatures. It is hypothesized that the effect of $BaAl_2O_4$ formation will have a decreased effect on NO_x storage profile with the increased temperature and total storage will be increased.

Figure 6-4 shows that the PBCA600 and PBCA500 catalysts have the longest complete uptake, as well as the largest amount of NO_x stored in the rapid uptake regime. It can be observed however that for this moderate storage temperature there is no observable difference between the PBCA500 and PBCA600 material in terms of uptake profile when compared with error overlaid. The PBCA700 material has a flatter uptake slope in the rapid regime when compared to the 250ºC uptake temperature. This change in slope translates to increased uptake

with increased operating temperature where, PBCA800 continues to show substantially decreased uptake in all regimes relative to PBCA500 and PBCA600. When the total uptakes are compared, the PBCA800 uptake is shown to achieve less than 34% of the total uptake observed for PBCA500, PBCA600.

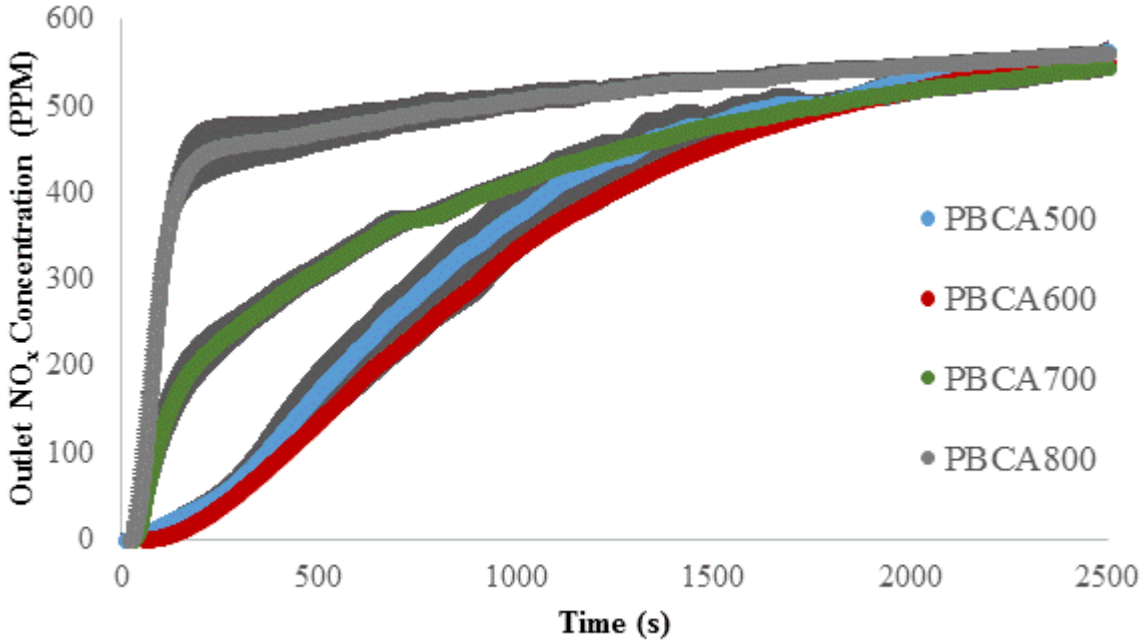

Figure 6-4: NO_x Uptake Profile at 300ºC for $Pt/Ba/CeO_2/Al_2O_3$

Figure 6-5 shows the total uptake integrated by regime for each catalyst profile shown in Figure 6-4 at 300ºC. The maximum uptake is once again observed over the PBCA600 catalyst. The PBCA600 catalyst shows an increase in complete uptake. The percentage of complete uptake represents of the total uptake shows an increase from 5% of the total uptake at 250ºC to 12% of the total uptake at 300ºC. Complete uptake for the PBCA600 catalyst is also two times greater than any of the other thermally aged catalysts. This shows that while the PBCA500 and PBCA700 catalysts have increased in conversion with increased uptake temperature, the

PBCA600 catalyst has much more complete uptake, which is associated with stable nitrates and increased Pt-Ba adjacency.

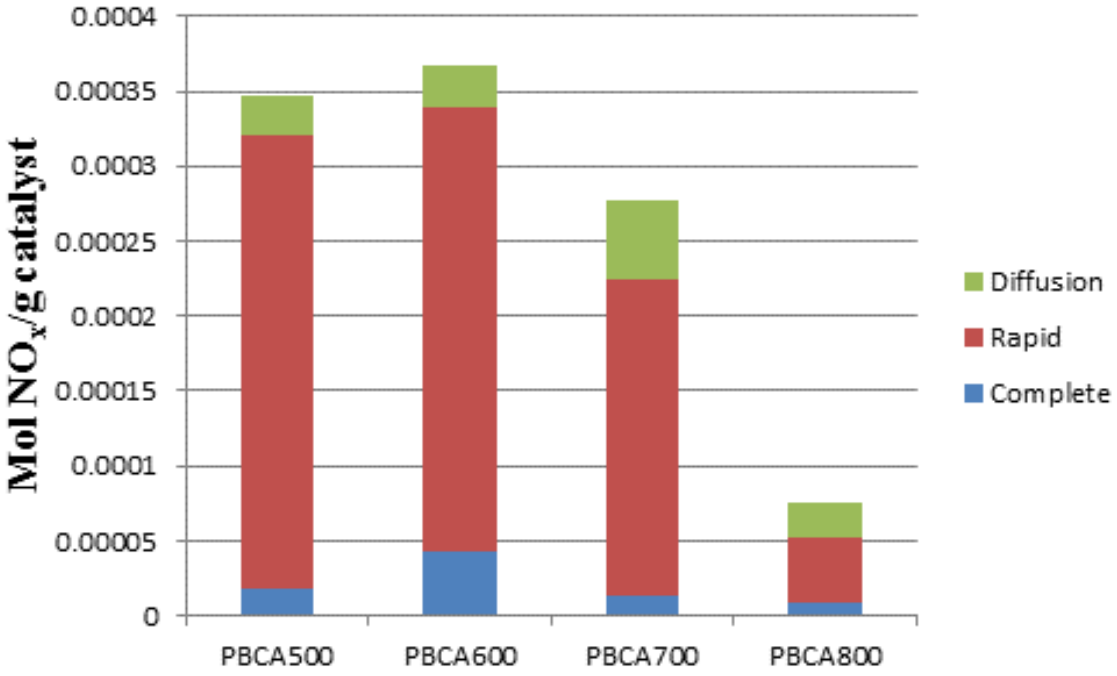

Figure 6-5: Total NO_x Storage at 300°C separated by uptake regime for PBCA catalysts with varying sintering temperature

Comparison of the total uptakes in Figure 6-3 and Figure 6-1 shows that the thermal aging temperature of 800ºC is sufficient not only to degrade low temperature uptake but also uptake in the moderate temperature regime. Less variation is observed in total uptake as uptake temperature is increased, specifically between the PBCA500 and PBCA600 catalysts. The PBCA600 catalyst still shows variation in complete uptake, although the total uptake for PBCA500 and PBCA600 are very close. The increase in complete uptake for the PBCA600 catalysts indicates that this catalyst has better storage properties than the PBCA500 material.

This is also an indicator that analysis of surface storage could increase the understanding of the storage change with thermal degradation beyond what can be obtained via the integration of uptake profiles by regime.

6.3 NO_x Storage over $Pt/Ba/CeO_2/Al_2O_3$ at 350ºC

The pervious data shows that as storage temperature is increased, the effect of catalyst aging is reduced. It is hypothesized that a further increase in sintering temperature will result in greater similarity in the uptake profiles between the aged catalysts. This is a result of the increased ability of $BaAl_2O_4$ to store NO_x with increased temperature.

Figure 6-6 contains the uptake profiles for the thermally aged catalyst with NO_x uptake conducted at the highest temperature measured, 350ºC. At 350ºC, the PBCA500, PBCA600, and PBCA700 materials all show similar uptake profiles through the rapid uptake regime. Also, similar to the first two uptake temperatures, the PBCA800 catalyst shows the fastest approach to the diffusion limited regime. The PBCA800 catalyst shows both the complete uptake and rapid uptake regimes are finished significantly earlier than the other three catalysts. As a result of the similarity in the uptake profiles, the total uptake for PBCA500, PBCA600, and PBCA700 vary by less than 5%.

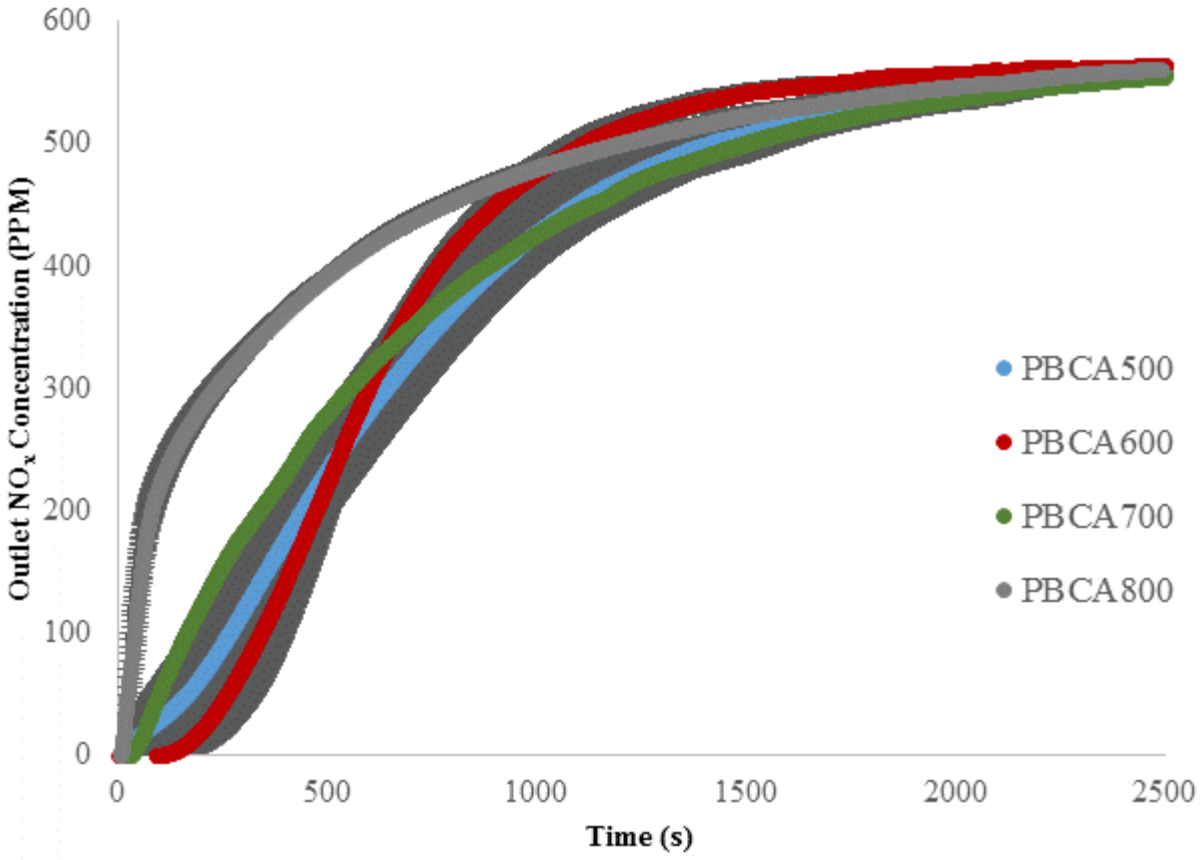

Figure 6-6: NO_x Uptake Profile at 350°C for $Pt/Ba/CeO_2/Al_2O_3$

As with the previous two uptake temperatures, the total uptake segmented by uptake regime is presented for each of the thermally aged catalysts in Figure 6-7. Uptake calculated for the PBCA800 catalyst is reduced by nearly 35% when compared to the other three catalysts. What is not initially obvious from Figure 6-6 is the difference in complete uptake when comparing the PBCA600 catalyst at the different uptake temperatures. Complete uptake is increased substantially with uptake temperature for the PBCA600 catalyst as uptake temperature is increased. This trend is not observed for the PBCA700 or PBCA800 catalysts. The complete uptake regime is associated with the rapid spillover of NO_x from Pt to adjacent barium sites, which coupled with the rapid uptake regime, represents the entire surface uptake. Because

$BaAl_2O_4$ is more available for storage at higher uptake temperatures, the increased Ba available from the $BaAl_2O_4$ – HT-$BaCO_3$ transition has become more accessible, which intern results in a greater number of Pt particles adjacent to active Ba sites. Thus, the increase in complete storage with temperature results in the increase in Pt-Ba adjacency and increased complete uptake.

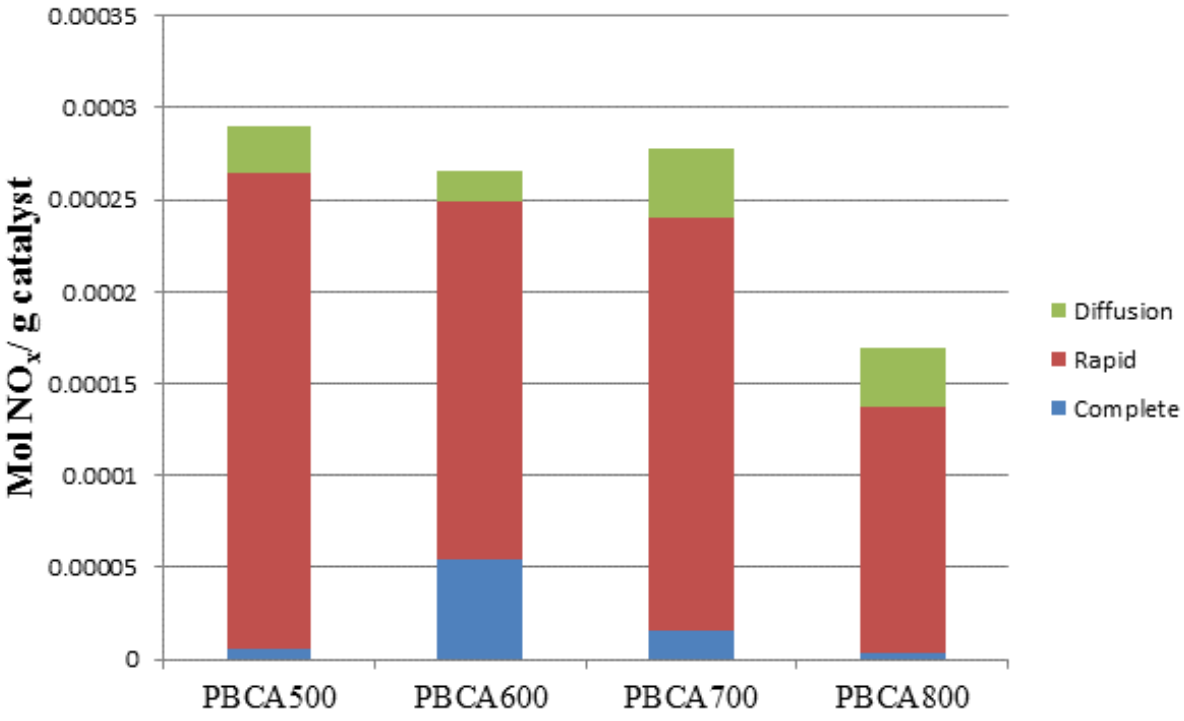

Figure 6-7: Total NO_x Storage at 350ºC separated by uptake regime for PBCA catalysts with varying sintering temperature

When the uptake temperature is increased from 250ºC to 350ºC, differences that were observed in the PBCA500, PBCA600, and PBCA700 catalysts at 250ºC are completely gone. The only catalyst that shows a decrease in total uptake is the PBCA800. Separating uptake by regime also shows that the 600ºC sintering temperature induces the most complete uptake when compared to the other catalysts at the highest uptake temperature.

In the following section, the uptake profiles and integrated NO_x uptakes have been connected to FT-IR both pre and post storage. Variations in consumed carbonates and observed nitrates can help to connect the performance of the aged catalysts in each regime to the nature of the barium as thermal aging is induced.

.

6.4 Surface Analysis of PBCA aged catalysts

FT- IR has been employed to determine the change in surface species with aging temperature and can be used to further examine the changes in uptake with catalyst sintering temperature and uptake conditions. Analysis of FT-IR to determine NO_x adsorption is sometimes complicated by the fact that nitrate adsorption peaks can be masked by the concurrent desorption of CO_3^- which occurs under storage conditions [7-9].

Figure 6-8 shows the FT-IR spectra of the as prepared catalysts with varying aging temperatures. A substantial CO_3^- peak at the 1420 cm^{-1} wave number is observed for all catalysts. The peak decreases with sintering temperature where the largest decrease in carbonate peak area exists between the PBCA500 and PBCA600 catalysts. The observation of decreasing carbonate is confirmed when the XRD spectra is compared for all catalysts.

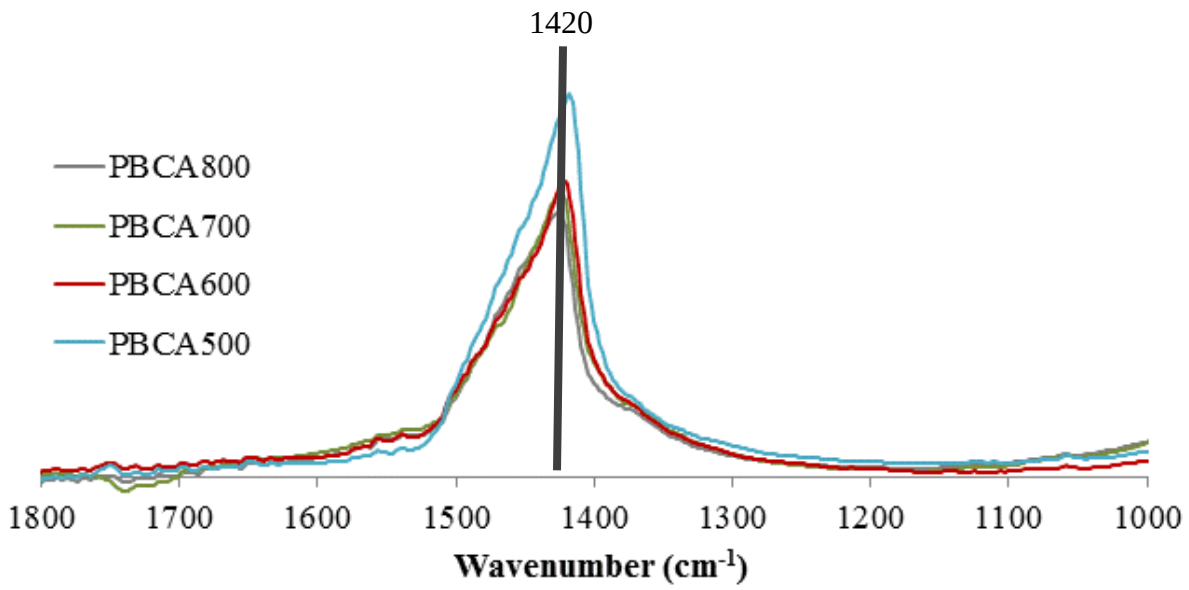

Figure 6-8: shows FT-IR spectra of PBCA catalysts prior to NO_x storage

It can be seen in Figure 6-9 that as sintering temperature is increased, the amount of bulk $BaCO_3$ observed via XRD is reduced significantly. When XRD is compared to the FT-IR of the as prepared catalysts, there is a strong correlation between surface carbonates and bulk carbonates. In both spectra, the PBCA500 catalyst has substantially more carbonates observed than the other three catalysts. The PBCA800 catalyst has very little bulk carbonate; however, there is still surface carbonates observed via FT-IR. The reduction in carbonates also coincides with an increase in $BaAl_2O_4$. The Ba in PBCA800 is almost entirely in the form of $BaAl_2O_4$. As shown in the literature, carbonates are observed on $BaAl_2O_4$ and $BaAl_2O_4$ has reduced NO_x uptake relative to $BaCO_3$ [10]. It is therefore expected that, even as the $BaAl_2O_4$ formation is increased, some carbonate formation is still observed and NO_x storage is still possible.

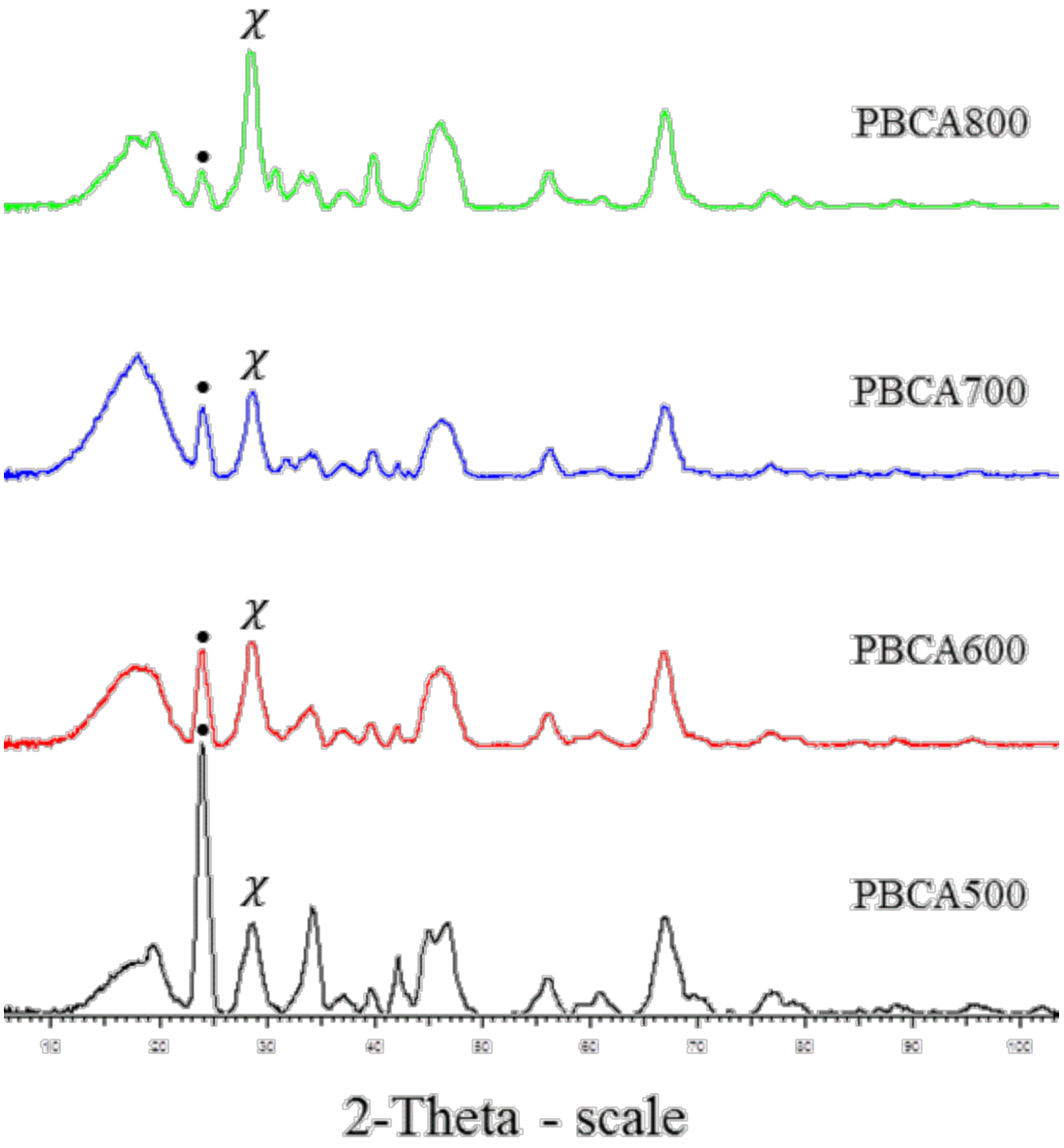

Figure 6-9: XRD spectra of thermally aged PBCA catalyst with the $Ba(CO_3)$ – (•) and $BaAl_2O_4$ - (χ)

It has been addressed previously that due to the CO_3^- peak consumption it is often difficult to observe changes in nitrate formation in the 1300-1400cm^{-1} wavelength region. The difficulty in identifying changes in FT-IR with NO_x storage can be observed in Figure 6-10

which shows the post storage FT-IR of all PBCA catalysts with varying sintering temperature. Both the 1348 and 1427cm^{-1} peaks are associated with monodenate nitrate formation[11].

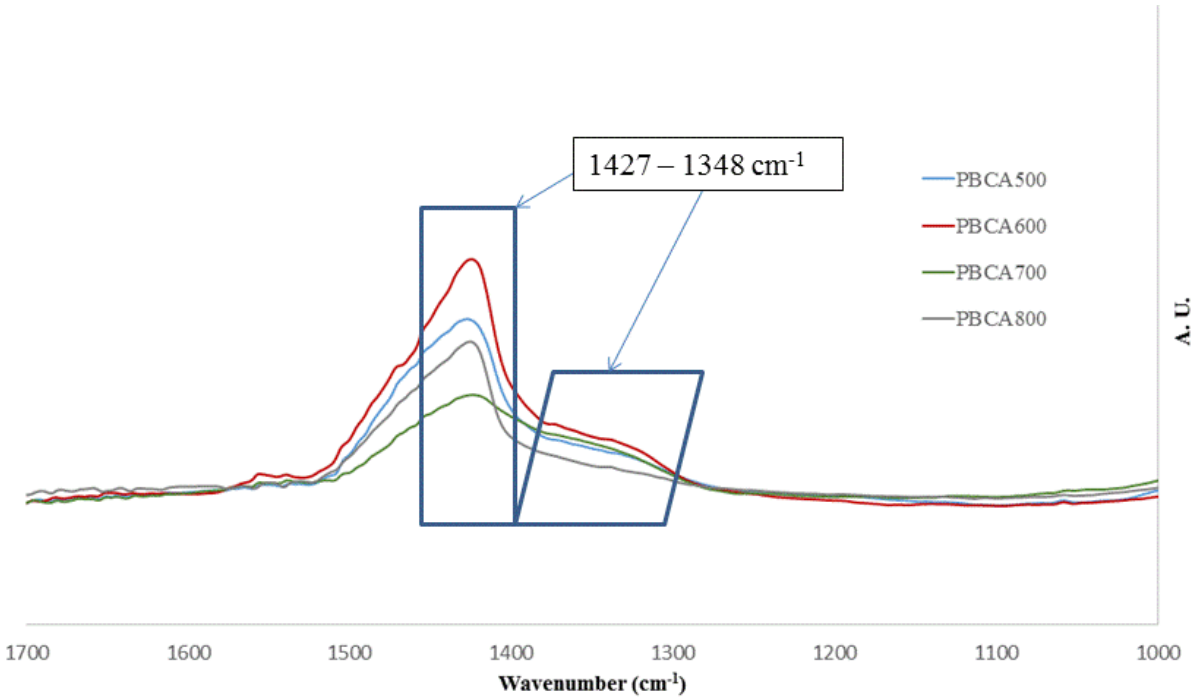

Figure 6-10: FT-IR of PBCA catalysts with varying aging temperature after 1hr NO_x storage at 350°C

Definitive determination of nitrate adsorption is difficult, as the 1427cm^{-1} nitrate peak overlaps with the carbonate peak at 1420 cm^{-1}. As identified, there is a difference in the amount of adsorbed carbonate that may be available to desorb upon NO_x storage as thermal aging is increased. Therefore, the only way to accurately identify the nitrate uptake via FT-IR is from the 1348cm^{-1} peak, which is represented as a shoulder to the larger nitrate/carbonate peak. As an attempt to better observe these changes, the FT-IR "storage spectra" has been calculated which represents the difference between the as prepared adsorption spectra (Figure 6-8) and the FT-IR after the NO_x storage has been conducted (Figure 6-10).

Figure 6-11 shows the FT-IR of the PBCA catalysts after storage at 250ºC with the as prepared catalyst spectra subtracted. The negative peak observed at 1420cm^{-1} is due to the desorbed CO_3^- and the variation in height of the negative peak can be attributed to CO_3^- desorption, as well as some adsorption contribution from nitrates. The two catalysts with the largest difference in negative peak at 1420cm^{-1} and positive nitrate peak at 1340cm^{-1} are the PBCA500 and PBCA600 catalysts. The difference indicates these two catalysts have the largest uptake in the form of nitrates and the nitrates are closely correlated to the loss of carbonate species. This is confirmed by the uptake data presented previously where the PBCA500 and PBCA600 catalysts show the highest NO_x uptake at the 250ºC uptake temperature. PBCA700 and PBCA800 have the smallest difference in carbonate to nitrate peaks, where the PBCA800 catalyst shows more carbonate desorbed than the PBCA700 material.

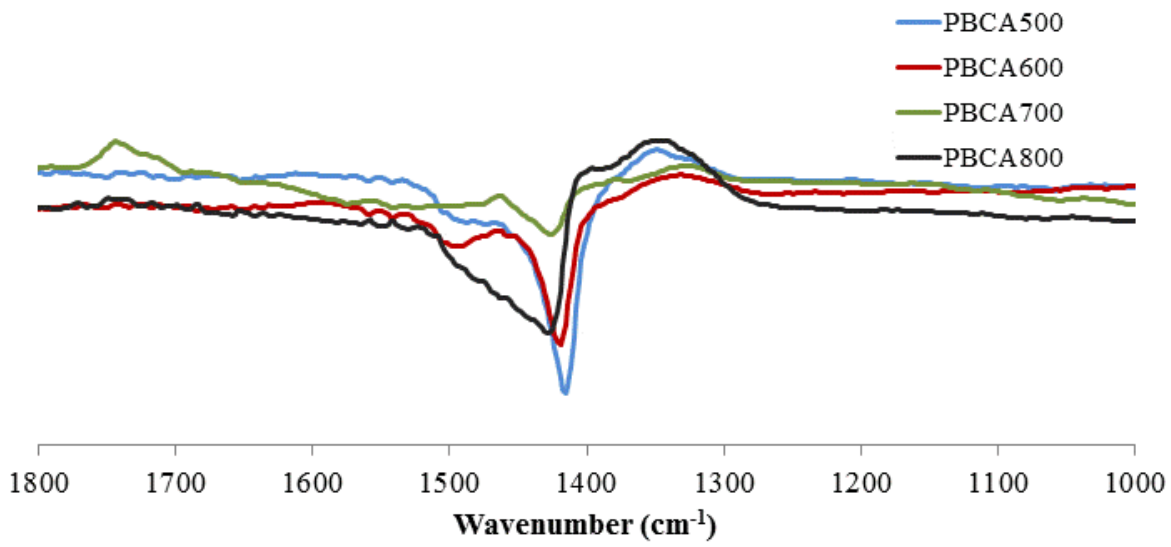

Figure 6-11: Figure FT-IR with Baseline subtracted with varying aging temperature after 1 hr NO_x storage at 250°C

In contrast to the low temperature uptake profiles and spectra, FT-IR spectra at 350ºC show strong carbonate/nitrate differences for the PBCA500 and PBCA700 catalysts when compared to the PBCA800 and PBCA600 materials. Figure 6-12 shows the storage spectra after NO_x storage at 350ºC. The negative carbonate consumption peak is largest for the PBCA700 and PBCA500 catalysts. Furthermore, the PBCA600 catalyst shows an absorbance peak at 1440cm^{-1} which is in part masking the carbonate consumption. While all catalysts except the PBCA800 catalyst show a clear nitrate peak at 1348cm^{-1}, the PBCA600 catalyst is the only catalyst which shows the secondary peak associated with the bidentate nitrate.

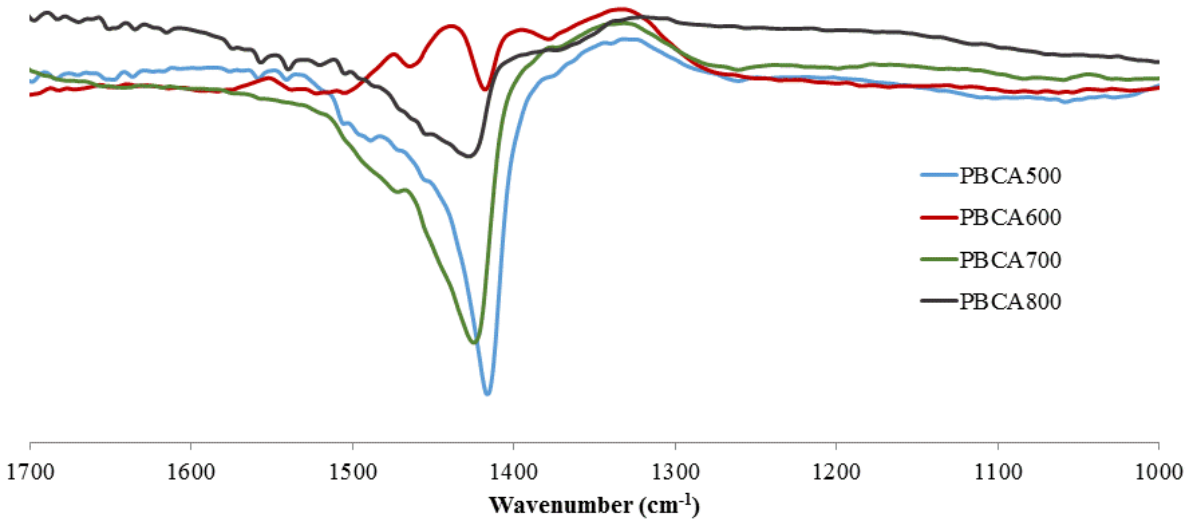

Figure 6-12: Figure FT-IR with Baseline subtracted with varying aging temperature after 1hr NO_x storage under 577ppm NO/4.7% O_2 in Ar at 350°C

The PBCA600 catalysts shows the most variation in the FT-IR spectra with increased NO_x storage spectra. When this is comparted to the storage profiles and uptake integrated by regime, it can also be seen that the PBCA600 catalysts has the largest variation in the regimes associated with surface uptake, specifically the complete uptake regime. Because complete uptake is associated with more rapid uptake and therefore more stable nitrate species, it is shown

that the enhanced Pt-Ba adjacency observed for the PBCA600 catalysts results in more stable nitrates.

6.5 Conclusions

NO_x uptake profiles show significant variation in the rapid uptake regime at low uptake temperatures. As uptake temperature is increased the deviation in uptake profile becomes less apparent. At an uptake temperature of 350ºC, PBCA500, PBCA600 and PBCA700 show very little deviation in the uptake profiles, with substantial overlap in error bars. PBCA800 shows decreased total uptake at all uptake temperatures. Low temperature total uptake for PBCA800 is less than 32% of total uptake achieved by the PBCA600 catalysts at 300ºC. During high temperature uptake, the PBCA800 catalyst achieves greater than 50% of uptake achieved by PBCA500, PBCA600 and PBCA800. This shows that $BaAl_2O_4$ is active for storage at elevated temperatures and that moderate thermal degradation does not affect NO_x storage at elevated temperatures.

XRD shows that Ba in the PBCA800 catalysts is almost completely present in the form of $BaAl_2O_4$. Because total NO_x storage is decreased substantially over the PBCA800 catalyst at all uptake temperatures, it can be concluded that complete incorporation of Ba into the $BaAl_2O_4$ form results in substantially decreased NO_x storage. However, PBCA700 shows substantial $BaAl_2O_4$ formation which results in reduced NO_x uptake at 250ºC and 300ºC but not at the 350ºC uptake temperature. Because, both the PBCA600 and PBCA700 catalysts show some $BaAl_2O_4$ formation and both catalysts perform similarly at high storage temperatures, it is clear that the

$BaAl_2O_4$ formation proceeds in a way that is not completely detrimental to NO_x uptake. Furthermore, the PBCA600 catalyst shows the highest low temperature NO_x uptake and PBCA600 has more $BaAl_2O_4$ formation than the PBCA500 catalysts. This finding strengthens the conclusion that the $BaAl_2O_4$ formation mechanism differs as formation is increased. Finally, all catalysts show that long term aging experiments with NO/O_2 generate only nitrates and carbonate consumption is strongly correlated to the amount of bulk $BaCO_3$ as measured by XRD.

FT-IR shows a secondary nitrate peak for PBCA600 with NO_x stored at 350ºC. The secondary peak is observed at 1440cm^{-1}, and can be explained by the large amount of NO_x uptake which takes place within the complete uptake regime. Complete uptake is associated with close Pt-Ba interaction, where the spill over mechanism is likely responsible for generating the bidenate or "bridged" nitrate species. At uptake temperatures above 250ºC catalysts show substantially less uptake in the complete regime as compared to the PBCA600 material. PBCA600 at 350ºC has greater than 20% of total uptake occurring in the complete uptake regime, which is due to an increase in Pt-Ba adjacency as inactive Ba is sintered to $BaAl_2O_4$ upon thermal aging. This is likely a result of the nature of species transition from Ba to $BaAl_2O_4$. Where, HT-$BaCO_3$ is consumed to form $BaAl_2O_4$ which participates in storage, this storage in combination with the storage capacity of LT-$BaCO_3$ has the potential to increase storage with moderate sintering.

The investigations of NO_x storage with degradation show that even with substantial thermal degradation, $Pt/Ba/CeO_2/Al_2O_3$ exhibits moderate NO_x storage throughout the range of ideal uptake temperatures. Thermal degradation has been shown to be predominately in the form of $BaAl_2O_4$ and even some $BaAl_2O_4$ formation has been shown to have negligible impact on NO_x storage. Furthermore, the initial formation of $BaAl_2O_4$ is associated with HT-$BaCO_3$

decomposition, which results in an increase in uptake. The degradation mechanism would benefit from further investigation into the HT-$BaCO_3$/LT-$BaCO_3$ transition which has been shown to occur between 600 – 700ºC during thermal aging.

6.6 Reference

1. Clayton, R., et al., *Pt Dispersion Effects During NOx Storage and Reduction on Pt/BaO/Al2O3 Catalysts.* Applied Catalysis B: Environmental 2009. **90**: p. 662-676.
2. Auvray, X., et al., *The effect gas composition during thermal aging on the dispersion and NO oxidation activity over Pt/Al2O3 catalysts.* Applied Catalysis B-Environmental, 2013. **129**: p. 517-527.
3. Roy, S. and A. Baiker, *NO x Storage− Reduction Catalysis: From Mechanism and Materials Properties to Storage− Reduction Performance.* Chemical Reviews, 2009. **109**(9): p. 4054-4091.
4. Kim, D.H., et al., *Relationship of Pt Particle Size to the NO x Storage Performance of Thermally Aged Pt/BaO/Al2O3 Lean NO x Trap Catalysts.* Industrial & engineering chemistry research, 2006. **45**(26): p. 8815-8821.
5. Casapu, M., et al., *Formation and stability of barium aluminate and cerate in NO x storage-reduction catalysts.* Applied Catalysis B: Environmental, 2006. **63**(3): p. 232-242.
6. Castoldi, L., et al., *Study of the effect of Ba loading for catalytic activity of Pt–Ba/Al 2 O 3 model catalysts.* Catalysis Today, 2004. **96**(1): p. 43-52.
7. Sedlmair, C., et al., *Elementary steps of NO x adsorption and surface reaction on a commercial storage–reduction catalyst.* Journal of Catalysis, 2003. **214**(2): p. 308-316.
8. Pereda-Ayo, B., et al., *Influence of ceria loading on the NO x storage and reduction performance of model Pt–Ba/Al 2 O 3 NSR catalyst.* Catalysis Today, 2015. **241**: p. 133-142.
9. Desikusumastuti, A., et al., *Nitrite and nitrate formation on model NO x storage materials: on the influence of particle size and composition.* Physical Chemistry Chemical Physics, 2009. **11**(14): p. 2514-2524.
10. Li, X., et al., *A Study on the Properties and Mechanisms for NO x Storage Over Pt/BaAl2O4-Al2O3 Catalyst.* Topics in catalysis, 2003. **22**(1-2): p. 111-115.
11. Caglar, B. and D. Uner, *NO oxidation and NO x storage over Ce–Zr mixed oxide supported catalysts.* Catalysis Communications, 2011. **12**(6): p. 450-453.

Chapter 7 Novel LNT Perovskite Catalyst

7.1 Introduction

Because LNT catalysts are an additional system which works alongside traditional TWC which already represent significant noble metal use, it is desirable to reduce or eliminate noble and precious metals in LNT formulations. As a result, platinum free LNT catalysts have attracted significant attention. The $LaCoO_3$ perovskites have shown the ability to both adsorb NO_x in lean environments and reduce NO_x during rich phase operation [1]. However, these catalysts also have significant challenges associated with implementation such as surface area, reactivity and tolerance to degradation.

Previous studies have shown the reduction of NO over high surface area $LaCoO_3$ based perovskite catalysts can reach conversions of up to 94% in ideal cycling conditions, where rich phases have contained only pure reductant, hydrogen, carbon monoxide or propene and lean phases contain only reacting components NO/NO_2 and O_2 [2]. The following work shows testing of the novel $La_{.8}Sr_{.2}CoO_x$ (LSCO) catalyst under the lean/rich operating conditions outlined in Chapter 3: Materials and Methods. The LSCO catalyst is also compared to the PBCA600 for conversion and oxidation of NO.

7.2 LSCO under Lean/Rich conditions

The following section presents three representative cycles of lean/rich oscillation over the LSCO catalyst during a one hour cycling run. The major features of the outlet concentrations in comparison to the cycling condition will be outlined for clarity. In Figure 7-1, when "NO_x Inlet"

is 500PPM, the catalyst system is operating in the "lean" mode and the inlet consists of $NO/O_2/H_2O/CO_2/Ar$. The "lean" mode is the mode in which NO_x is stored. When the NO_x in the inlet (represented by the blue line) is 0, the system is operating in "rich" mode. Rich mode inlet gas consists of $H_2/CO/H_2O/CO_2/Ar$. This is the operating mode in which stored NO_x is reduced to N_2.

Figure 7-1: LSCO catalyst used in NO_x Oscillating Lean/Rich experiment with calculated NO_x inlet (blue) and real time NO_x outlet (red)

To measure NO, NO_2 and total NO_x, the NO_x analyzer is operated in "switching mode". More information on switching mode can be found in Chapter 3: Materials and Methods. Because the analyzer is operating in switching mode, switching between NO/NO_x measurements, the real time NO_x analysis shows oscillation. Real time mode only shows the measurement that

is being taken in real time (i.e., NO or NO_x depending on which mode the analyzers has switched to). Therefore, real time is used to compare outlet concentrations to the NO_x inlet only as a gauge. It can be observed in Figure 7-1 that during lean operation, real time NO_x concentrations (red line) are low but continue to increase as the catalyst becomes more saturated. During rich operation, real time NO_x concentration is decreased for the first 50 seconds until nearly all the adsorbed NO_x is released (indicated by the large spikes in real time analysis concentration at 1060, 1240, 1520 seconds). The amount of NO_x released cannot be determined because the concentration exceeded the detection limit of the analyzer. However, these concentrations spikes are obvious indicators that very little of the stored NO_x is reduced over the LSCO catalyst during the rich phase.

For comparison, the most efficient NO_x storage catalyst PBCA600 from the previous work was also operated under the lean/rich conditions. Figure 7-2 shows the real time NO_x concentration and calculated NO_x inlet for the PBCA600 catalyst operated in lean/rich oscillating experiments. The PBCA catalyst is shown to effectively reduce stored NO_x during rich phase operation. After 20 seconds of rich phase operation, less than 30ppm NO_x is observed. The catalyst also effectively stores NO_x. The maximum NO_x concentration reached during lean phase operating is 120ppm.

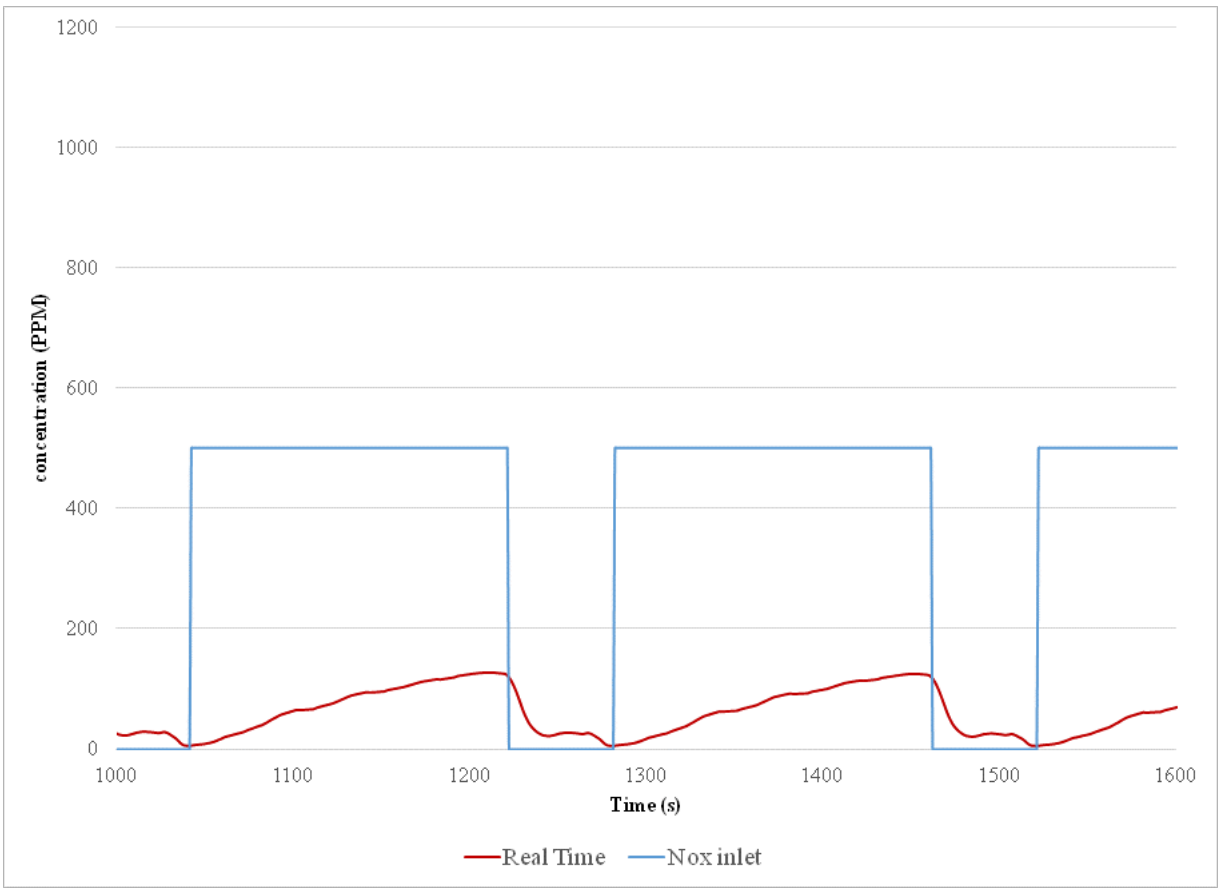

Figure 7-2: PBCA catalyst NO_x Oscillating Lean/Rich experiment with calculated NO_x inlet (blue) and real time NO_x outlet (red)

Comparison of Figure 7-1 and Figure 7-2 show two important differences. First, where the LSCO catalyst releases NO_x in large quantities during rich operation, the PBCA catalyst converts nearly all of the stored NO_x. Second, the LSCO catalyst oxidizes significantly more NO_x during lean phase operation, which is represented by the oscillation of the real time measurement.

7.3 Dual catalyst system under lean/rich conditions

Due to the increase in oxidative ability of the LSCO catalyst and the far superior NO_x reduction of the PBCA catalyst, a combination of the two has the potential to impact NO_x conversion positively. To facilitate this, a "dual catalyst" system was employed where LSCO/PBCA catalysts were used in tandem. LSCO was used as the front half of the bed and PBCA600 was used as the back half of the bed. The results of the LSCO/PBCA dual bed set-up (Figure 7-3) shows a combination of the features found in Figure 7-1 and Figure 7-2. Lean phase concentrations show the oscillating real time NO_x measurements which indicate significant oxidation of NO. More importantly, the dual bed set-up is able to effectively reduce NO_x during rich phase operation.

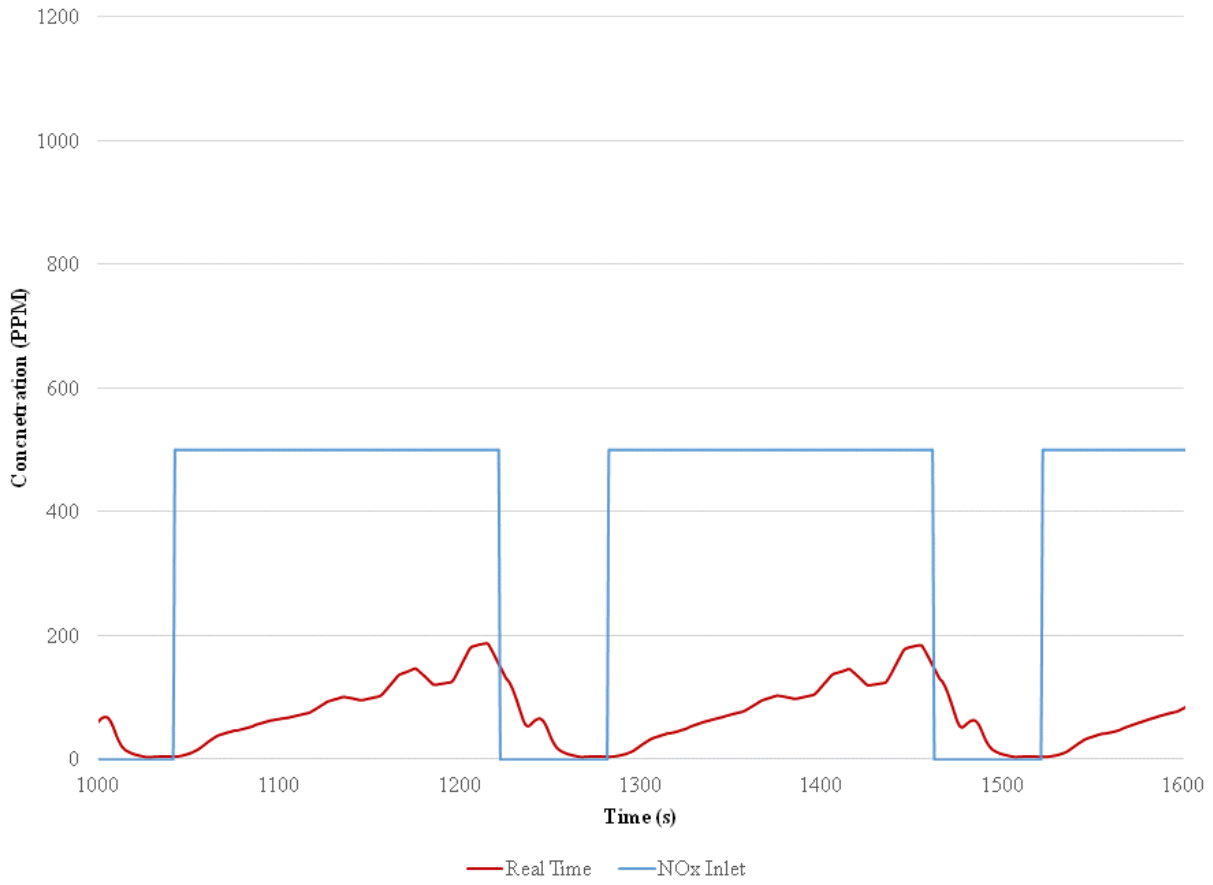

Figure 7-3: LSCO/PBCA bed on bed catalyst for Oscillating Lean/Rich experiment with calculated NO_x inlet (blue) and real time NO_x outlet (red).

It is also observed in Figure 7-3 that the real time NO_x concentration is less than 5ppm for the final 20 seconds of the rich phase. In comparison, the PBCA catalyst continues to desorb unreacted NO_x at greater than 20ppm during the final 20 seconds of rich phase operation.

Another combinatory effect of the dual bed system is exhibited when comparing the change in NO oxidation with number of cycles. Figure 7-4 shows that the LSCO catalyst exhibits a six fold increase in maximum lean phase NO_2 concentration after six cycles. The opposite trend is observed for the PBCA catalysts. Maximum NO_2 concentration is decreased by 60% after the 6 cycles. When the dual bed system is employed the NO_2 concentration varies by less than 5% from the starting concentration for the cycle measurement period.

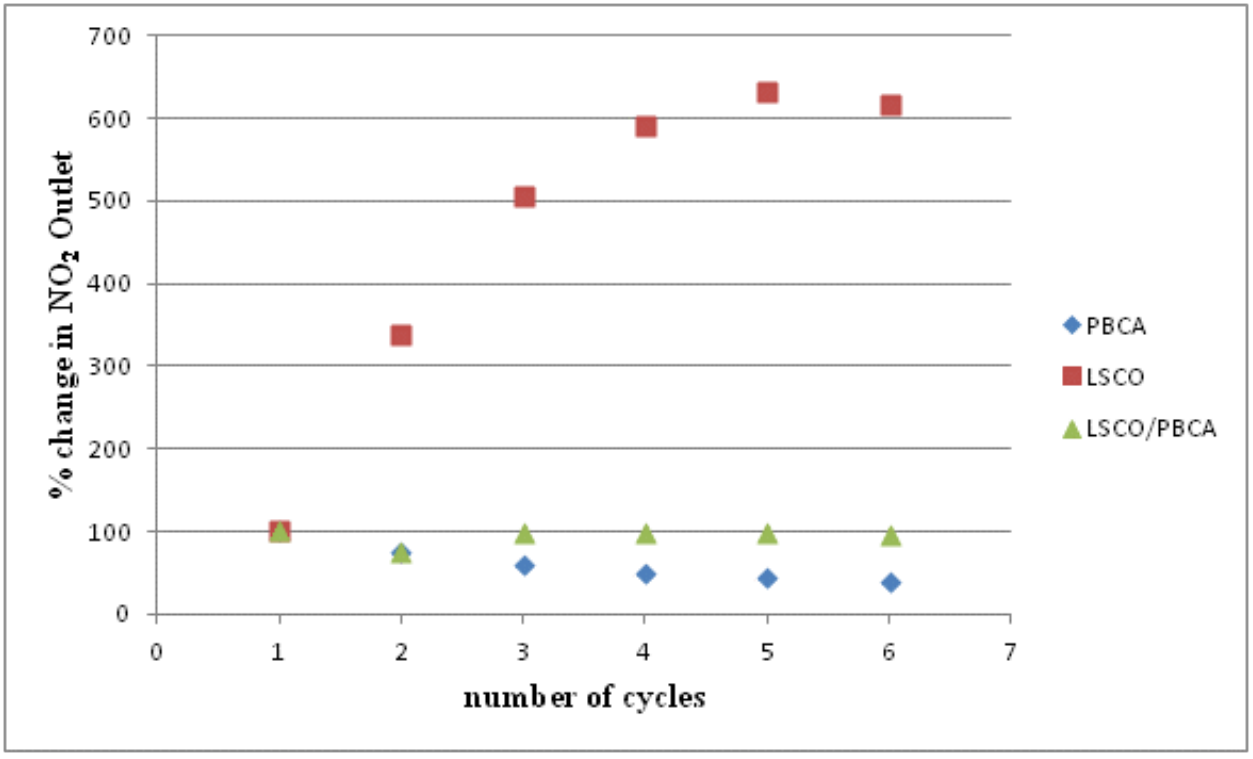

Figure 7-4: % change in maximum lean phase NO_2 concentration with number of cycles for PBCA (blue), LSCO (red) and LSCO/PBCA dual bed (green)

While it is not initially clear that increased NO oxidation is a positive conclusion, this result yields a potential for other applications. One potential application is in tuning the outlet concentrations of the LNT system for applications in the multiple catalyst systems of TWC. This dual bed system could be used to optimize LNT/SCR systems where NO_x reduction is important for the LNT section but oxidation of remaining NO is required to increase effectiveness of the inline SCR catalyst. Also, increased NO_2 concentration could increase storage efficiency if the LSCO/PBCA catalyst ratios were tuned to increase the PBCA section and could perhaps result in increased conversions. Because LSCO the catalyst shows large variations in NO oxidation over short cycle times it is also important to understand what if any changes are occurring to the structure of the perovskite. Figure 7-5 shows the XRD spectra of used LSCO catalysts. The catalyst has been used for cycling experiments from 1 to 4 hours. The large peak at 33° is indicative of the $LaCoO_3$ perovskite as are the smaller peaks between 40-50° and around 60°. Because the Sr dopant in the LSCO is only 20% of the A site, the material should maintain the XRD spectra of the $LaCoO_3$ if no degradation has taken place. There appears to be no degradation that can be observed via XRD of the LSCO material through four hours of lean rich cycling.

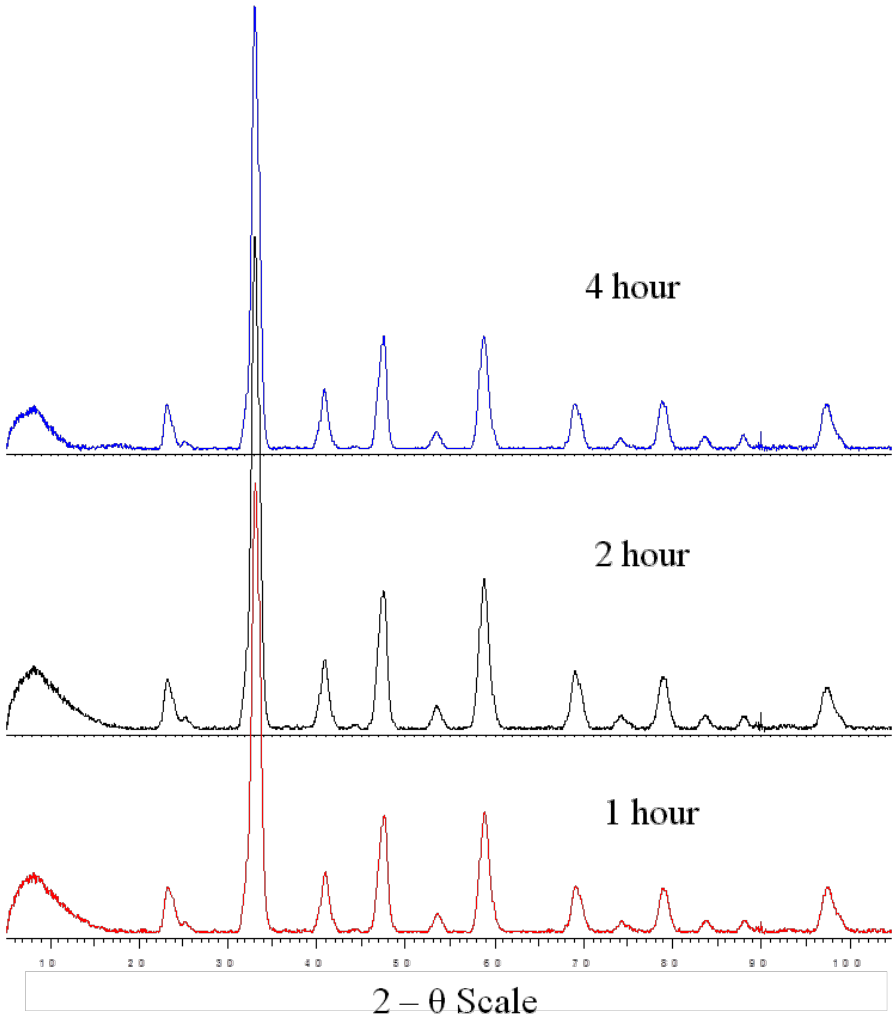

Figure 7-5: XRD of LSCO catalysts after Lean/Rich cycling ranging from 1-4 hours

Although the LSCO catalyst showed no reduction ability in the rich phase after NO_x storage, several positives have been identified from the LSCO/PBCA, lean/rich experiments. NO oxidation occurs more readily over the LSCO catalyst. The LSCO/PBCA system has shown potential in outlet tuning applications, and most importantly the LSCO catalyst has been shown to retain the perovskite structure in a CO_2/H_2O environment for up to 4 hours of oscillating operation.

7.4 Conclusions

The LSCO catalyst has shown the ability to both store and oxidize NO. However, the material has shown little to no ability to reduce stored NO_x in the cyclic lean/rich environment of LNT catalysis. The PBCA600 catalyst has been identified in Chapter 6: Thermal Degradation Effects on NO_x Storage, as the most effect storage catalyst, and as such, was tested in the lean/rich environment as well. The PBCA600 catalyst shows substantial NO_x storage and reduction, but showed little NO oxidation during lean phase operation when compared to the LSCO catalyst. Combining the LSCO and PBCA600 catalysts in dual bed configuration resulted in increased NO oxidation during lean phase operation and decreased NO_x slip during that later time periods of rich phase operation. As a result of the combinatory effects of the dual bed set-up it is proposed that system tuning could be used to produce desired effects such as increased NO oxidation for storage or further decreases in NO_x slip. A number of new set-ups are available when considering the combination of the two catalysts. The catalysts could be physically mixed or calcined in tandem. Another option would be to vary the bed lengths of each section in order to determine minimum loadings for each catalyst to continue the combinatory effects observed in the 50/50 dual bed set-up.

7.5 Reference

1. Ye, J., et al., *Highly efficient NOx purification in alternating lean/rich atmospheres over non-platinic mesoporous perovskite-based catalyst K/LaCoO3.* Catalysis Science & Technology, 2013. **3**(8): p. 1915-1918.
2. You, R., et al., *YCeZrO Ternary Oxide Solid Solution Supported Nonplatinic Lean-Burn NOx Trap Catalysts Using LaCoO3 Perovskite as Active Phase.* The Journal of Physical Chemistry C, 2014. **118**(44): p. 25403-25420.

Chapter 8: Conclusions and Recommendations

This chapter details the recommendations of future work based upon the conclusions of this thesis. Areas of future interest are broken down into three distinct sections; NO oxidation, NO_x storage, and perovskite catalysis.

8.1 NO Oxidation in LNT catalysts

Modeling of NO oxidation over Pt/Al_2O_3 catalysts has shown that adapting kinetic parameters to changes in Pt morphology can accurately represent the trends observed in the experimental data. Specifically, increases in Pt particle size from 2-10 nm showed increased conversion for NO oxidation. The increase in conversion can be attributed to greater abundance of the Pt(111) crystal face as well as the decreased oxidation in larger Pt particles. The model was adapted by varying activation energy of NO and NO_2 desorption as well as O_2 adsorption, where method of variation was determined through literature review. However, LNT catalysts also contain additional promoters and, in an effort to understand variations in NO oxidation with thermal aging over fully formulated LNT catalysts, the $Pt/Ba/Al_2O_3$ and $Pt/Ba/Ce/Al_2O_3$ systems were investigated.

The work in Chapter 5: Effects of thermal degradation on NO Oxidation, clearly shows there is a strong correlation between the oxidation state of platinum and the catalytic oxidation of NO over the LNT catalysts. The Pt-Ba interaction negatively impacted the oxidation state of Pt during NO oxidation for both the PBA and PBCA catalysts. Furthermore, addition of Ce was shown to further oxidized platinum which resulted in decreased conversion after low thermal aging. Ce addition showed a second effect upon thermal aging identified as the “Ce anchoring effect”, which resulted in a reduction in the effect of thermal aging on Pt particles (i.e. particles

in the PBCA catalyst did not grow as rapidly under thermal aging when compared to the PBA catalysts). Due to the competing effects of oxidized Pt particles and Ce anchoring, PBCA showed less NO oxidation when compared to PBA at 600ºC and outperformed the PBA catalyst after thermal aging at 800ºC. Because the oxidation state of Pt and Ce were shown to be critically important in NO oxidation over PBA and PBCA catalysts, analyzing these states would provide valuable information to help interpret the change in NO oxidation with catalyst degradation.

8.1.1 Investigation of Pt-Ce interaction with thermal aging

The mechanism of the Pt-Ce interaction should be investigated further via surface analysis techniques. X-ray photoelectron spectroscopy (XPS) is a surface analysis technique that allows for analysis of the surface chemistry of solid samples. Olsson et al used XPS to determine the oxidation state of Pt as it effected NO oxidation in $Pt/Ba/Al_2O_3$ catalyst under different pretreatment conditions[1]. XPS has also been used to analyze the Ce oxidation state and surface availability of Ce in LNT catalysts[2]. The use of XPS in tandem with additional characterization techniques such as O_2-TPD and NO/NO_2 – TPD, would give further insight into the availability of surface oxygen, and the role the available oxygen plays in the both the oxidation of Ce, and Pt, in thermally aged catalysts.

8.2 NO_x storage in $Pt/Ba/CeO_2/Al_2O_3$ catalysts

It has been shown that long term NO_x storage experiments are altered by thermal degradation of the LNT catalysts. Low temperature storage showed the largest variation with thermal aging. When aging temperature increased from 500ºC to 800ºC, an 80% reduction in total uptake was observed. Additionally, it was shown that increased thermal aging resulted in increased $BaAl_2O_4$ formation. $BaAl_2O_4$ formation initially resulted in an increase in NO_x storage,

where the PBCA600 catalyst showed the most NO_x storage at 250 ºC and 300ºC. The PBCA600 catalyst also showed the most complete uptake at 350ºC, indicating an increase in the Pt-Ba adjacency. Based upon the increase in NO_x storage with the initial formation of $BaAl_2O_4$, it has been hypothesized that thermal aging proceeds via the consumption of HT-$BaCO_3$ initially, which is then followed by the consumption of the LT-$BaCO_3$. Surface analysis allowed for observation of the changes in surface species with NO_x uptake and thermal degradation. The carbonate desorption peak was observed to decrease as aging temperature was increased, and the observed nitrate peaks were larger as aging temperature was decreased. The PBCA600 catalyst also showed an increase in stable nitrates, when NO_x was stored at 350ºC, with bridged, bidenate, and mondenate nitrates observed. This is another indicator of the improved NO_x uptake with moderate aging.

While FT-IR of the used catalysts proved useful in identifying surface changes, it was unable to identify any changes associated with individual uptake regimes. This is because FT-IR is an ex-situ technique and, as such, analysis was conducted after NO_x storage experiments were completed.

8.2.1 In-Situ DRIFTS of NO_x Storage

Employing an in-situ technique would identify the changes in surface species as storage is occurring. Diffuse Reflectance Infrared Fourier Transform Spectroscopy (DRIFTS) can be employed as an in in-situ technique to analyze the surface components as the uptake experiments are taking place. It has been shown that with low temperatures (<200ºC), and short uptake times, storage intermediates can be effectively identified. Less stable NO_x storage surface components have also been observed over pure $BaAl_2O_4$ and intermediates such as linear nitrates, linear and bridged nitrites have all been identified under these “less optimal” uptake conditions[3, 4].

Low temperatures and high sintering conditions produced the largest variations in NO_x storage profile and total uptake. Therefore, it is suggested that in-situ surface analysis via DRIFTS and increased experimental resolution in the area of 600-700ºC degree sintering temperatures, and 250-300ºC storage temperatures would further the understanding of the degradation in NO_x storage with thermal aging for $Pt/Ba/CeO_2/Al_2O_3$ catalysts. The proposed conditions would result in the widest range of observed surface species based upon the observed uptake profiles and variations in FT-IR. The suggested experimental range should also capture the transition in $BaAl_2O_4$ formation from HT-$BaCO_3$ consumption, to consumption of LT-$BaCO_3$, which can then be correlated to variation in both storage profiles and DRIFTS spectra.

8.3 Perovskite LNT catalyst investigations

The LSCO catalyst showed promise as a platinum free NO oxidation and NO_x storage catalyst. However, there was no observable NO_x reduction due to the large quantities of NO_x desorbed from the catalyst during rich phase of operation. The perovskite catalyst did show good hydrothermal stability and resistance to carbonate formation during lean/rich cycling. The lack of NO_x reduction during the rich cycle resulted in the investigation of a dual bed catalyst system in which PBCA600 was used to help facilitate the reduction of NO_x released by the LSCO catalyst. The combination of LSCO/PBCA600 materials in the "dual bed" configuration showed interesting trends, including decreased NO_x slip and increased NO oxidation. Based on the above conclusions the following avenues have been identified for additional research in the perovskite LNT catalyst system.

8.3.1 Additives for increased NO_x reduction

Literature has shown that the addition of Pd to the $LaCoO_3$ perovskite increases the ability of the catalyst to reduce NO_x in lean rich cycling[5]. It was also known that perovskite catalysts produced via EDTA/citrate complexation suffer from low surface area which results in lower catalytic activity. It is hypothesized that the addition of Pd will increase NO_x conversion in the long term cycling experiments. Furthermore, it is proposed that surface area can be increased by co-impregnation of the LSCO catalyst with a higher surface area support during complexation. Due to the increase in surface area and activity, the catalyst stability during lean/rich cycling is likely to decrease. Thus, the extended time lean/rich cycling experiments should be conducted with the new catalyst formulation to identify viability of the catalyst under real world cycling conditions.

8.4 Variations in Dual Bed configuration

Because the dual bed configuration showed features which were a combination of the features observed for the two catalysts, it is proposed that the dual bed configuration be optimized to increase NO_x reduction. The study will be designed to find the optimum condition for NO_x slip reduction. The dual bed investigated in Chapter 7: Degradation of a novel Pt Free LNT catalyst was a 50/50 split of the two catalysts. From these experiments, two outcomes are likely when the ratio of LSCO to PBCA is changed in the dual bed configuration. First it is possible reducing the PBCA catalysts bed section could have little effect in changing the combinatory catalyst properties observed for the 50/50 split and therefore the amount of PBCA catalyst used could be reduced to an optimal amount whilst maintaining performance. The second outcome which is believed to be more likely is NO_x slip can be further reduced through increasing the PBCA section of the bed while maintaining the properties of the bed through small loadings of LSCO in the front section of the dual bed. The optimization of the bed

configuration should be done in tandem with expanded analysis of the outlet gases via gas chromatography (GC) and mass spectroscopy(MS). GC/MS will allow for quantified outlet concentrations of reduced NO_x components like NH_3, N_2O. This will make it possible to close the nitrogen balance and determine selectivity of reduction to NH_3 or N_2 with the varying dual bed configurations.

8.5 Final remarks

The investigations presented have advanced the field of LNT catalyst research by providing an enhanced understanding of the degradation of LNT catalysts. The studies have tied the changes observed physically and catalytically to specific surface properties and surface components. Further investigation into the degradation mechanism of LNT catalysts is critical to the affective implementation of these catalysts in automotive exhausts.

8.6 Reference

1. Olsson, L. and E. Fridell, *The influence of Pt oxide formation and Pt dispersion on the reactions NO2 <-> NO+1/2 O-2 over Pt/Al2O3 and Pt/BaO/Al2O3.* Journal of Catalysis, 2002. **210**(2): p. 340-353.
2. Lv, L., et al., *The lean NOx traps behavior of (1–5%) BaO/CeO2 mixed with Pt/Al2O3 at low temperature (100–300 °C): The effect of barium dispersion.* Chemical Engineering Journal, 2013. **222**: p. 401-410.
3. Liu, Z. and J.A. Anderson, *Influence of reductant on the thermal stability of stored NOx in Pt/Ba/Al2O3 NOx storage and reduction traps.* Journal of Catalysis, 2004. **224**(1): p. 18-27.
4. Disselkamp, R., et al., *II. B. 1 Fundamental Studies of NOx Adsorber Materials.*
5. Kim, C.H., et al., *Strontium-doped perovskites rival platinum catalysts for treating NOx in simulated diesel exhaust.* Science, 2010. **327**(5973): p. 1624-1627.

Appendix I

9.1 X-Ray Diffraction Profiles

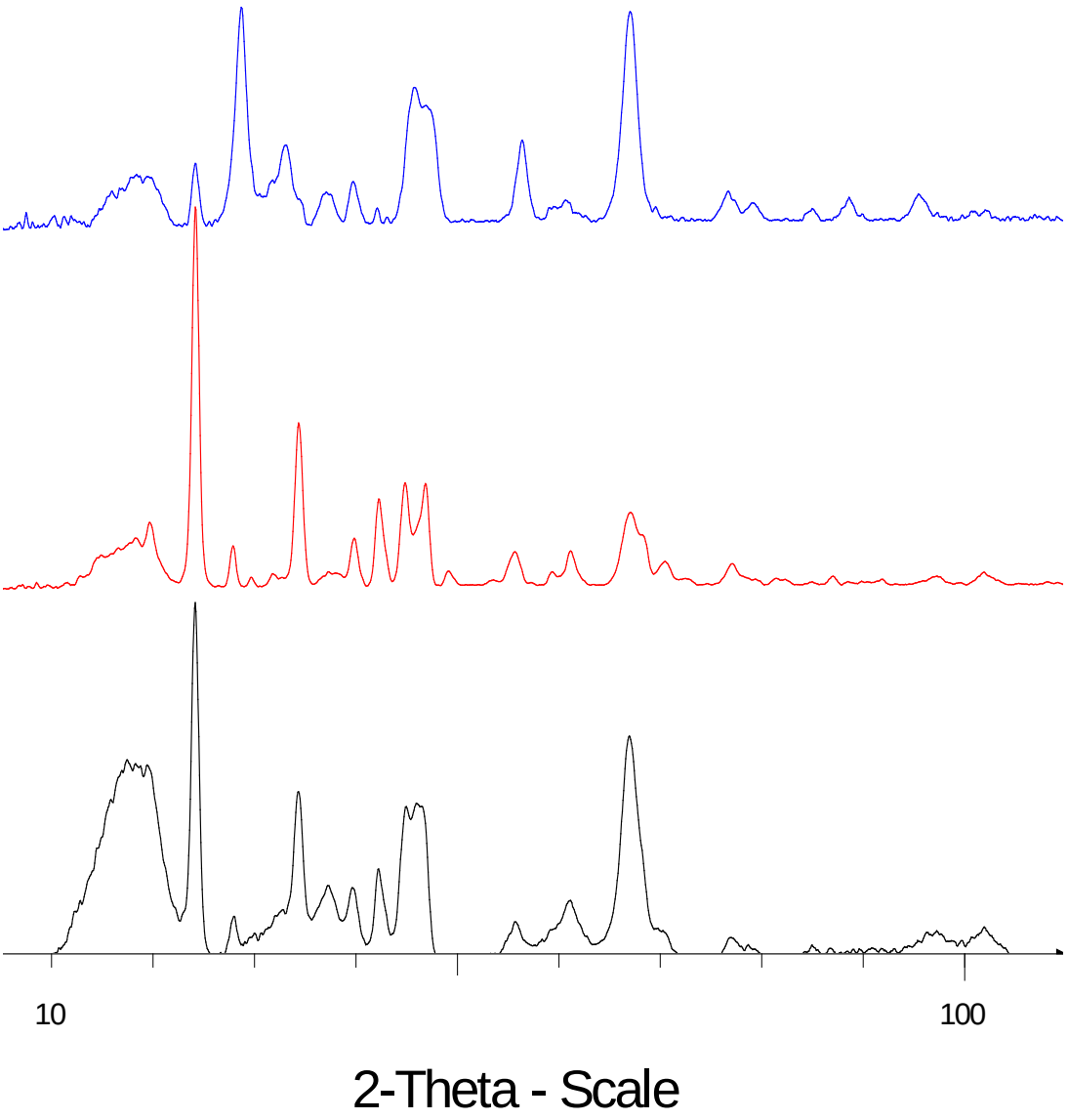

Figure 9-1: XRD PBA catalyst 600-800°C sintering temperatures

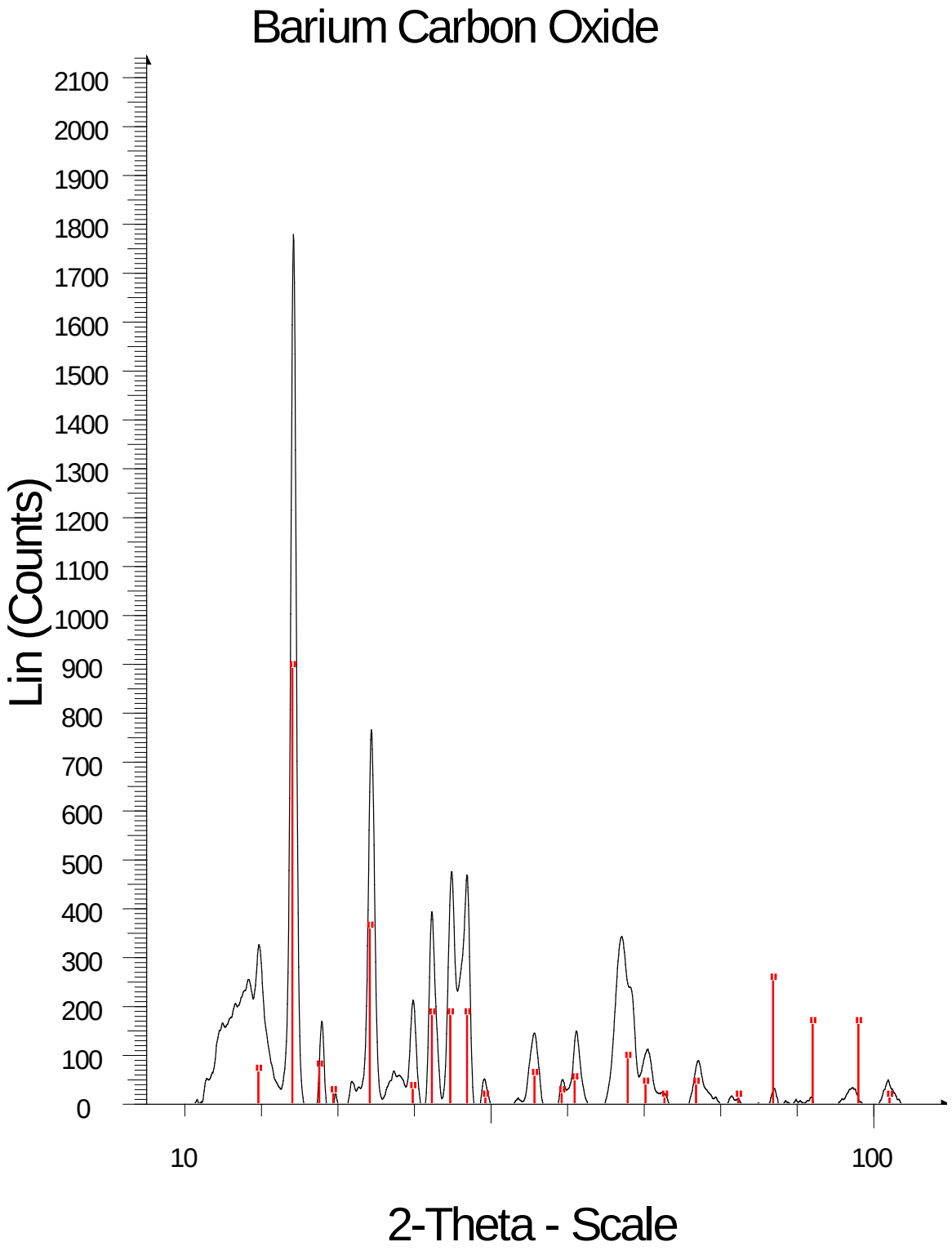

Figure 9-2: XRD PBA600 with $BaCO_3$ diffraction profile overlaid

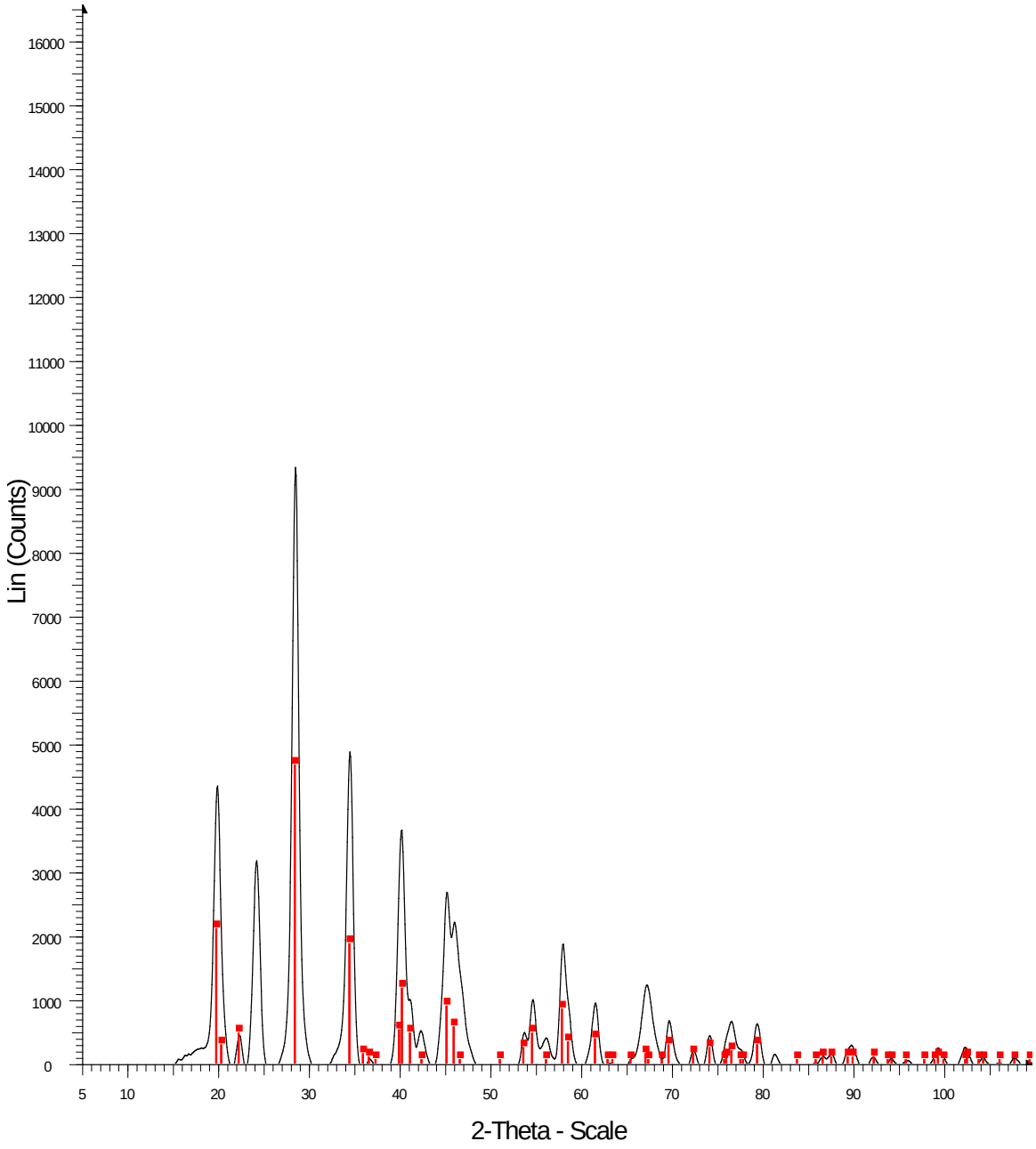

Figure 9-3: XRD of PBCA800 with $BaAl_2O_4$ Diffraction profile overlaid

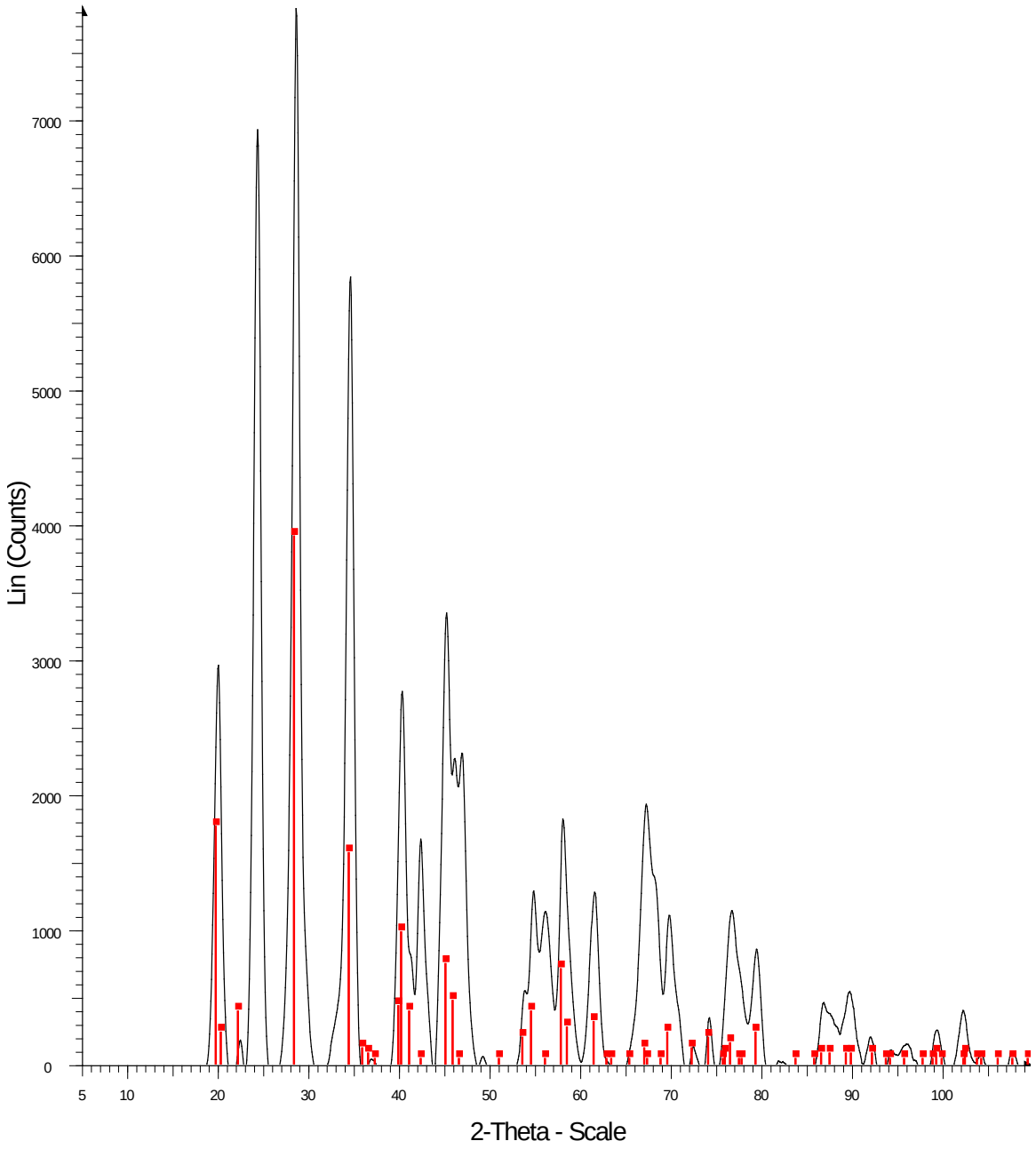

Figure 9-4: XRD of PBCA600 with $BaAl_2O_4$ Diffraction profile overlaid

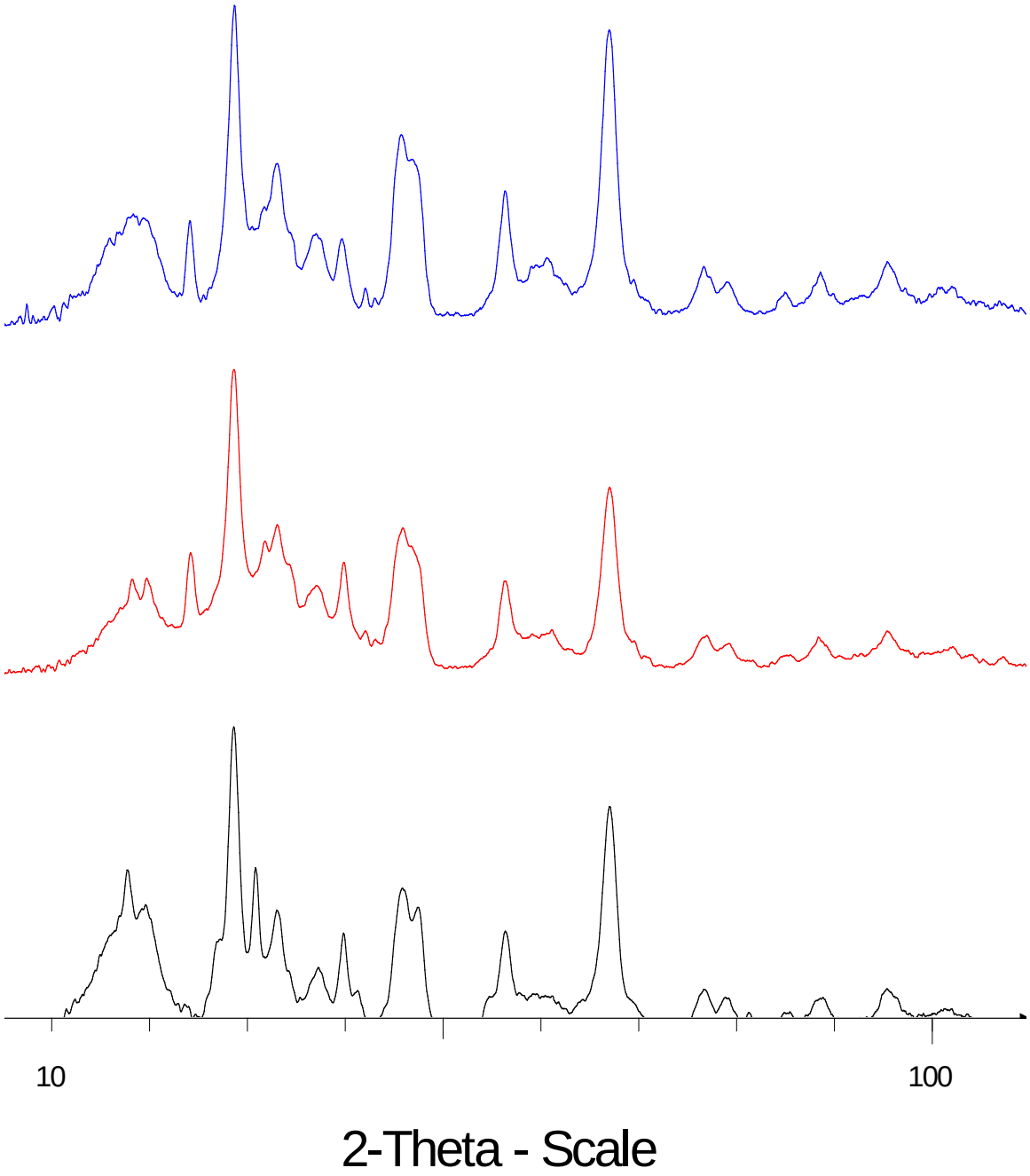

Figure 9-5: XRD of PBCA 600-800ºC sintering temperatures

9.2 TEM Images of PBA and PBCA catalysts

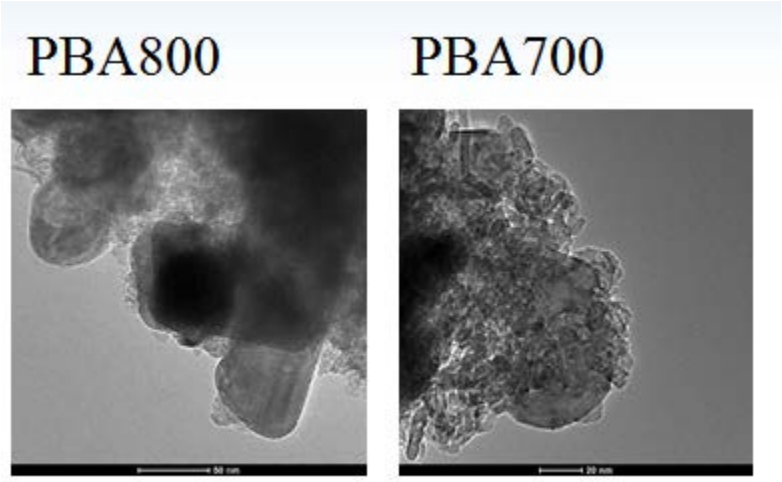

Figure 9-6: TEM images of PBA700 and PBA800 catalysts

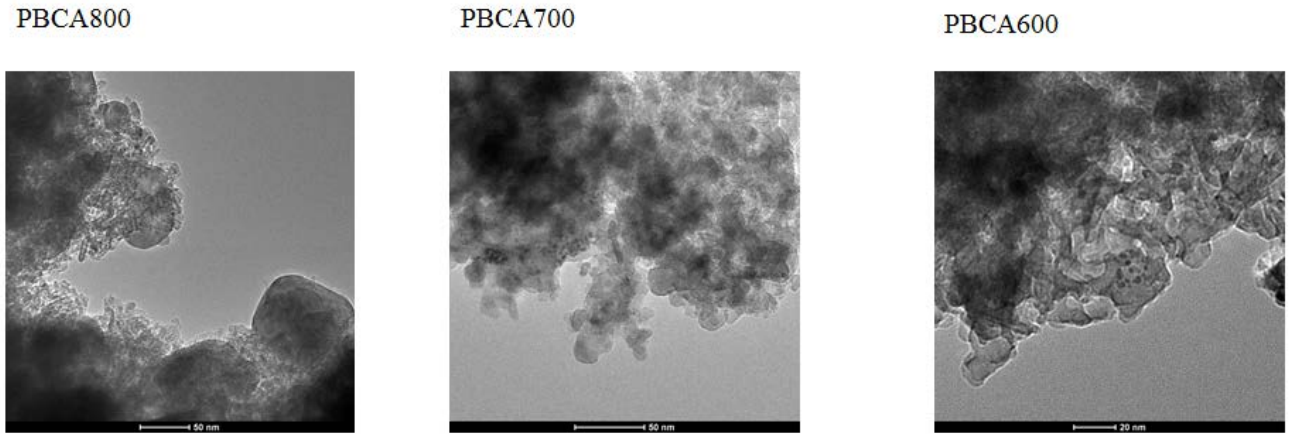

Figure 9-7: TEM Images of PBCA600, PBCA700 and PBCA800 catalysts